Portland State University
PDXScholar

Dissertations and Theses | Dissertations and Theses

Fall 11-6-2018

Ensemble Data Assimilation for Flood Forecasting in Operational Settings: from Noah-MP to WRF-Hydro and the National Water Model

Mahkameh Zarekarizi
Portland State University

Let us know how access to this document benefits you.

Follow this and additional works at: https://pdxscholar.library.pdx.edu/open_access_etds


Part of the Civil and Environmental Engineering Commons, and the Hydrology Commons

Recommended Citation
Zarekarizi, Mahkameh, "Ensemble Data Assimilation for Flood Forecasting in Operational Settings: from Noah-MP to WRF-Hydro and the National Water Model" (2018). *Dissertations and Theses.* Paper 4651.

10.15760/etd.6535

This Dissertation is brought to you for free and open access. It has been accepted for inclusion in Dissertations and Theses by an authorized administrator of PDXScholar. For more information, please contact pdxscholar@pdx.edu.

Ensemble Data Assimilation for Flood Forecasting in Operational Settings:

From Noah-MP to WRF-Hydro and the National Water Model

by

Mahkameh Zarekarizi

A dissertation submitted in partial fulfillment of the
requirements for the degree of

Doctor of Philosophy
in
Civil and Environmental Engineering

Dissertation Committee:
Hamid Moradkhani, Chair
Dacian Daescu
Gwynn Johnson
Paul Loikith

Portland State University
2018

Abstract

The National Water Center (NWC) started using the National Water Model (NWM) in 2016. The NWM delivers state-of-the-science hydrologic forecasts in the nation. The NWM aims at operationally forecasting streamflow in more than 2,000,000 river reaches while currently river forecasts are issued for 4,000. The NWM is a specific configuration of the community WRF-Hydro Land Surface Model (LSM) which has recently been introduced to the hydrologic community. The WRF-Hydro model, itself, uses another newly-developed LSM called Noah-MP as the core hydrologic model. In WRF-Hydro, Noah-MP results (such as soil moisture and runoff) are passed to routing modules. Riverine water level and discharge, among other variables, are outputted by WRF-Hydro. The NWM, WRF-Hydro, and Noah-MP have recently been developed and more research for operational accuracy is required on these models. The overarching goal in this dissertation is improving the ability of these three models in simulating and forecasting hydrological variables such as streamflow and soil moisture. Therefore, data assimilation (DA) is implemented on these models throughout this dissertation. State-of-the art DA is a procedure to integrate observations obtained from in situ gages or remotely sensed products with model output in order to improve the model forecast. In the first chapter, remotely sensed satellite soil moisture data are assimilated into the Noah-MP model in order to improve the model simulations. The performances of two DA techniques are evaluated and compared in this chapter. To tackle the computational burden of DA, Massage Passing Interface protocols are used to augment the

computational power. Successful implementation of this algorithm is demonstrated to simulate soil moisture during the Colorado flood of 2013. In the second chapter, the focus is on the WRF-Hydro model. Similarly, the ability of DA techniques in improving the performance of WRF-Hydro in simulating soil moisture and streamflow is investigated. The results of chapter 2 show that the assimilation of soil moisture can significantly improve the performance of WRF-Hydro. The improvement can reach 58% depending on the study location. Also, assimilation of USGS streamflow observations can improve the performance up to 25%. It was also observed that soil moisture assimilation does not affect streamflow. Similarly, streamflow assimilation does not improve soil moisture. Therefore, joint assimilation of soil moisture and streamflow using multivariate DA is suggested. Finally, in chapter 3, the uncertainties associated with flood forecasting are studied. Currently, the only uncertainty source that is taken into account is the meteorological forcings uncertainty. However, the results of the third chapter show that the initial condition uncertainty associated with the land state at the time of forecast is an important factor that has been overlooked in practice. The initial condition uncertainty is quantified using the DA. USGS streamflow observations are assimilated into the WRF-Hydro model for the past ten days before the forecasting date. The results show that short-range forecasts are significantly sensitive to the initial condition and its associated uncertainty. It is shown that quantification of this uncertainty can improve the forecasts by approximately 80%. The findings of this dissertation highlight the importance of DA to extract the information content from the observations

and then incorporate this information into the land surface models. The findings could be beneficial for flood forecasting in research and operation.

Dedication

To Mahasti and Faramarz

Mom, Dad, I lived my life in the past four years to make every second of not seeing you worth living. I failed a lot and I wanted to give up so many times. However, whenever I asked myself "Is that why I left my home?" I stood back up and worked even harder. You dedicated your lives to me and dedicating this book to you is the least I could do.

Acknowledgments

I would like to express my deepest gratitude to my advisor, Dr. Hamid Moradkhani. He taught me a lot more than hydrology and data assimilation. I thank him for all the opportunities and supports he provided. He helped me become the researcher, I am today.

I thank my dissertation committee, Dr. Gwynn Johnson, Dr. Paul Loikith, and Dr. Dacian Daescu for offering their time to review my dissertation and providing me with their valuable comments.

Special thanks to Dr. Ali Ahmadalipour for reviewing and editing my dissertaion. His comments helped me improve the quality of this dissertation.

I thank Dr. Hongxiang Yan, former PSU student and my mentor for teaching me many things I could not imagine to learn by myself. He was always helpful and available whenever I needed him even after he left PSU.

I thank William Garrick, the Research Computing Manager in the Office of Information Technology, Portland State University. He truly helped me whenever I needed help with the Coeus cluster. He always immediately replied my emails no matter if it was after hours or holidays. A significant portion of this dissertation could not happen without his assistance.

I deeply thank Roxanne Treece, Assistant Director of Graduate Academic Services for supporting me during the graduation process. Her assistance made my

transition after Ph.D. much easier. Also, thanks to CEE faculty and staff especially Dr. Chris Monsere, Megan Falcone and Samantha Parsons for their consistent help in my program.

I thank NWC, WRF-Hydro, and CUAHSI teams for hosting me in NWC summer school and WRF-Hydro training workshop. They patiently answered my questions when I was learning about the NWM, and they made data required for this dissertation available for me. Special thanks to Dr. David Gochis and Dr. Arezoo RafieeiNasab.

I thank my dearest colleagues and friends Dr. Arun Rana, Dr. Ali Ahamdalipour and Sepideh Khajehei. Arun was my mentor when I had just started my program in PSU. Ali always encouraged and supported me. Sepideh was always there for me no matter if I was in Portland or Alabama. I thank everyone in the "Remote Sensing and Water Resources" lab, especially Maysoun Hameed.

I appreciate all the support from my beloved partner, Hamed who unconditionally supported me in every moment of happiness or frustration. He kept me inspired and motivated, and he always believed in me even when I did not.

Last but not least, my warm acknowledgments to my parents and Ardeshir, my only and favorite brother for unconditionally loving me and supporting me when I decided to leave them in pursuit of my dreams.

Table of Contents

List of Tables

List of Figures

List of Abbreviations

CCI……....Climate Change Initiative

DA……..…….. Data assimilation

EnKF…….……..... Ensemble Kalman Filter

ESA ……..…… European Space Agency

LAI……..….. Leaf Area Index

LSM……..…….. Land Surface Model

MCMC……...…….. Markov Chain Monte Carlo

MPI……..…….. Massage Passing Interface

NASA…….. National Aeronautics and Space Administration

NLDAS…….. North American Land Data Assimilation System

NOAA……..….. National Oceanic and Atmospheric Administration

NWC……..... National Water Center

NWM…….….. National Water Model

NWS…….….. National Weather Service

OL…….. Open Loop

OWP…….. Office of Water Prediction

PF…….….. Particle Filter

RFC…….….. River Forecast Center

SMAP……..….. Soil Moisture Active Passive

UNOOSA…….. United Nation's Office for Outer Space

WRF…….….. Weather Research and Forecast

WRF-Hydro…….. WRF-Hydrological modeling system

1 Motivation

As the costliest natural hazard, floods have affected 2,490 million people between 1980 and 2004 over the globe (Strömberg, 2007). From 1900 to 2015, the U.S. has had 35,000 disasters out of which 40 percent are floods (Cigler, 2017). Two most recent examples of disasters that led to widespread flood are hurricane Harvey (Omranian et al., 2018) in September 2017 and Hurricane Florence in September 2018. Another example is the 2013 flood in Colorado Front Range that affected 18,000 people with a cost of around $2 billion. This highlights the need for an efficient and effective operational flood forecasting system. Currently, River Forecast Centers (RFCs) are in charge of flood monitoring and forecasting up to a week in advance. There are 13 RFCs in the U.S. including Missouri, North Central, Northeast, Northwest, Ohio, Southeast, West Gulf, Arkansas-Red, Alaska River, Colorado, California-Nevada, Lower Mississippi, and Mid-Atlantic. RFCs are in charge of approximately 4,000 river locations over the U.S. The need for a more comprehensive and process-based forecasting system with a longer lead-time and a better spatial coverage over the U.S., brought the National Water Center (NWC) into operation. The NWC has taken the lead for operational flood forecasting over the U.S. since 2015. The primary model in the NWC is the National Water Model (NWM). With the goal of improving water prediction services in National Oceanic and Atmospheric Administration (NOAA), the NWM started operating in August 2016. The distinct feature of the NWM is that it increases the 4,000 prediction locations to 2,700,000 locations over the Continental United States for streamflow prediction. In

addition to streamflow prediction, it simulates hydrological variables such as soil moisture and runoff. These variables are delivered at two spatial resolutions of 1 (km) and 250 (m). Another mission of the NWM is providing hyper-resolution (street-level) water predictions (Deo et al., 2018) for the National Weather Service (NWS) in order to improve decision making (http://water.noaa.gov/about/nwm; accessed on 9/18/2018). This feature is valuable in cases of hurricane-related flooding such as Harvey and Florence. The NWM is run operationally in four configurations including "Analysis and Assimilation", "Short-Range", "Medium-Range", and "Long-Range". The first run operates every hour and runs the NWM for the past 3 hours for a better estimation of the current land surface states and initializing the next three runs. The second run operates every hour and predicts streamflow and other hydrologic variables for the next 0-18 hours, the third run operates four times a day and issues forecasts up to the next ten days, and the last run, operates daily and issues forecasts for up to 30 days. The NWC has been successful in operationally running the model with high resolution over a large scale, and the quality of forecasts is constantly increasing through research. The NWC encourages research on the NWM by holding summer schools that gather graduate students from all over the nation to develop and work on research projects that directly help improve the model (Afshari et al., 2016; Brazil, 2018; Deo et al., 2018).

The NWM is a specific configuration of the community WRF-Hydro Land Surface Model (LSM) which has recently been introduced to the hydrologic community (Gochis et al., 2015, 2018). The WRF-Hydro model, itself, uses another newly-developed

column LSM called Noah-MP (Niu et al., 2011; Yang et al., 2011) as the core hydrologic model. In WRF-Hydro, Noah-MP results (such as soil moisture and runoff) are passed to surface and subsurface routing modules. The results are then passed to a channel routing model. Riverine water level and discharge, among other variables, are outputted by WRF-Hydro.

The Noah-MP and WRF-Hydro models are of particular interest in this dissertation. Previous studies (Lin et al., 2018; Yang et al., 2011; Zhang et al., 2016) had shown the effectiveness of these models in simulating hydrological variables (i.e., soil moisture, runoff, and river discharge); however, they (similar to other LSMs) are subject to uncertainties. These uncertainties are associated with climate change (Ahmadalipour et al., 2017a, 2017c; Barlage et al., 2015; Rana and Moradkhani, 2016), urbanization (Pathiraja et al., 2018a), climate variability (Loikith et al., 2017; Zarekarizi et al., 2017), and model structure and parameterization (Moradkhani et al., 2018; Pathiraja et al., 2016a).

To quantify and reduce uncertainty, Data Assimilation (DA) can be used (Liu and Gupta, 2007; Moradkhani et al., 2005a). Hydrologic DA is a mathematical discipline to integrate land surface model simulations with observations to improve the forecast skills (Chen et al., 2013; Moradkhani et al., 2012, 2005b; Pathiraja et al., 2018a, 2018b; Pathiraja et al., 2016a; Piazzi et al., 2018; Zaitchik et al., 2008). Commonly used DA methods in the hydrologic community are the Ensemble Kalman Filter (EnKF) (Clark et al., 2008), Particle Filter (PF) (Moradkhani et al., 2005; 2012; 2018), and Variational DA

(Daescu and Langland, 2017; Hamill and Snyder, 2000; Shaw and Daescu, 2016). EnKF was introduced by Evensen (1994) to build upon the well-known Kalman Filter (Kalman, 1960) and has been used to improve hydrologic modeling and prediction (Clark et al., 2008; Komma et al., 2008; Moradkhani et al., 2005b; Pathiraja et al., 2016a). Even though the EnKF is a statistically optimal estimation of a linear, Gaussian system, its widespread application in non-Gaussian and linear problems, has made this method a popular tool in hydrologic modeling (Maneta and Howitt, 2014; Moradkhani et al., 2005b; Pathiraja et al., 2016a). On the other hand, PF-based methods are not subject to the limitation of the EnKF such as (1) Gaussian assumption of errors in model states and observations, (2) linear updating of model states, and (3) violation of the water balance due to linearly adjusting (updating) the states. In the PF, the water balance is not violated since ensemble members are resampled instead of being adjusted (Moradkhani, 2008). The PF has been used for a variety of purposes from streamflow modeling and prediction (Dechant and Moradkhani, 2011) to extreme drought and flood forecasting (Ahmadalipour et al., 2017b; Yan et al., 2018, 2017). The PF has evolved over time and one of the recent advancements resulted in the Particle Filter Markov Chain Monte Carlo (PF-MCMC) (Andrieu et al., 2010; Moradkhani et al., 2012) and recently to Evolutionary Particle Filter which combines the strengths of PF-MCMC and an Evolutionary optimization, i.e., Genetic algorithm (Abbaszadeh et al., 2018). Yan et al. (2018) employed a parallel PF-MCMC to assimilate remotely sensed soil moisture observations into the Variable Infiltration Capacity (VIC) model. They demonstrated a better drought monitoring skill than currently implemented drought monitoring products. Yan et al.

(2017 and 2018) used the PF-MCMC and assimilated satellite soil moisture into the VIC model and combined the results with a multivariate statistical drought forecasting approach showed that initializing the drought forecasting model with updated soil moisture states from DA results in more accurate drought forecasts. They tested their methodology to hindcast the widespread drought of 2012 in the U.S. and showed that with DA, the drought could have been predicted weeks in advance.

Similarly, the goal of this dissertation is to answer this question in the context of flood forecasting. Therefore, the overarching goal of this dissertation is to improve the performance of Noah-MP, WRF-Hydro, and the NWM in simulating and forecasting flood. Specifically, answering the following questions is targeted:

(1) What are the main sources of uncertainty in flood forecasting? How could these sources be quantified? How sensitive are the forecasts to the uncertainties? Is initial condition uncertainty an important source? How long does it take for the system to forget about the initial conditions?

(2) Are DA techniques able to improve the performance of Noah-MP in simulating soil moisture? How well are they able to improve the model? Which DA technique has better performance? How efficient are these methods?

(3) How well are DA techniques able to improve the performance of the WRF-Hydro model? Does assimilation of satellite soil moisture into WRF-Hydro affect the streamflow simulations? Does assimilation of USGS streamflow observations lead to improved soil moisture simulations?

Research and operation could benefit from the outcomes of this dissertation toward improving the skill of current flood forecasting systems while reducing the uncertainties. The outcomes help identify potential additions for future improvements in flood forecasting, especially in the NWM. The assessments provided in this dissertation are important preliminary steps toward a better land surface modeling practice for a better weather prediction skill and more accurate large-scale flood forecasts.

The dissertation is organized as follows: In the second chapter, a literature review on Noah-MP and DA techniques are first provided and then, two experiments are designed and illustrated. The results and implications of these experiments are discussed in the end. In the third chapter, the WRF-Hydro model is targeted. Again, the relevant experiments are designed and the analyses and results are discussed. In the third chapter, initial condition uncertainty in flood forecasting is quantified. Synthetic and real data experiments are elaborated in that chapter and their findings and significance are discussed. The dissertation concludes with an overall summary of the main findings, discussion, and future work.

2 Data Assimilation to enhance Noah-MP soil moisture predictions

2.1 Abstract

Noah-MP is a land surface model that has recently attracted attention from the meteorological community because it can be coupled with weather forecasting models such as Weather Research and Forecast (WRF). The ability of the model to accurately simulate soil moisture is of particular interest because soil moisture plays an important role in agriculture productivity and flood/drought prediction. This chapter investigates the possibility to further improve the model's skill in simulating soil moisture. Besides using a land surface model, soil moisture can be obtained from satellite measurements, and it has been shown that combining remotely-sensed and model-simulated soil moisture through data assimilation (DA) techniques can result in more accurate hydrologic forecasts. In this study, data assimilation methods are evaluated on the Noah-MP model. Particularly, two commonly used techniques, the Ensemble Kalman Filter (EnKF) and Particle Filter Markov Chain Monte Carlo (PF-MCMC) are assessed and compared. Additionally, an algorithm is proposed to handle the computational demand of such a large-scale DA implementation. The algorithm is designed for high-performance computing infrastructure and clusters of computational nodes. The results indicate that the DA successfully improves Noah-MP's ability in simulating soil moisture. Results of comparing EnKF and PF-MCMC indicate that the PF-MCMC has a higher skill in

improving soil moisture. Finally, the proposed parallel algorithm is implemented for simulating soil moisture during the Colorado Front Range flood in 2013.

2.2 Highlights

(1) Two commonly used data assimilation methods, the Ensemble Kalman Filter and Particle Filter Markov Chain Monte Carlo, are successfully implemented on Noah-MP.

(2) Particle Filter DA shows a higher skill in improving Noah-MP's soil moisture simulations.

(3) A high-performance-computing method is implemented to meet the computational demand.

2.3 Introduction

Noah-MP (Yang et al., 2011) is a Land Surface Model (LSM) that plays an important role in earth system modeling. The water stored in the land during a wet season will eventually return to the atmosphere in the dry season through evapotranspiration (Niu et al., 2011). Noah-MP is capable of modeling this feedback. Soil moisture (the water stored in the land) plays a key role in this feedback because it has a persistence characteristic. This means that the water stored in soil needs weeks or even seasons to evaporate. Therefore, soil moisture can provide information about the future of the atmosphere and is known to affect weather predictability (Niu et al., 2011). On the other hand, it determines onset, duration, and termination of agricultural droughts

(Ahmadalipour et al., 2017b; Madadgar and Moradkhani, 2013; Yan et al., 2017; Yan et al., 2018) and it also is one of the important predictands of (flash) floods (Cenci et al., 2017). Previous research (Gao et al., 2015; Martinez et al., 2016; Xia et al., 2017; Zhang et al., 2016) has shown that Noah-MP is significant in simulating soil moisture. For example, Cai et al. (2014a) concluded that Noah-MP has a significant capability in modeling the soil moisture. Also, Yang et al. (2011) studied the performance of soil moisture modeling in Noah-MP as compared with the Noah LSM (the previous version on Noah-MP) and found that Noah-MP improves the simulations.

In addition to land surface modeling of soil moisture, this land surface variable can be measured from a variety of in-situ and remote sensors. Two types of soil moisture measurements include observed gauge measurements and satellite measurements. In-situ or gauge soil moisture networks are available for a limited number of points across the U.S., while satellite soil moisture observations are available over a grid.

Both sources of obtaining soil moisture (LSMs and observations) are subject to a great deal of uncertainty. To reduce and quantify uncertainty, Data Assimilation (DA) is used (Liu and Gupta, 2007; Moradkhani et al., 2018, 2005a). In DA, observations are integrated with a dynamic land surface model[1].

[1] In simple words, suppose a land surface model is running. This model has numerous variables. One variable of interest, x, is also observable by a satellite. When the satellite passes the area of interest, the value x is recorded. To make the model-generated values closer to observed satellite data, DA is used. The DA updates the model to reflect the values recorded by the satellite.

DA methods have been frequently discussed in the literature of hydrologic modeling (Chen et al., 2013; Moradkhani et al., 2012, 2005b; Pathiraja et al., 2016a; Pathiraja et al., 2018c; Piazzi et al., 2018; Zaitchik et al., 2008). In DA, one or multiple variables are updated every time an observation becomes available. Common variables that have been assimilated into land surface models include snowpack (Kumar et al., 2016, 2014; Piazzi et al., 2018), streamflow (Aubert et al., 2003; DeChant and Moradkhani, 2014a, 2012), and soil moisture (Chen et al., 2011; Hain et al., 2012; Reichle et al., 2007; Marc Etienne Ridler et al., 2014). Soil moisture, in particular, has been assimilated into land surface models with objectives such as drought monitoring/prediction (Ahmadalipour et al., 2017b; Yan et al., 2018, 2017), flood prediction (DeChant and Moradkhani, 2014b; Moradkhani et al., 2012) , or obtaining a better estimation of soil moisture (Hain et al., 2012; Yan et al., 2015).

Successful assimilations of soil moisture observations on LSMs such as VIC (Yan et al., 2018), PRMS (Yan et al., 2017), and NASA LIS (Hain et al., 2012) have been reported in the literature. However, limited research has been done on Noah-MP soil moisture DA. The limited number of research on the assimilation of observed soil moisture into the Noah-MP model may be attributed to the computational burden and the complexity of this model.

Consequently, improving Noah-MP and its representation of soil moisture is the main goal of this chapter. Specifically, this chapter aims as the following:

(1) Assessing the performance of data assimilation techniques on the Noah-MP simulations.

(2) Comparing the skill of commonly used DA techniques.

(3) Introducing a high-performance-computing process to tackle the high computation demand of such DA techniques.

The value of this research lies in weather predictability and flood forecasting. Further improving the current ability in simulating soil moisture is intended in this study which can improve the current skills in weather and flood prediction. The results of this study could help the operational agencies such as the National Water Center in improving flood forecasts and the NCEP for further improving climate forecasts.

The rest of the chapter is structured as follows: more information about the study area, data, and the event of interest are provided in the next section. The data assimilation and parallel computing methodologies are explained in the methodology section, followed by a section illustrating the pre-processing of the Noah-MP model. The results of a simple model run are provided in the first part of the results section. The results section is followed by the DA results and the designed experiments. Finally, the chapter is concluded with a short summary and discussions/conclusions.

2.4 Study area and data

2.4.1 Colorado Front Range and the 2013 flood

Since one of the goals of this study is to investigate the role of soil moisture assimilation targeting operational flood forecasting systems, modeling floods is of interest. In particular, The great Colorado flood of September 2013 is studied. This flood happened during the period of 9-16 September 2013 due to heavy rainfall (>450 mm) in the Colorado Front Range foothills. The flood caused $2 billion in damage, 8 flood-related fatalities and forced 18,000 people to evacuate their houses (Gochis et al., 2015). Record atmospheric moisture was brought to the region by large-scale moisture advection features and led to heavy rainfall. While numerical weather predictions were able to identify this rainfall, they had significant errors in its magnitude and spatial pattern (Gochis et al., 2015). For a detailed assessment of the causes and impacts of this flood, interested readers are referred to Uccellini (2014). Figure 2-1 shows the location and imagery of this area.

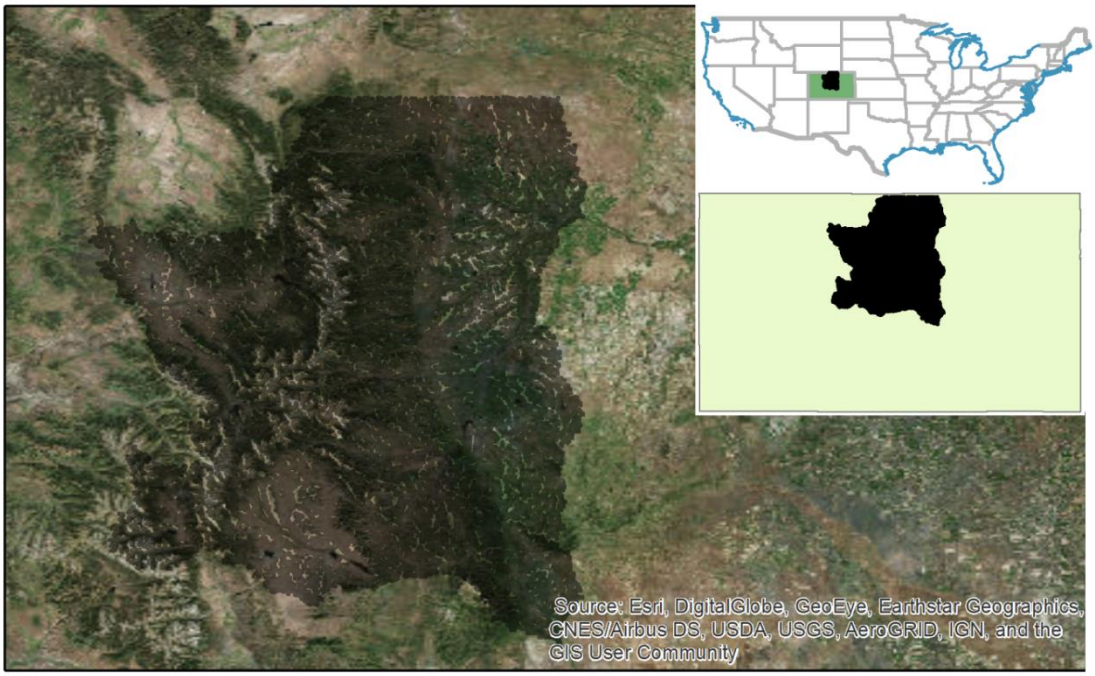

Figure 2-1: Imagery and location of the studied area, Colorado Front Range

2.4.2 Satellite soil moisture observations

Frequently used satellite soil moisture products are the Climate Change Initiative (CCI), Soil Moisture and Ocean Salinity (SMOS), Advanced Scatterometer (ASCAT) by European Space Agency (ESA), and Soil Moisture Active Passive (SMAP) by National Aeronautics and Space Administration (NASA).

Available from March 31, 2015, SMAP (Entekhabi et al., 2010) monitors the Earth's land surface for soil moisture. A unique feature of this mission is its ability to distinguish frozen and thawed land surfaces. SMAP provides more than 20 data products

with different spatiotemporal resolutions under four levels of L1, L2, L3, and L4, representing the processing levels. The L1 and L2 products contain instrument-related data based on half orbits of the SMAP satellite. The L3 products are a daily composite of L2. The L4 data are the output from NASA's land surface model estimated by assimilation of L-band brightness temperature observations. While SMAP measurements provide soil moisture in the upper 5 cm of the soil column, L4 products are designed to provide root zone soil moisture by informing model simulations of surface soil moisture within data assimilation processes. One application that can directly benefit from remotely sensed soil moisture measurements is flood forecasting (Entekhabi et al., 2010) since soil moisture plays an essential role in partitioning rainfall into infiltration and runoff. Accurate observations of current soil moisture status lead to improved flood forecasts. This study investigates the advantages of updated soil moisture states.

Since SMAP data were not available for the 2013 flood, the Climate Change Initiative (CCI) v02.2 (Dorigo et al., 2017; Liu et al., 2011) is used for this case study. Four passive and two active microwaves are blended to form the CCI products including the Scanning Multichannel Microwave Radiometer (SMMR), Special Sensor Microwave Imager (SSM/I), Tropical Rainfall Measure Mission (TRMM) Microwave Imager (TMI), Advanced Microwave Scanning Radiometer for Earth Observing System (AMSR-E), Advanced Microwave Instrument (AMI), and ASCAT. The temporal resolution of CCI data is daily and the spatial resolution is 0.25˚.

2.4.3 Meteorological forcing

Two datasets that could potentially be used for Noah-MP are GLDAS (Global Land Data Assimilation System) and NLDAS (North American Land Data Assimilation System). The Global Land Data Assimilation System (GLDAS) (Rodell et al., 2004), built upon the North American Land Data Assimilation System (NLDAS), provides support for improved forecast initial conditions by integrating data from advanced observing systems. GLDAS is a multi-institutional product developed jointly by National Aeronautics and Space Administration (NASA), Goddard Space Flight Center (GSFC), and the National Oceanic and Atmospheric Administration National Centers for Environmental Prediction (NOAA NCEP) and is run at NCEP, NASA GSFC, Princeton University, the University of Washington, and NOAA's Office of Hydrologic Development. GLDAS drives Mosaic, Noah, CLM, and VIC land surface models with the goal of simulating the transfer of mass, energy, and momentum. Then, it updates the simulations by merging them with satellite- and ground-based observations through data assimilation techniques such as the Ensemble Kalman Filter and the Extended Kalman Filter. GLDAS runs are performed on $0.25^{\circ} \times 0.25^{\circ}$ (standard operational run), $0.5^{\circ} \times 0.5^{\circ}$, $1.0^{\circ} \times 1.0^{\circ}$, and $2.0^{\circ} \times 2.5^{\circ}$ grids and the results are publicly available in near-real time.

Multiple versions of GLDAS are available including GLDAS-2, which refers to simulations forced entirely with Princeton meteorological forcing data, GLDAS-2.1 referring to simulations forced with a combination of model- and observation-based data, and GLDAS-1 which includes simulations forced by combination of NOAA/GLDAS

atmospheric analysis fields, spatially and temporally disaggregated NOAA Climate Prediction Center Merged Analysis of Precipitation (CMAP) fields[2].

Land surface models, in particular, Noah-MP (Niu et al., 2011; Yang et al., 2011), can be forced with the GLDAS meteorological data such as precipitation, short- (and long-) wave radiation, air temperature, air pressure, specific humidity, and wind speed. For example, Yang et al. (2011) run Noah-MP at a global scale with meteorological forcing data from GLDAS for the period of 1980-2006 in order to assess the performance of Noah-MP.

In this study, the Noah-MP model is forced with surface meteorological data including daily or sub-daily precipitation, wind speed, air temperature, specific humidity, air pressure, and incoming longwave and shortwave radiation. Meteorological forcings were obtained from the Phase II North American Land Data Assimilation System (NLDAS-2) (Xia et al., 2012b), gridded to the 1/8˚ resolution. NLDAS is a multi-institution project aiming at providing reliable initial land states to improve weather predictions. NLDAS runs Noah, Mosaic, Sacramento Soil Moisture Accounting (SAC-SMA), and VIC to generate land states over 1/8˚ CONUS domain (Xia et al., 2012a). NLDAS-1 was first introduced by Mitchell et al. (2004) and later in 2012 NLDAS-2 which builds on NLDAS-1 was published. The second phase increased the accuracy and consistency of the data and upgraded the model codes and parameters.

[2] For more information, visit
https://disc.gsfc.nasa.gov/datasets/GLDAS_NOAH025_M_V2.1/summary?keywords=GLDAS

2.5 Noah-MP Land Surface Model

A Land Surface Model (LSM) is a mathematical representation of a hydrologic system that simulates energy and water fluxes. LSMs are categorized into two categories of lumped and distributed. While lumped models simulate the entire basin as one entity with forcing data (input) uniformly distributed across the basin, distributed models divide the watershed into smaller units (e.g., grid cells) and solve the energy and water balance for each unit. Some well-known distributed models include (but are not limited to) Variable Infiltration Capacity (VIC) (Liang et al., 1994; Nijssen et al., 2001), Community Land Model (CLM) (Oleson Lawrence, D. M., Bonan, G. B., Flanner, M. G., et al., 2010), Noah (Ek, 2003), and Noah-MP (Yang et al., 2011).

Noah LSM is a result of multi-institutional cooperation including the Air Force Weather Agency, Weather Research and Forecast (WRF), and the National Center for Environmental Prediction (NCEP). The model is reported to have shortcomings on the following processes:

1) Runoff and snowmelt simulations (Bowling et al., 2003; Slater et al., 2007).

2) Snow skin temperature prediction as a result of combining vegetation and snow layers in snowy days (Niu et al., 2011).

3) Capturing the Earth's critical zone because the model considers just a shallow soil column (only two meters) which then results in a relatively short soil memory (Niu et al., 2011).

4) Representing infiltration in the presence of frozen soil (Shanley and Chalmers, 1999).

However, Noah-MP (Yang et al., 2011) attempts to resolve the above weaknesses by adding a vegetation canopy layer, modifying the radiation transfer system, and relating stomatal resilience to photosynthesis. In addition to solving the aforementioned problems (Barlage et al., 2015), Noah-MP offers alternatives for various physical processes. For instance, multiple options are provided for dynamic vegetation, frozen soil permeability, conversion of precipitation into rainfall/snowfall, generation of runoff/groundwater, and more processes as discussed in Niu et al. (2011). A performance assessment of Noah-MP (Yang et al., 2011) concluded that despite the amplified computational time, the model demonstrates improvements in skin temperature, runoff, snow, and soil moisture simulations as compared to the original Noah LSM. Furthermore, the optional parameterization schemas of the Noah-MP model was proven beneficial after conducting 36 experiments with 36 different combinations of parameter schemas concluding that the ensemble mean performs better than any individual ensemble member (Yang et al., 2011).

Noah-MP has attracted attention from the meteorological and hydrological communities. The meteorological community is interested in this model mainly because it has been coupled with the Weather Research and Forecast (WRF) model. Such coupling enables the modeling of the land-atmosphere feedbacks. Coupled Noah LSM has been used in operational agencies such as the National Center for Environmental

Prediction (NCEP) for weather prediction and downscaling of the climate models (Yang et al., 2011); Noah-MP is a possible replacement. Additionally, Noah-MP was tested for inclusion in the next phase of the North American Land Data Assimilation System (NLDAS) (Cai et al., 2014b). On the other hand, the hydrologic community has become interested in this model because it is the main LSM in the National Water Model (NWM) operated by the National Weather Service (NWS) for flood forecasting in more than 2 million river reaches over the Continental United States.

A brief literature review on the Noah-MP model is presented in the following. More specific information such as setting up the model is discussed in the "results" section.

Model background: Noah-MP is developed in FORTRAN and is forced with the air temperature at height z above ground, snowfall, rainfall, surface downward solar radiation, surface downward longwave radiation, specific humidity at height z above ground, and surface pressure at height z above ground. It is noteworthy that the entire forcing variables are available through the Global Land Data Assimilation System (GLDAS) (Rodell et al., 2004).

Xia et al. (2017) discussed the next generation of NLDAS using three LSMs including Noah-MP, Community Land Model version 4.0 (CLM4.0), and Catchment LSM-Fortuna 2.5 (CLSM-F2.5). They concluded that all three models were able to capture monthly to inter-annual variability. They also discussed that current LSMs in

NLDAS have a simple snow model, which causes an unrealistic runoff simulation and thus, Noah-MP can be of interest.

Model sensitivity*:* Cuntz et al. (2016) performed a global sensitivity analysis of Noah-MP parameters. In addition to 71 model parameters, they found 139 hard-coded parameters and included them in their analysis and found that the most sensitive parameter is a hard-coded one that controls soil surface against direct evaporation. They find that latent heat[3] and runoff have similar sensitivities and that surface runoff is sensitive to almost all of the hard-coded parameters. They also argue that the model is sensitive to the quality of incoming radiation. They suggested that the user should take care of the amount of direct diffusive radiation and the amount of visible to near-infrared radiation in the input files.

Arsenault et al. (2018) conducted a sensitivity analysis of Noah-MP. They used a variance decomposition method to assess model sensitivity to its parameters. Their target variables were soil moisture, sensible heat, latent heat, and net ecosystem exchange. They have done the analysis on 10 international Fluxnet stations over the globe. They considered four configurations and concluded that in dynamic vegetation configuration, all output variables were very sensitive to wilting point, unsaturated soil conductivity exponent, baseline light use efficiency, baseline carboxylation, leaf turnover, and single-sided leaf area. Particularly for soil moisture, they considered porosity and saturated soil

[3] The hidden (latent=hidden) heat absorbed or released in processes that the temperature remains the same, such as evaporation, condensation, melting, freezing, or sublimation.

hydraulic conductivity. They also conclude that dynamic vegetation configuration makes soil moisture more sensitive to vegetation parameters. This highlights the potential of using a land surface model with dynamic vegetation option to improve soil moisture state estimates (Yang et al., 2011).

Model performance: Model performance of Noah-MP was first evaluated by Yang et al. (2011) where global-scale tests were conducted on the model. By comparing model simulations against satellite and ground-based observations, they showed improvements in modeling runoff, soil moisture, snow, and skin temperature as compared to the Noah LSM. They design six experiments ranging from Noah LSM to fully augmented Noah-MP with dynamic vegetation. They also made an ensemble of different schemas and recommended that the model should be used in an ensemble format. An important note regarding the Noah-MP LSM is that the mean state and variability of the model are controlled by ET but modulated by the buffering effects due to groundwater (Yang et al., 2011). Yang et al. (2011)discuss that the runoff schema plays a vital role in soil moisture-ET relationship. Four options are provided for calculating runoff. These options include Simple Top Runoff and Groundwater Model (SIMGM), Simple Top Runoff Model (SIMTOP), and Schaake96. SIMGM refers to TOPMODEL-based runoff scheme with the simple groundwater (Niu et al., 2011), SIMTOP refers to a simple TOPMODEL-based runoff scheme with an equilibrium water table (Niu et al., 2011), and Schaake96 refers to an infiltration-excess-based surface runoff scheme. This scheme uses a gravitational free-drainage subsurface runoff process which was used in the original

Noah model as well (Schaake et al., 1996). The last runoff schema option is BATS. Surface runoff in BATS is parameterized as a 4th power function of the top 2 m soil wetness. The subsurface runoff is parameterized as gravitational free drainage (Niu et al., 2011). Yang et al. (2011) discuss that some schemas such as SIMTOP result in the wetter soil as they impose a lower boundary condition (zero-flux). Runoff schemas with gravitational free drainage (such as BATS) tend to underestimate soil moisture, which in turn leads to underestimation of ET as compared to models with a groundwater component. While the runoff schema is a key schema for soil moisture modeling, as concluded by Yang et al. (2011), the β factor (a factor in Noah-MP that controls stomatal resistance), dynamic vegetation, and stomatal resistance are not as important.

The 2m maximum temperature is very sensitive to the choice of the LSM as Burakowski et al. (2016) showed. Zhang et al., (2016) showed that these subprocess schemas have the highest uncertainty: canopy resistance, soil moisture threshold for evaporation, runoff and groundwater, and surface-layer parameterization. Ma et al. (2017) evaluate Noah-MP's performance over 18 HUC2 regions across the CONUS. They observed that the model performs better in simulating evapotranspiration when the dynamic vegetation option is off and they conclude that the dynamic vegetation option needs to be improved. Ma et al. (2017),Niu et al. (2011), and Yang et al. (2011) confirmed that Noah-MP performs well in simulating snow depth and snow water equivalent (SWE).

Martinez et al. (2016) concluded that an increase in root-zone soil moisture (top 2 meters) results in an increase of evapotranspiration, mostly in areas where ET is more water limited. They also found that the groundwater schemas induce an increase in the simulated moisture where the water table is close to the surface. They discussed that when the increase in ET takes place in areas that water table is in the root-zone, part of the extra ET comes from direct uptake of moisture from the saturated layers below the water table (i.e., direct groundwater uptake).

Model spin-up: Cai et al. (2014a) analyzed the required spin-up duration for soil moisture and suggested that 8 years is enough for the analysis. Gao et al. (2015) discussed the spin-up period for the Noah-MP model and highlighted the importance of spin-up in Noah-MP. The required spin-up period may vary from a couple of years to more than 30 years, depending on the variable of interest and the physics of the model. For example, Gao et al., (2015) discussed that for a simple soil physics, 4 years of spin-up would be enough, while in case of adding organic matter and spare to dense rhizosphere parameterization, 30 years of spin-up is needed.

Coupling with climate models: Gao et al. (2015) discussed that the interactions between land and atmosphere are not well represented in the current LSMs. Therefore, they used Noah-MP to assess the parameterization role in Tibetan Plateau (TP). They concluded that uncertainty in soil initialization significantly affects deep-soil temperature and moisture. They discussed that the uncertainties in atmospheric forcings affects topsoil variables, and therefore the surface energy fluxes. They showed that the default Noah-MP

has large dry biases (about 50%) in topsoil moisture in the monsoon season. They reported successful results when the rhizosphere effect is taken into consideration.

2.6 Methodology

2.6.1 Data Assimilation

In this study, both EnKF and PF-MCMC are used and their performance in improving soil moisture simulations is assessed. In the following section, a brief literature review on both methods is presented.

2.6.1.1 Particle Filter

Particle Filter (PF) methods have been frequently demonstrated to be effective in hydrologic modeling (Dechant and Moradkhani, 2011; Moradkhani et al., 2018, 2012; Yan and Moradkhani, 2016). Similar to all PFs, PF-MCMC is also based on Sequential Importance Resampling (SIS) (Liu et al., 2001). Due to weight degeneracy as a shortcoming of SIS, a resampling step is introduced where particles with significant weights are replicated and particles with insignificant weights are neglected (Moradkhani et al., 2012). Markov Chain Monte Carlo (MCMC) methods are introduced as an alternative of PFs that are based on the Ergodic theory[4] while PFs are based on the law of large numbers (Moradkhani et al., 2012). These techniques explore the posterior distribution using one or more chains and are more efficient than the PF methods (Moradkhani et al., 2012). MCMC methods are one of the ten most influential algorithms

[4] A branch of statistics where the main concern is the behavior of dynamic systems.

of the 20th century (Dongarra and Sullivan, 2000). In simple words, the goal of MCMC is to sample from a complicated, high-dimensional function. However, the function is too complicated to sample from. One way to tackle this problem is importance sampling where there is a proposal distribution to sample from. This proposal distribution could successfully mimic the original posterior distribution in low dimensions; however, for higher dimensions, the proposal distribution can incorrectly assign higher probabilities. Therefore, the proposal distribution could fail in high dimensions. MCMC methods propose to tackle this problem by a random walk in the areas with high probabilities.

The particle filter (PF) based ensemble DA algorithm is used in this study to update the model states and quantify the initial condition uncertainty. Compared with the popular ensemble Kalman filter (EnKF), the PF can relax the Gaussian error assumption, maintain water balance, and provide a more complete representation of state/parameter posterior distribution (Dechant and Moradkhani, 2014; Moradkhani et al., 2012; Yan and Moradkhani, 2016; Yan et al., 2015).

As demonstrated by Moradkhani (2008), the state-space models that describe the generic earth system are as follows:

$$x_t = f(x_{t-1}, u_t, \theta) + w_t \tag{1}$$

$$y_t = h(x_t) + v_t \tag{2}$$

where $x_t \in \mathbb{R}^n$ is a vector of the uncertain state variables at a current time step, $y_t \in \mathbb{R}^m$ is a vector of observation data, u_t is the uncertain forcing data, $\theta \in \mathbb{R}^d$ is the

model parameters, h is a non-linear function that relates the states x_t to the observations y_t, w_t represents the model error, and v_t indicates the observation error. The errors w_t and v_t are assumed to be white noise with mean zero and covariance Q_t and R_t, respectively. The posterior distribution of the state variables x_t given a realization of the observations $y_{1:t}$ is written as follows:

$$p(x_t|y_{1:t}) = p(x_t|y_{1:t-1}, y_t) = \frac{p(y_t|x_t)p(x_t|y_{1:t-1})}{p(y_t|y_{1:t-1})} = \frac{p(y_t|x_t)p(x_t|y_{1:t-1})}{\int p(y_t|x_t)p(x_t|y_{1:t-1})dx_t} \tag{3}$$

$$p(x_t|y_{1:t-1}) = \int p(x_t, x_{t-1}|y_{1:t-1})dx_{t-1} = \int p(x_t|x_{t-1})p(x_{t-1}|y_{1:t-1})dx_{t-1} \tag{4}$$

where $p(y_t|x_t)$ is the likelihood, $p(x_t|y_{1:t-1})$ is the prior distribution, and $p(y_t|y_{1:t-1})$ is the normalization factor. In practice, Equation (3) does not have an analytic solution except for a few special cases. Instead, the posterior distribution $p(x_t|y_{1:t})$ is usually approximated using a set of Monte Carlo (MC) random samples as:

$$p(x_t|y_{1:t}) \approx \sum_{i=1}^{N} w_t^{i+} \delta(x_t - x_t^i) \tag{5}$$

where w_t^{i+} is the posterior weight of the i^{th} particle, δ is the Dirac delta function, and N is the ensemble size. The normalized weights are calculated as follows:

$$w_t^{i+} = w_t^{i-} \frac{p(y_t|x_t^i)}{\sum_{i=1}^{N} w_t^{i-} p(y_t|x_t^i)} \tag{6}$$

where w_t^{i-} is the prior particle weights, and $p(y_t|x_t^i)$ can be computed from the likelihood $L(y_t|x_t^i)$. Generally, a Gaussian distribution is used to estimate $L(y_t|x_t^i)$:

$$L(y_t|x_t^i) = \frac{1}{\sqrt{(2\pi)^m |R_t|}} exp\left[-\frac{1}{2}\left(y_t - h(x_t^i)\right)^T {R_t}^{-1}\left(y_t - h(x_t^i)\right)\right] \tag{7}$$

To obtain approximate samples from $p(x_t|y_{1:t})$, a resampling operation is necessary. Moradkhani et al. (2005a) suggest resampling the particles with a probability greater than the uniform probability. After resampling, all the particle weights are set equal to $1/N$.

To further reduce the weight degeneration problem (where all but one of the importance weights are close to zero), the particle filter with sampling importance resampling (PF-SIR) algorithm can be combined with Markov chain Monte Carlo (MCMC) (Andrieu et al., 2010; Moradkhani et al., 2012). The recently developed particle Markov chain Monte Carlo (PMCMC) (Andrieu et al., 2010) is used in this study for large-scale DA applications. The PMCMC is an extension of the PF-SIR and uses the PF-SIR to design efficient high-dimensional proposal distributions for the MCMC algorithm.

The PMCMC consists of the following three steps: (1) Initialization ($j = 0$): run PF-SIR targeting $p(x_t|y_{1:t})$, sample $X_t(0) \sim p(x_t|y_{1:t})$ and let $p(y_{1:t})(0)$ denote the corresponding marginal likelihood estimate. (2) Iteration ($j \geq 1$): sample $X_t^* \sim p(x_t|y_{1:t})$

again and let $p(y_{1:t})^*$ denote the corresponding marginal likelihood estimate. (3) Calculate the acceptance ratio as:

$$min\left\{1, \quad \frac{p(y_{1:t})^*}{p(y_{1:t})(j-1)}\right\} \tag{8}$$

and set $X_t(j) = X_t^*$ and $p(y_{1:t})(j) = p(y_{1:t})^*$; otherwise set $X_t(j) = X_t(j-1)$ and $p(y_{1:t})(j) = p(y_{1:t})(j-1)$.

It is worth noting that the assimilation of soil moisture in Noah-MP is done separately for each grid cell. Therefore, each grid cell is updated separately without receiving any information from the adjacent cells.

2.6.1.2 Ensemble Kalman Filter

Unlike the Particle Filter methods that assign weights to ensemble members, the EnKF adjusts the value of the state variables according to the observations. EnKF (Evensen, 1994) is an extension of Kalman Filter (Kalman, 1960). If x is the state variable, at each time step that an observation becomes available, the state is updated through the following equation:

$$x_t^{i+} = x_t^{i-} + K\left(y_t - Hx_t^{i-} + r_t\right) \tag{9}$$

where x_t^{i+} is the posterior state vector for the i^{th} ensemble member, x_t^{i-} is the priori state vector, H is the linearized observation operator ($H = \partial h/\partial x$) that translates model space to observation space, and K is the Kalman gain calculated as:

$$K = P^{-}H^{T}(HP^{-}H^{T} + R_t)^{-1} = C_{xy}\left(C_{yy} + R_t\right)^{-1} \quad (10)$$

where P^{-} is the model state error covariance, $P^{-}H^{T} = C_{xy}$ is the covariance of the state ensembles with the predicted observations, and $HP^{-}H^{T} = C_{yy}$ is the variance of the predicted observations.

2.6.2 High-Performance Computing

Large-scale, high-resolution ensemble DA with land surface modeling is computationally very expensive. One possible solution is parallel computing that uses multiple computational sources to augment the computational power. Parallel processing uses multiple processing nodes concurrently. Since in ensemble data assimilation, there are no dependencies between ensemble members, parallel computing is of interest. In ensemble data assimilation, and particularly PF-MCMC each ensemble member is an evolving Markov chain and different chains are independent of each other and can be run in parallel. The bottleneck of using parallel computing in data assimilation is the time dependence. Although ensemble members are independent of each other, they need information from the previous time step.

Parallel computing is defined as the simultaneous use of multiple computing sources. Depending on the hardware, parallel computing is referred to as high-performance computing. If the resources are as small as a desktop computer or a laptop, it is called parallel computing, but when the resources increase to cluster where hundreds of nodes are used or supercomputers, where thousands of nodes are used, it is referred to as

high-performance computing (HPC). The most commonly used Application Programming Interface[5] (API) for parallel processing is Massage Passing Interface or MPI. One can think of MPI as a set of subroutines and communication protocols with fixed functionality. However, MPI is available for many languages such as Python, C, C++, FORTRAN, etc. Multiple MPI APIs are available including OpenMPI, HP-MPI, MPICH. All of these APIs follow the same standard.

Two commonly used ways of parallel programming are shared memory and distributed memory. In the shared memory system, multiple processes are created and each has access to the entire memory. For example, if the value of a matrix changes, every process uses the updated values. On the other side, in distributed memory systems, multiple copies of the main program are provided for each process. Processes are not aware of changes that other processes make. To pass the information along, processes need to use communication protocols such as send and receive, broadcast, etc. Communications in MPI programs are expensive; therefore, the number of communications should be optimized in an MPI-based program.

Conventionally for parallel data assimilation, two methods have been used: model decomposition and domain decomposition. Every data assimilation technique has these two steps: “simulation” and “update”. A parallel program could focus on one or both of them. As discussed in Yan et al. (2018) , model decomposition starts from grid

[5] A set of clearly defined subroutines

cell #1, completes the “simulation” and “update” and proceeds to grid cell #2. The update section of this schema is in parallel meaning that ensemble members are distributed between processors. Since the “update” step needs the ensemble members to communicate (for adding noise to the simulations, for example), this schema will be very expensive in modern supercomputers and clusters due to the frequent need to communicate. As discussed in Yan et al. (2018) , model decomposition is more suitable for small watersheds and shared memory programming (for example, using OpenMP).

The domain decomposition schema completes the “simulation”, and then for updating, it distributes the cells between processors and completes the “update” step in parallel. While cells are updated in parallel, one processor handles all the ensemble members of one cell. In other words, different grid cell states can be updated concurrently where each processor only updates the grid cell states which belong to its own. This way, a significant amount of communications between different grid cells is saved (Marc E. Ridler et al., 2014; Yan et al., 2018). As a result, the domain decomposition implementation has attracted more attention in the community and in operation (Gochis et al., 2018).

The overall parallel structure of this study is described in the following steps and a schematic of these steps is presented in Figure 2-2. It should be noted that the parallel algorithm used by Yan et al. (2018) was on the VIC model while in this chapter the focus is on Noah-MP.

(1) The program is initialized and *n* processes for Δt time steps are created. Numbers (ranks) are assigned to processors. The process with rank 0 is called the master process and the rest are called the worker processes; however, there is no difference between rank 0 and the rest. The DA ensemble size is *s*. The total number of cells is *nc*.

(2) Perturbing[6] forcings: Each processor takes responsibility of Δt(i)=Δt/n time steps. It goes over all the assigned time steps, reads the forcing file for this time step, perturbs rainfall and temperature and makes an ensemble with size *n*, and writes the ensemble.

(3) DA starts; t=0

(4) Each worker takes responsibility of *s(i)=s/n* members of the DA ensemble. For the assigned ensemble portion, it runs the model for a time step. The simulations are automatically written by Noah-MP. Then the processes wait until all of them have completed the job. The forcings of the succeeding step are the results of the previous step.

(5) The master processor reads soil moisture (or streamflow, depending on the purpose of DA) from all the simulations and aggregates them. It broadcasts the aggregated data to all the processors.

[6] Add noise

(6) The master processor assigns a block of domain grid cells to each worker. Roughly, each worker will have $\Delta c=nc/n$ cells. It then broadcasts the assignments to every worker.

(7) Each worker (but not the master) updates (based on PF-MCMC or EnKF) the simulations for every cell that it is in charge of (Δc) sequentially. For each grid cell, the "update" routine is initialized where s simulations are compared against the observation at that time and that cell. Then PF-MCMC or EnKF is run.

Every time a worker finishes updating a cell, it will communicate the updated ensemble to the master process.

(8) The master process that has collected all the updated ensemble members will gather all the information, re-order them and broadcast the results for the entire crew.

(9) Each worker becomes in charge of $s(i)=s/n$ DA ensemble members and writes the DA updated states in the restart files so it could be used in the next time step.

(10) The DA is completed for this time step. All the processors go to the next time step and start from step (1).

In this study, Portland State University's Coeus HPC cluster is used. This cluster is comprised of (1) 128 general computing nodes each with 20 cores and 128GB of RAM (medium partition), (2) 12 PHI processor nodes each with 96GB of RAM and 64 cores (3) 2 nodes with high memories each with 768 GB of RAM and 24 cores. All the programs in this study are written in Python3 and for parallel processing, MPI in Python

using package mpi4py (Dalcín et al., 2008, 2005, 2011) is used. A simplified flowchart of the algorithm, presented in Figure 2-2, shows the process of parallel computing in this study.

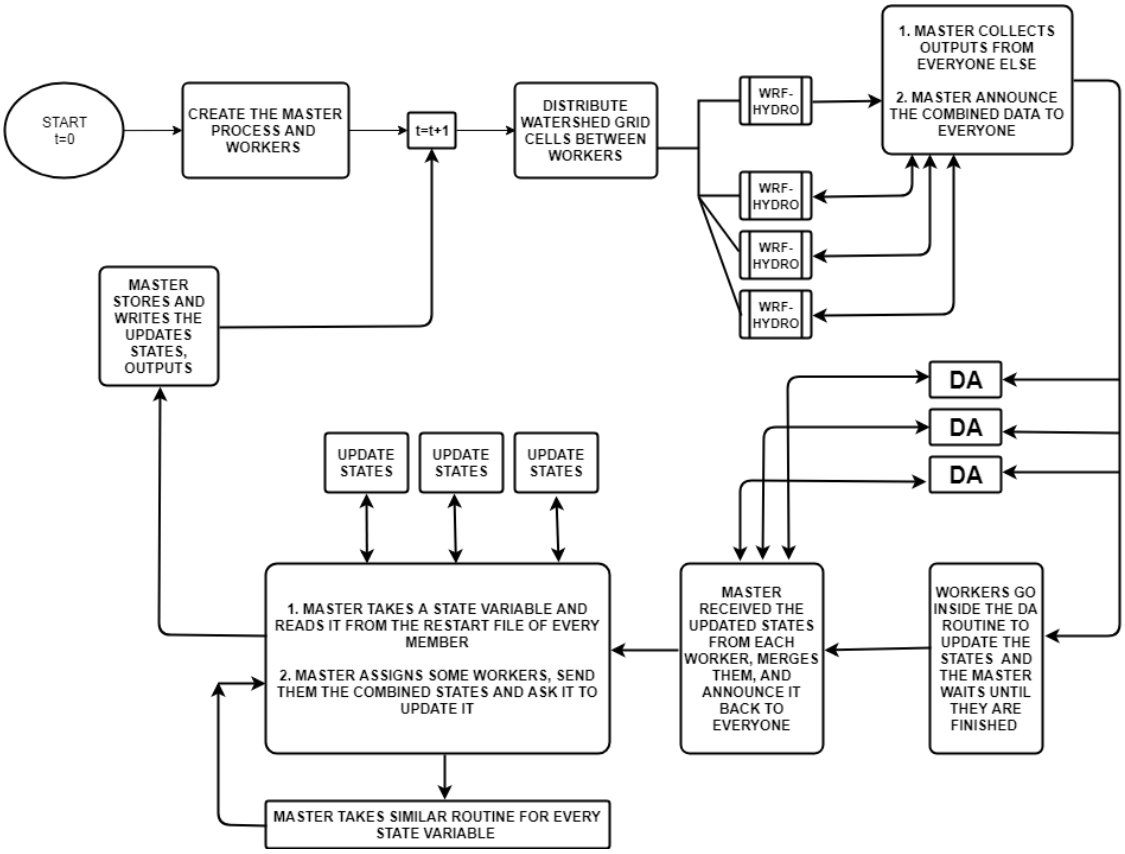

Figure 2-2: Parallel ensemble data assimilation flowchart used in this dissertation

2.6.3 Performance assessment

In this chapter, two commonly used performance measures including Normalized Information Criterion (NIC) and Bias are applied. NIC has been frequently used to measure the improvements by the DA and it is defined as below (Yan et al., 2018, 2017).

$$NIC = (RMSE_{ol} - RMSE_{da})/RMSE_{ol} \tag{11}$$

Where RMSE is defined as

$$RMSE = \sqrt{\sum_{i=1}^{n}(y_{oi} - y_{pi})^{2}\ /N} \tag{12}$$

To assess the performance temporally, Bias, as defined by the following equation, is used.

$$Bias = \sum_{i=1}^{n}|y_{oi} - y_{pi}| \tag{13}$$

In all the equations, y indicates the variable of interest (soil moisture or streamflow in this dissertation), o indicates “observed”, and p indicated “predicted”. N is the length of the dataset.

2.6.4 Characterization of uncertainties

Uncertainties in forcing data (precipitation and temperature) and soil moisture observations are quantified by building a parametric distribution around the expected

value. For precipitation, it is assumed that the data follow a lognormal distribution with mean zero and coefficient of variation of 35%. The added errors to precipitation are heteroscedastic which means that the error is proportional to the rain intensity. However, for temperature, the homoscedastic assumption is used which means the errors are not dependent on the value of temperature. Similarly, for soil moisture observations, a fixed standard deviation of 0.04 m^3/m^3 is considered. Model structure uncertainty is also represented through perturbing simulated soil moisture simulations, which assumes a coefficient of variation of 10%.

2.7 Model setup and pre-processing

In this section, the primary steps before running the Noah-MP model are explained. First, re-gridding the forcing files are explained and then selected variables in the domain files are shown and discussed.

The model is run with a spatial resolution of 1 (km) and temporal resolution of 1 hour for the period of 1 January 2013 to 1 October 2013 over the Colorado Front Range area.

2.7.1 Re-gridding the forcing inputs

For preprocessing and running the model, WRF-Hydro (Weather Research and Forecast-Hydrological Processing) (Gochis et al., 2018) is employed. WRF-Hydro V3 is a land surface model that uses Noah-MP as the core column land surface model combined with surface, sub-surface, and channel routing modules. In all model runs of

this chapter, the routing and groundwater modules were turned off. Forcing inputs are re-gridded and prepared by WRF-Hydro's available pre-processing scripts at (https://ral.ucar.edu/projects/wrf_hydro/regridding-scripts). These scripts are available for multiple datasets. Given that NLDAS data are utilized in this study, NLDAS re-gridding script that is written in NCAR Command Language (NCL) is downloaded and used. Forcing variables include incoming shortwave radiation (W/m^2), incoming longwave radiation (W/m^2), specific humidity (kg/kg), air temperature (K), surface pressure (Pa), the horizontal component of wind speed (m/s), the vertical component of wind speed (m/s), and liquid water precipitation rate (mm/s) are downloaded from NLDAS-2 database. Two of these input variables, rainfall and temperature, are presented in Figure 2-3. In this figure, temperature and rainfall are mapped over the study area, the Colorado Front Range. As mentioned in 2.4.3, both variables are obtained from the North American Land Data Assimilation dataset.

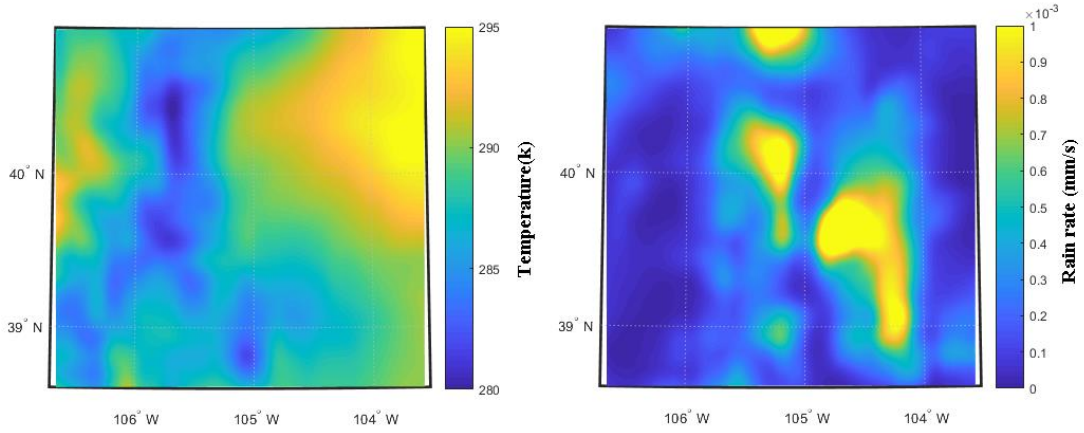

Figure 2-3: Temperature and rainfall inputs obtained from the NLDAS dataset and mapped over the study area. Both datasets are mapped for September 12, 2018 12:00 PM.

2.7.2 Domain files

Domain input files were acquired from the example case study provided along with WRF-Hydro V3. These files include terrain (such as elevation) and vegetation (such as monthly green fraction) information. Two select variables including elevation and monthly green fraction are presented in the following. The elevation map of the study area is shown in Figure 2-4 and monthly green fraction is for January (top left panel) to December (bottom right panel) is mapped in Figure 2-5. It is worth noting that the monthly green fraction data are generated by the WRF preprocessing tool that is available through NCAR website (https://ral.ucar.edu/projects/wrf_hydro/overview)

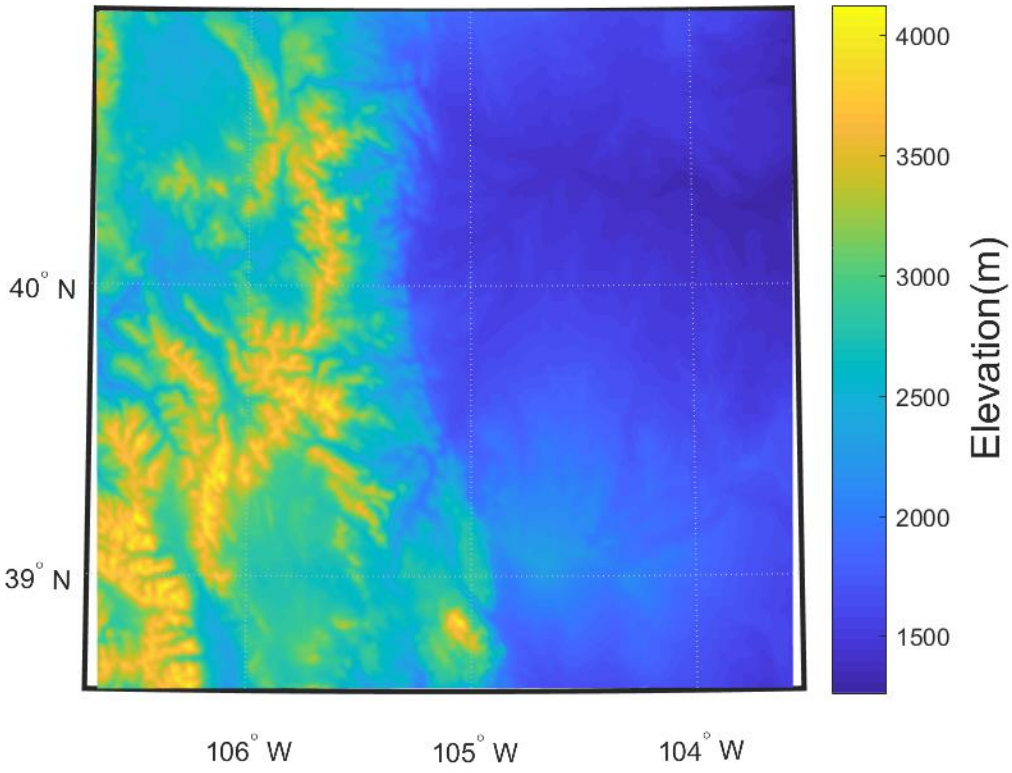

Figure 2-4: Height (m) as used in the domain file to run the Noah-MP model.

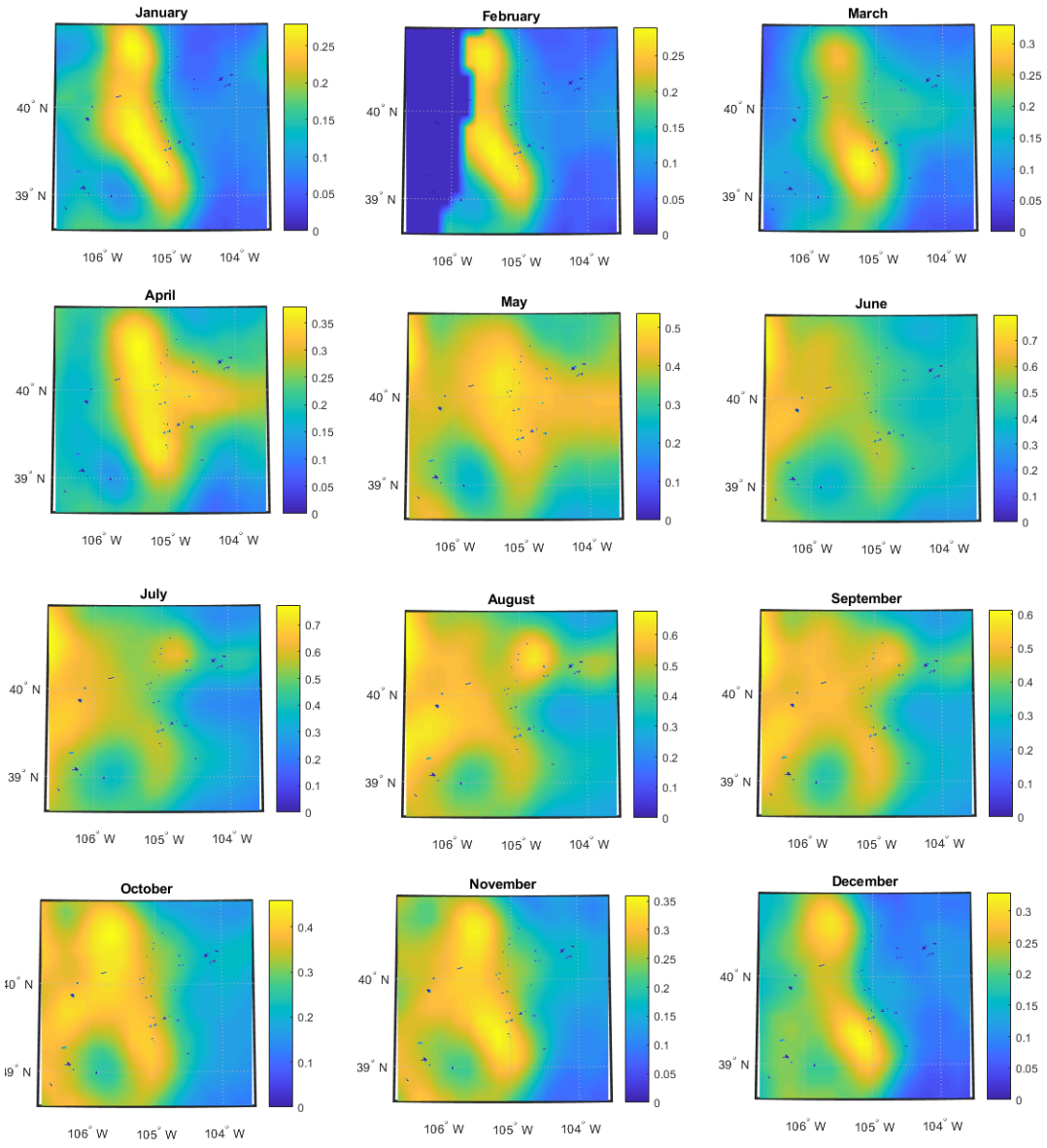

Figure 2-5: Monthly green fraction fields used as input in the Noah-MP domain file. Data are obtained from the WRF pre-processing tool.

As mentioned, Noah-MP introduced multi-parameterization to land surface modeling. Different options are provided for a single process. For example, four options are provided for calculating runoff. The options that were chosen in this study are listed in Table 2-1.

Table 2-1: Noah-MP parameterization options and the selected schemes used in this study

***Parameterization* option**	**Description**	**Chosen option**
DYNAMIC_VEG_OPTION	*Dynamic vegetation*	Table LAI
CANOPY_STOMATAL_RESISTANCE_OPTION	*Canopy stomatal resistance*	Ball-Berry
BTR_OPTION	*Soil moisture factor controlling stomatal Resistance*	Noah
RUNOFF_OPTION	*Runoff and groundwater*	Schaake96
SURFACE_DRAG_OPTION	*Surface exchange coefficient for heat*	1: M-O (Brutsaert, 1982)
SUPERCOOLED_WATER_OPTION	*Supercooled liquid water in frozen soil*	NY06
RADIATIVE_TRANSFER_OPTION	*Radiation transfer*	Gap=1-Fveg
SNOW_ALBEDO_OPTION	*Snow surface albedo*	CLASS
PCP_PARTITION_OPTION	*Partitioning precipitation into rainfall and snowfall*	Jordan91
TBOT_OPTION	*The lower boundary condition of soil temperature*	Noah
TEMP_TIME_SCHEME_OPTION	*The first-layer snow or soil temperature time schema*	Semi-implicit

2.8 Results

2.8.1 Example: A simple model run results

In this section, the results of a simple model run are provided as an example. In this model run, no data assimilation is conducted. The period of interest is September 2013 and the area of interest is the Colorado Front Range. The resulting variables include (but are not limited to) surface soil moisture, root-zone soil moisture, runoff, and evapotranspiration. In the following figures, sample output variables including runoff and soil moisture are mapped. Runoff is shown in Figure 2-6 . A cluster of high values is observed in the center of the domain. The yellow parts are where urbanized areas are located. Loveland is located in mid-north, Boulder is located in the center of the domain, and Denver is located in the mid-south of the domain. As expected, model simulations show high runoff values in urbanized areas that could be assigned to low infiltration rate which does not allow the water to penetrate to the ground. Soil moisture is mapped in Figure 2-7:. In this figure, spatial variations of soil moisture at different soil layers (on 9/12/2018 when the flood reached the peak) are demonstrated. The cluster of low soil moisture values in the upper right of the domain is attributed to the soil type in that area. The soil in that area is mostly comprised of sand which drains very fast and justifies low soil moisture values. The temporal variation of area-averaged soil moisture is shown in Figure 2-8: Noah-MP example run results without data assimilation. It is noticed that soil moisture peak occurs near the rainfall peak which was reported (Gochis et al., 2015) to be on September 12th. It is noted that the simulated peak of soil moisture happens later than

the reported peak of rainfall. This is explained by the runoff generation mechanisms during this event. The rainfall peak was in the night of 11-12 and due to "infiltration excess[7]" runoff generation, water was ponded before penetrating to the ground. Therefore, soil moisture peak is expected to happen later than rainfall peak. Infiltration excess runoff generation during 11-12th September is also confirmed by Gochis et al. (2015). While this would be an approximate validation of the simulations, detailed validation of the model results is out of the scope of this study and other studies (cited in section 2.5) have addressed such evaluations.

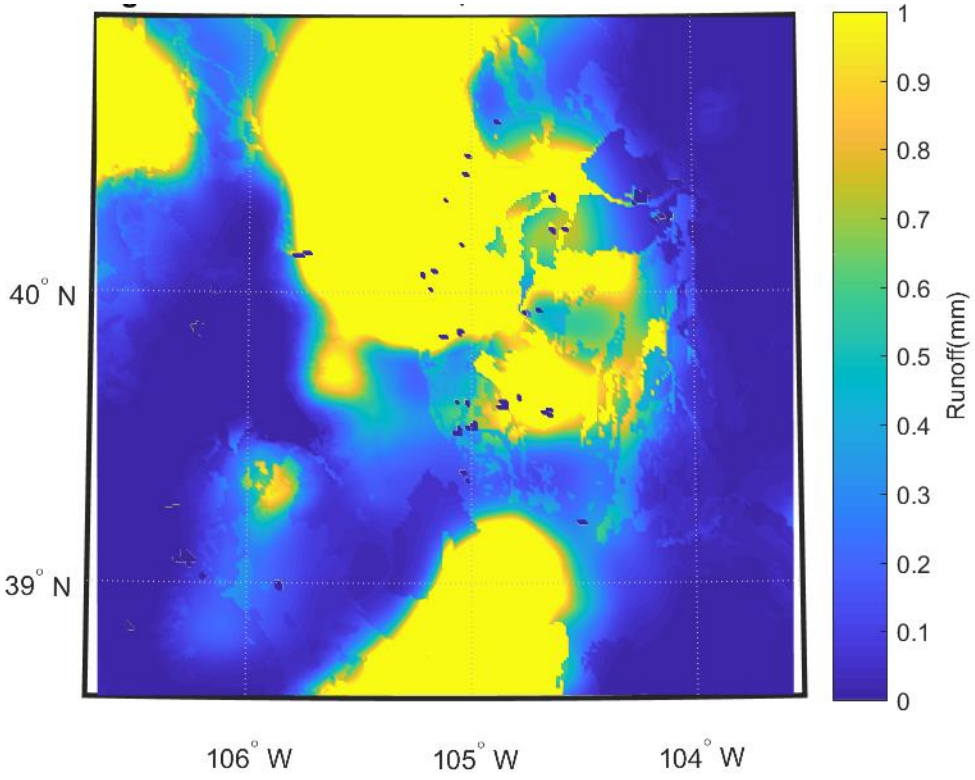

[7] When rainfall rate exceeds infiltration rate

Figure 2-6: Noah-MP example run results without data assimilation. Spatial variation of simulated runoff on Sep 12, 2013, when rainfall was at the peak. The yellow parts indicate where the water is ponded due to infiltration excess over the urbanized areas

The observed volumetric soil moisture peak according to Gochis et al. (2015) in Mountain Research Laboratory is around 0.45 (m^3/m^3) while the peak of soil moisture simulations is around 0.33 (m^3/m^3). This is attributed to ignoring the groundwater effects in this chapter due to the long spin-up period needed by the groundwater modules.

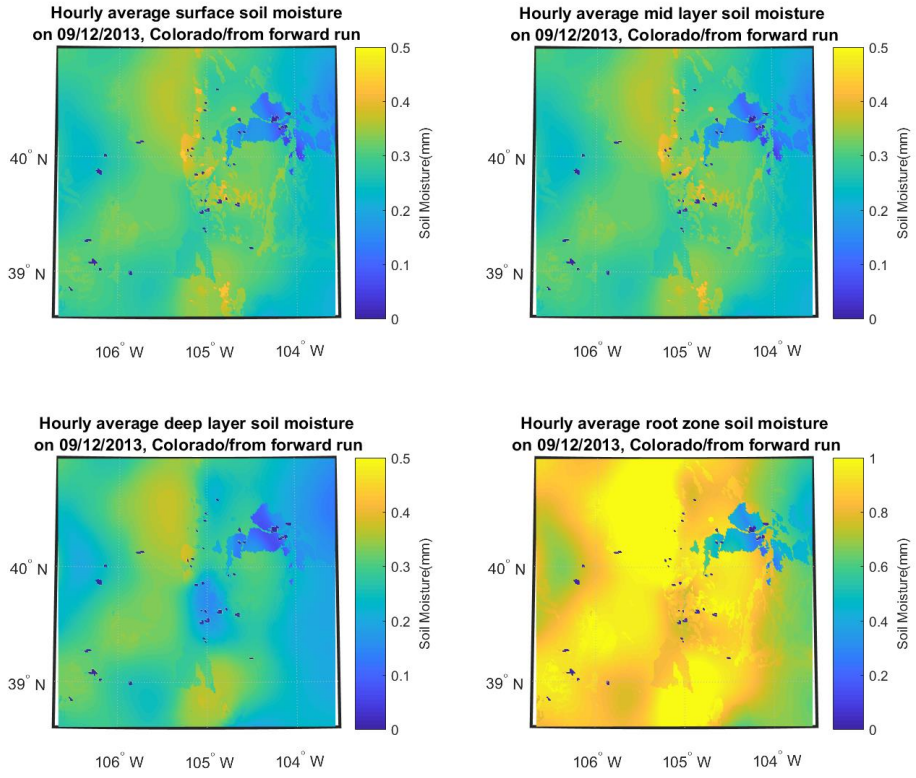

Figure 2-7: Noah-MP example run results without data assimilation. Spatial variation of simulated soil moisture. The top layer (upper left) is 10 cm, the second layer (top right) is 30 cm, the third layer (bottom left) is 60 cm, and the deep layer (bottom right) layer is 100 cm.

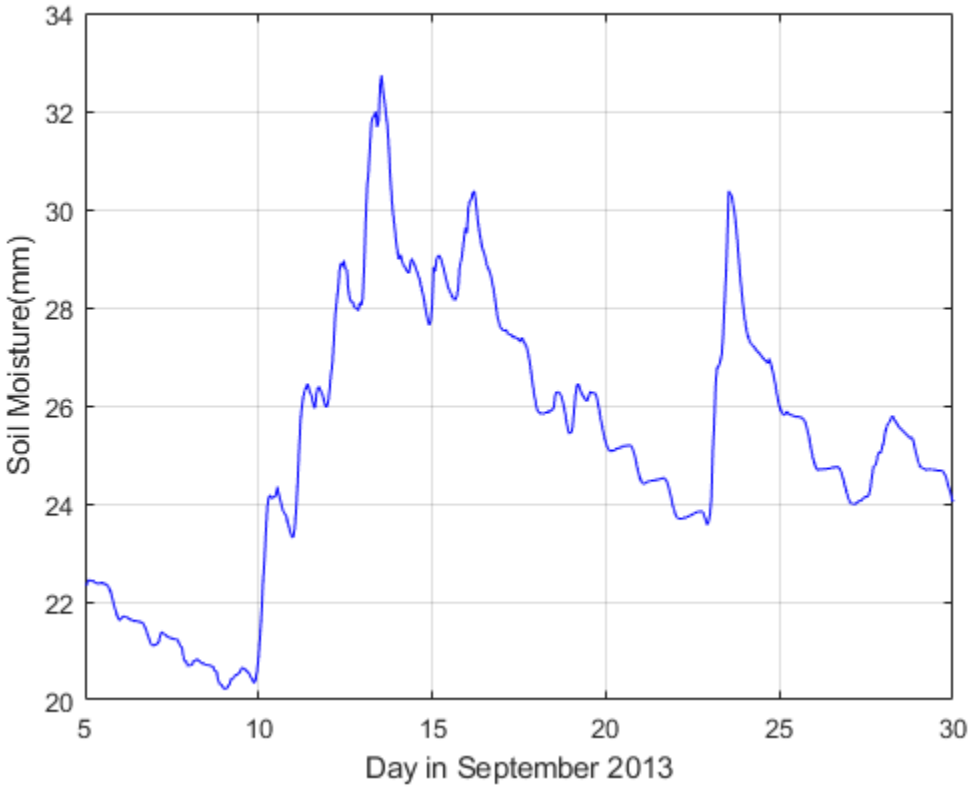

Figure 2-8: Noah-MP example run results without data assimilation. Temporal variation of soil moisture, averaged over the area, converted to mm in September 2013.

2.8.2 Synthetic Study

Synthetic experiments are beneficial in DA studies (Moradkhani, 2008). The steps of building a synthetic study, also known as Observing System Simulation Experiment (OSSE) is illustrated in (Moradkhani, 2008). Unlike real-world DA studies, in a synthetic

study, the true soil moisture is known. This makes the comparisons easier. The synthetic experiment is developed according to the following steps:

(1) Generate truth: the model is run and the simulated soil moisture is considered "truth" (as shown in Figure 2-9).

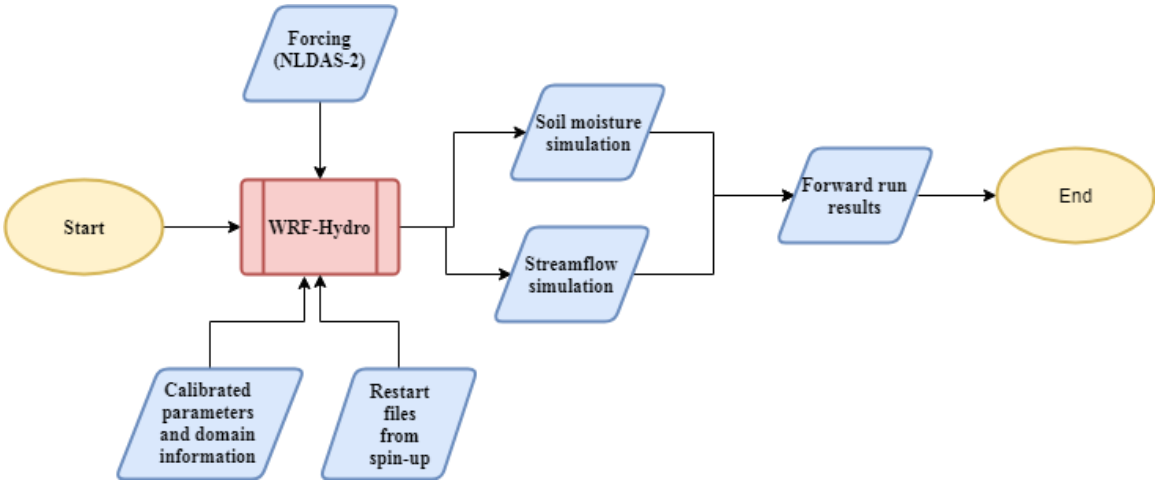

Figure 2-9: Steps of creating true soil moisture in the synthetic study. Noah-MP is run through WRF-Hydro.

(2) Generate synthetic satellite soil moisture: Observational error is incorporated into the true soil moisture from the previous step and is considered as the synthetic satellite observation. Similar to previous studies (Kumar et al., 2014; Yan et al., 2017, 2018), the white noise for CCI satellite soil moisture is set to 0.04 m^3/m^3.

(3) The OL run: Noah-MP is rerun for the period of interest with perturbed forcing which is called the open loop (OL) run. Perturbation is referred to adding noise to a variable.

(4) The DA run: Noah-MP is run for the same period but with the assimilation of synthetic satellite observations (DA) as depicted in Figure 2-10. To account for the uncertainty in forcing, additive errors with mean zero and standard deviation of 3˚C are added to air temperature. Precipitation is perturbed using a lognormal distribution with a coefficient of variation of 0.35. OL and DA runs share similar errors, initial states, and ensemble size (50 members) and all errors are assumed uncorrelated. The DA run uses PF-MCMC and incorporates synthetic satellite soil moisture obtained from step 2.

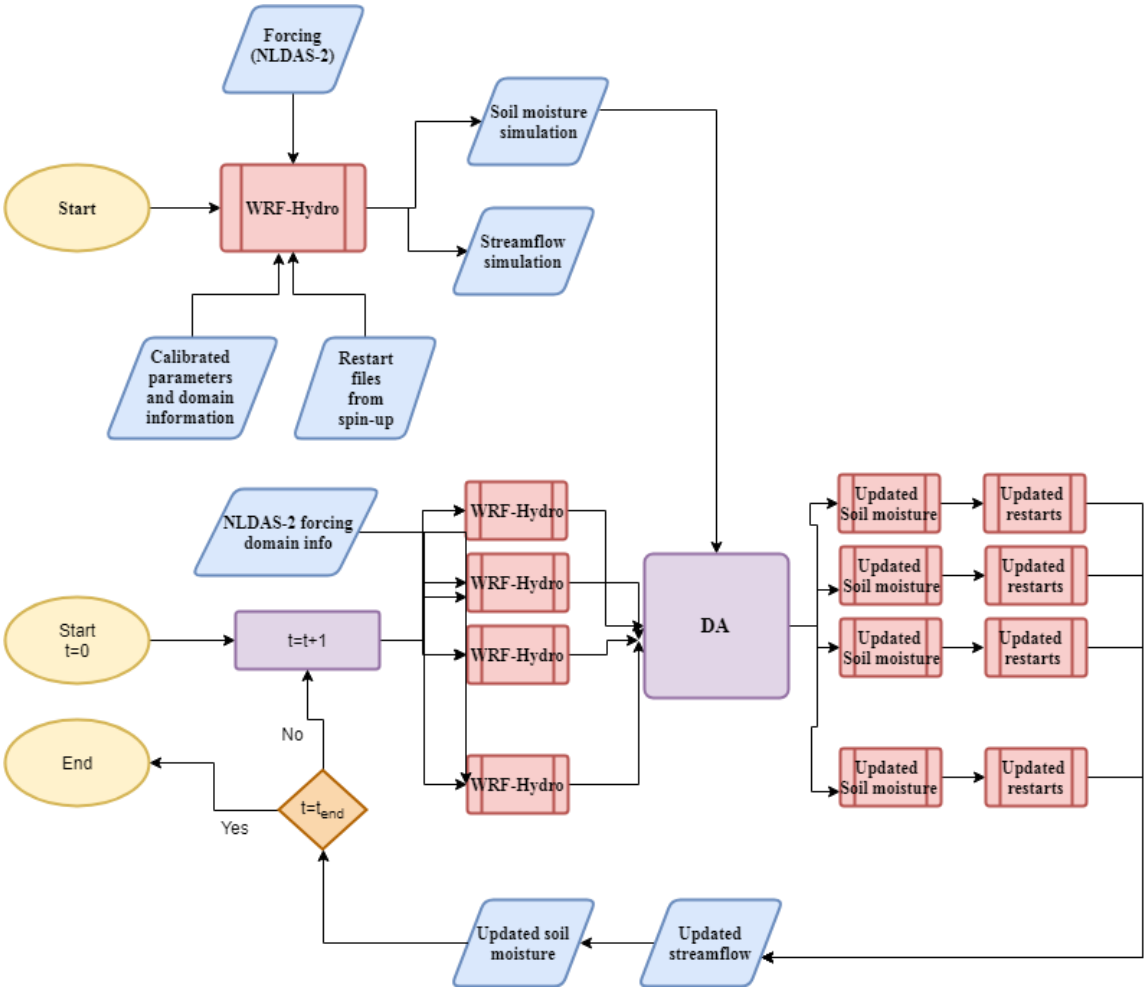

Figure 2-10: A schematic of synthetic soil moisture assimilation. The upper part shows the generation of the synthetic soil moisture data and the lower part is associated with assimilating the synthetic data. Noah-MP and WRF-Hydro are interchangeable in this figure.

The results of the synthetic study are presented in the following. First, the open loop run with no data assimilation that accounts for the uncertainty of rainfall and temperature are presented in Figure 2-11. In this figure, the open loop run is an ensemble of model runs. The ensemble is created by perturbing the forcing data. Precipitation and temperature are perturbed for this OL run. The 50% predictive intervals are shown with dashed lines. The uncertainty of soil moisture simulations originated from forcing uncertainties is of interested.

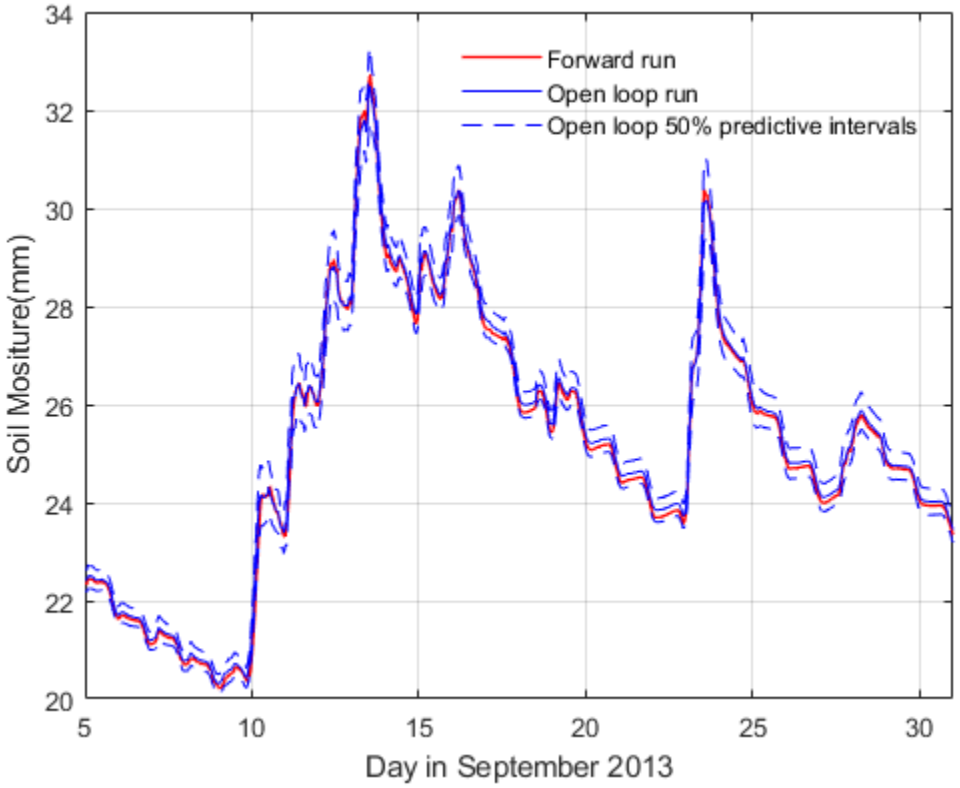

Figure 2-11: Synthetic experiment results. Surface soil moisture simulations from the forward run (red line) and the open loop run (blue lines). The open loop run is an ensemble of model runs with perturbed forcings. The 50% predictive intervals are shown with dashed lines

Then, the DA analysis was conducted. In DA, the synthetic soil moisture observations that are derived from the model forward run are assimilated into the model at an hourly step for 9/1/2013-9/31/2013. In the data assimilation, surface soil moisture is assimilated and only surface soil moisture is updated; however, updating soil moisture in other layers could be easily done as shown by Yan et al. (2015; 2017; 2018). Two methods are used for DA: EnKF and PF. Similar observations are used for both methods. The errors and the perturbations are also similar. The results of both DA methods and the OL run are then compared against the true soil moisture. Bias is then calculated as the absolute difference between the simulated soil moisture and true soil moisture. Biases are compared in Figure 2-12. In this figure, the temporal variation of hourly biases during the assimilation time is shown. It is observed that the open loop shows the higher bias than both DA methods. Between the two DA methods, PFMCMC is performing better than EnKF. It is noted that PF-MCMC shows higher bias at the beginning of the DA run. This is attributed to the spin-up period for the PF needs. It is also observed that around the peak of soil moisture, EnKF and OL biases are high while PF biases are lower. This is an indication of the effectiveness of PF-MCMC in simulating extremes.

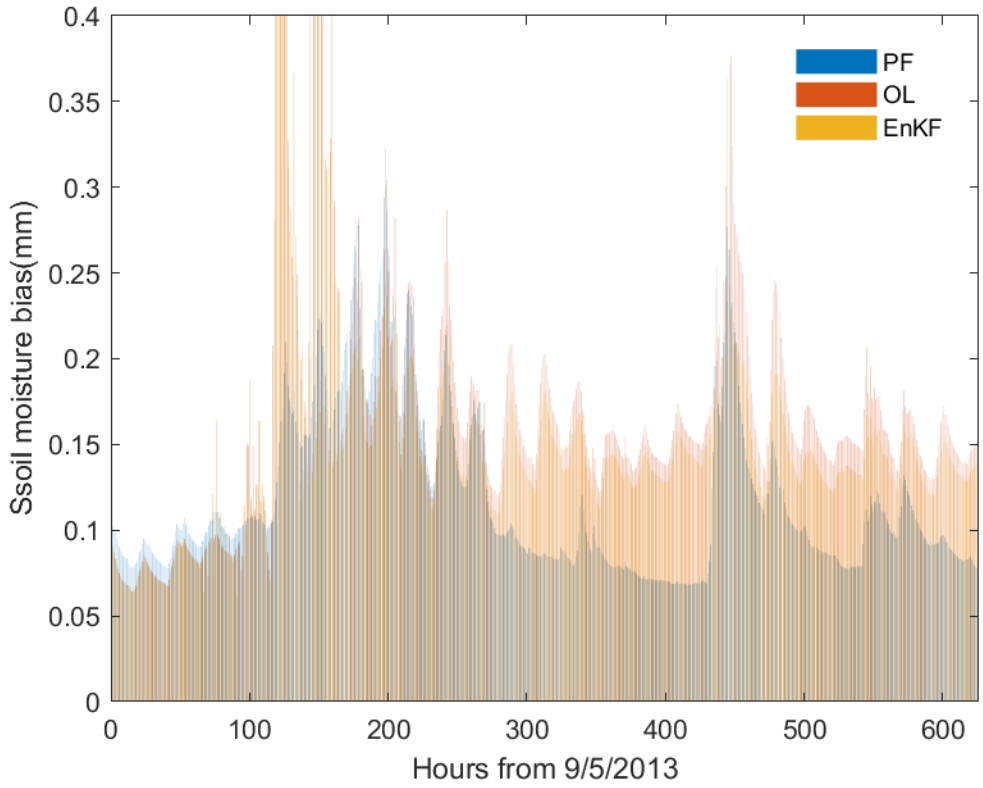

Figure 2-12: Synthetic experiment results. Temporal variation of bias from the PF-MCMC, the EnKF, and the OL runs. In PF and EnKF, similar observations are assimilated. Biases are averaged over the area. The simulation starts on 9/5/2013.

The average biases of all three runs over the area and over September are compared in the bar chart of Figure 2-13. On average, PF-MCMC shows the lowest bias followed by the EnKF and the OL. OL, with an average bias of 0.17 (mm), demonstrates the highest average bias. Both DA techniques have lower biases than the OL run which highlight the added value of ensemble data assimilation. The spatial variation of biases is presented in Figure 2-14 for 9/12/2013 when the Colorado Front Range flood reached its peak. A cluster of high biases in OL are identified in the urbanized Loveland area located

in the mid-north of the basin. EnKF also shows high (but still lower than OL) bias in that area.

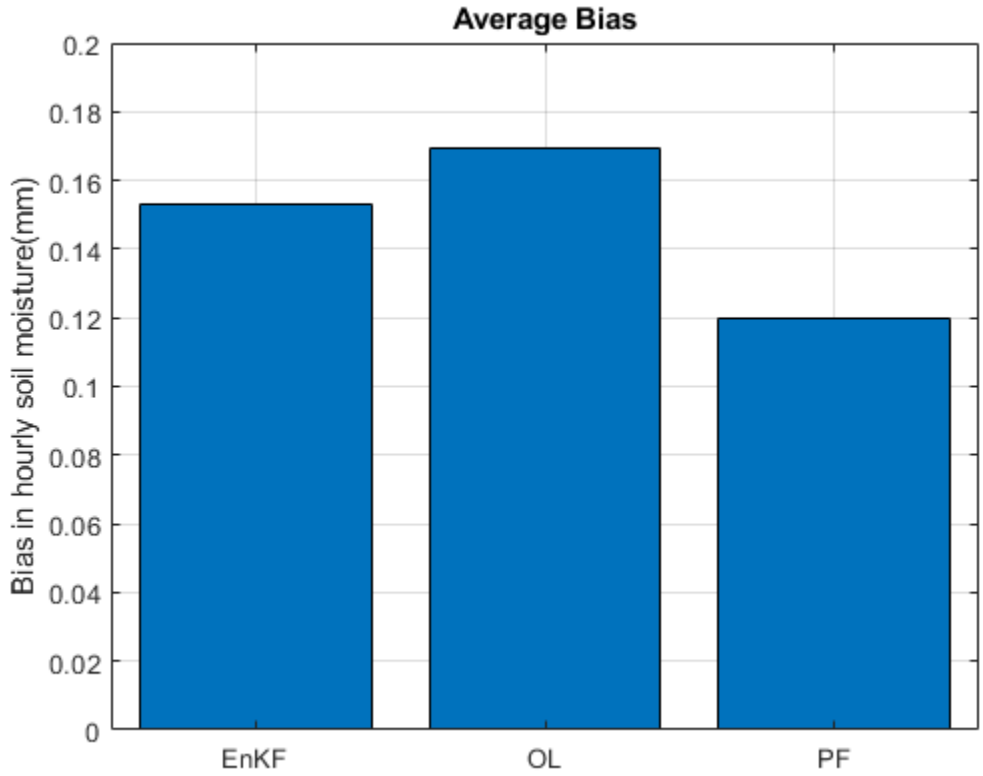

Figure 2-13: Synthetic experiment results. Comparison of average biases in the (from left to right) EnKF, the OL, and the PF runs. Biases are spatiotemporally averaged over the domain and over the simulation period (September 2013).

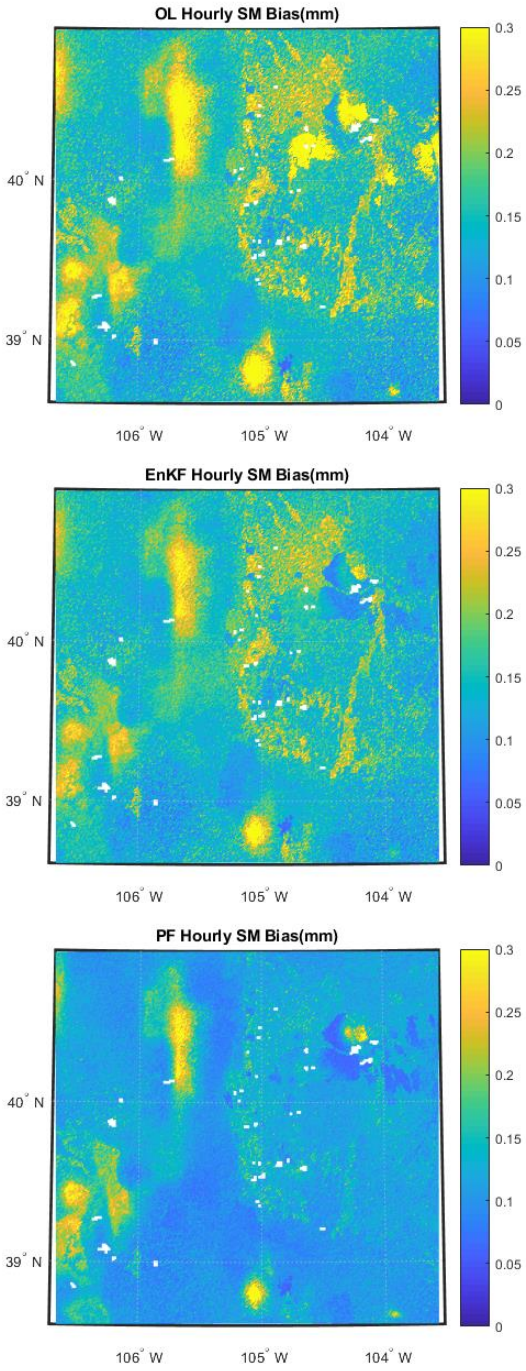

Figure 2-14: Synthetic experiment results. Spatial variation of biases in the OL (top panel), the OL (middle panel), and the EnKF (bottom panel). Biases are calculated on 9/12/203, at the peak of the rainfall.

Besides bias, the NIC is used to measure improvements of DA against OL. Positive values of NIC indicate improvements and negative values indicate degradation. Figure 2-15 shows the spatial distribution of the NICs of both methods. The left panel shows the improvements made by EnKF and the right panel shows the improvements made by PF-MCMC. In more than 88% of the area, the PF is improving the performance of Noah-MP in simulating soil moisture. These improvements reach up to 50% in the northern part of the domain. On the other hand, EnKF shows improvements in more than 98% of the domain (positive NICs are observed in 98% of the area). These improvements are as high as 15%, on average. It is noted that the NIC values of PF-MCMC are higher than the NIC values of the EnKF. This indicates that higher improvements are achieved by PF-MCMC than the EnKF. This superiority of PF-MCMC to the EnKF is also proved in Figure 2-16. In this figure, the RMSEs of PF-MCMC and EnKF are compared through NIC. The NIC in his figure shows the improvements by PF-MCMC than the EnKF. Positive values indicate the superiority of PF-MCMC and negative values indicates that PF-MCMC performs worse than EnKF. The NIC is positive in 80% of the area. This means that in the majority of the domain, the PF-MCMC has a better performance than the EnKF.

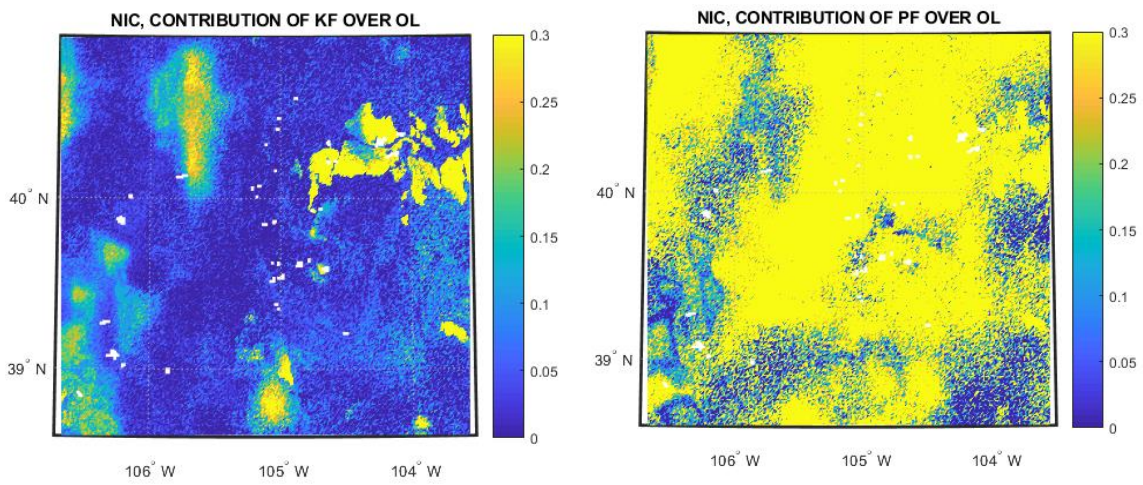

Figure 2-15: Synthetic study results. The degree of improvements achieved by DA. EnKF improvements are mapped on the left and the PF improvements are mapped on the right. The improvements are quantified through Normalized Information Contribution.

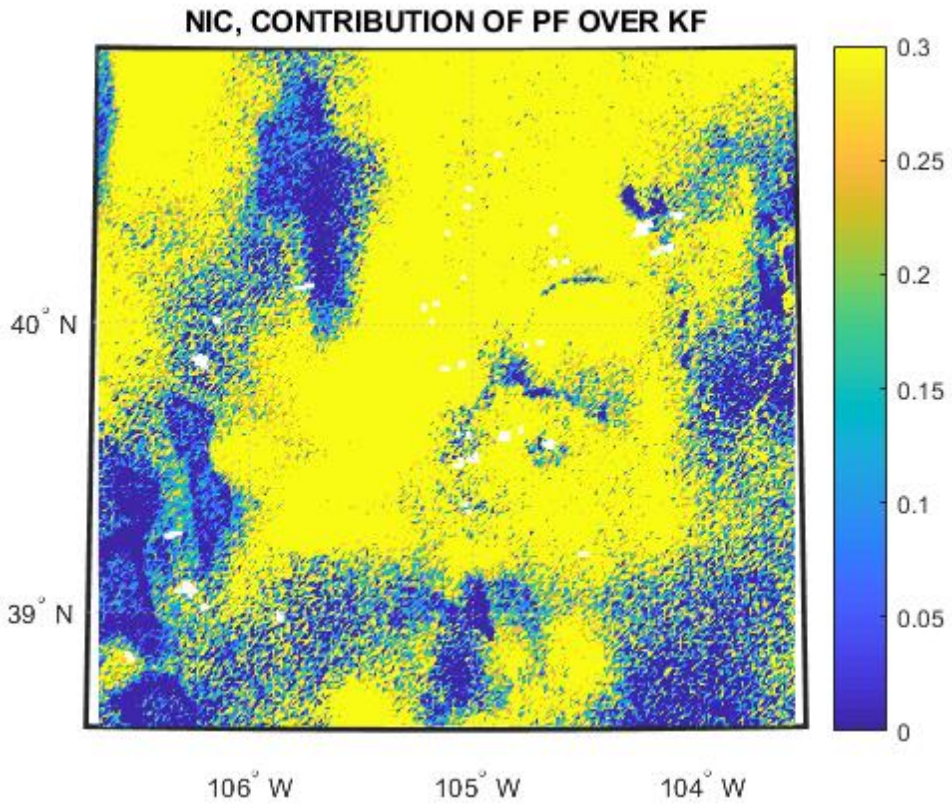

Figure 2-16: Synthetic study results. Comparison of EnKF and PF performances. The performance is quantified by Normalized Information Contribution. Higher positive values indicate the superiority of PF over EnKF and negative values indicate the superiority of EnKF.

2.8.3 Real Study

After demonstrating the added value of the methodology through synthetic experiments, a real experiment was conducted. In this experiment, real satellite data are assimilated to simulate the flood of September 2013 in Colorado. CCI data were used because, at the time this flood event happened, SMAP had not been launched. In this section, the results of the real study are presented. Before DA, one needs to perform a

rescaling step in order to make the climatology of model and observations match. This is called a re-scaling step. For rescaling, CDF-matching approach which is very common in hydrology is used (Yan et al., 2018). The spatial distribution of observed soil moisture after rescaling is presented in. The cluster of low soil moisture values is also observed in the rescaled satellite soil moisture maps, as shown in this figure. This map is comparable with model simulations presented in the background map of Figure 2-17.

Similar to the synthetic study, the real study was conducted for September 2013. Two DA techniques, EnKF and the PF-MCMC, were used. For both DAs, rescaled CCI satellite observations were assimilated into the Noah-MP model. To evaluate the performance of the DAs, the results are compared with gauge soil moisture observations throughout the domain. Gauges is shown as points in Figure 2-17. The numbers assigned to stations are the numbers used in this study.

The performances of both DAs are quantified by NIC as shown in Figure 2-18. The upper panel shows the performance of EnKF for all the gages. Positive values show improvements by the DA and the higher NICs confirm higher improvements. Out of 27 gauges, the EnKF improves soil moisture simulations in 17 gauges. These improvements are as high as 20% at the 26^{th} station. The PF-MCM, on the other hand, improves soil moisture simulations in 19 gauges and the improvements are as high as 30%. This shows that both DA techniques are capable of improving soil moisture simulations over the study area.

This NIC values of PF are generally higher than the NIC values of PF-MCMC which confirms the effectiveness of the PF-MCMC that the EnKF. The superiority of PF-MCMC to the EnKF is also depicted in figure 2-19. In this figure, the improvement of PF-MCMC to the EnKF is shown. Out of 29 gauges, the PF-MCMC is performing better than the EnKF. The PF-MCMC improves the EnKF simulations by up to 15% at the 24th station.

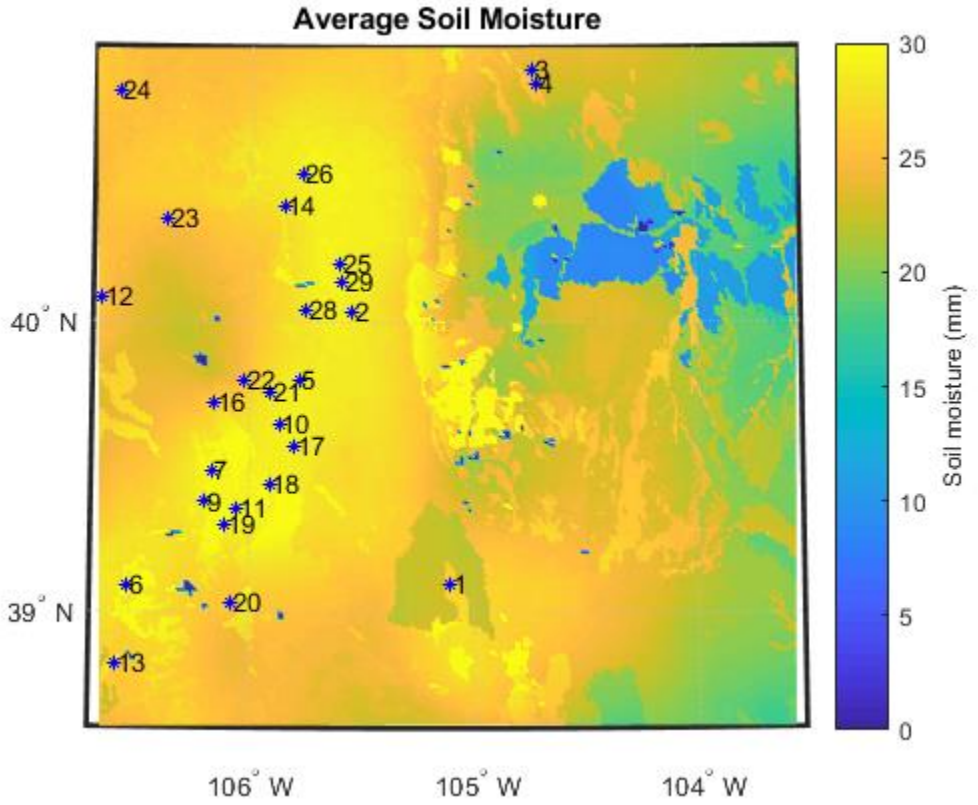

Figure 2-17: Background: Rescaled CCI satellite soil moisture in Colorado Front Range averaged over all hours in September 2013 over the study area. Points: Location of in-situ soil moisture gauges. Stations are labeled with the numbers assigned to stations for the analyses of this chapter.

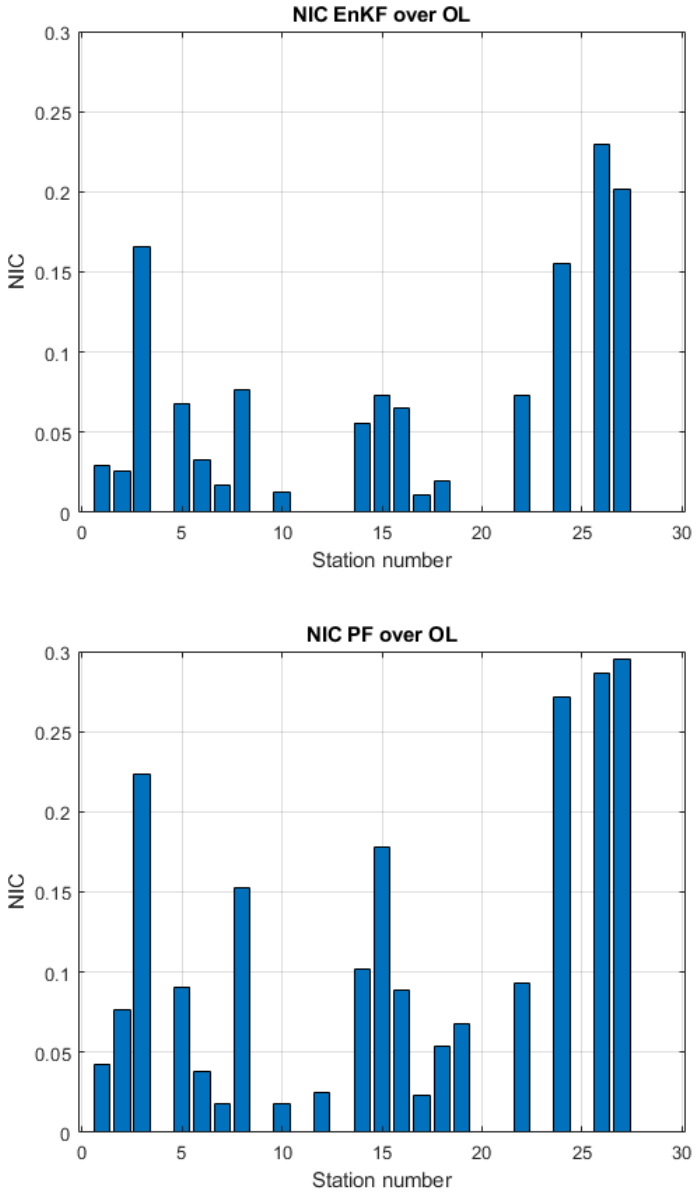

Figure 2-18: Real experiment results. Performance evaluation of EnKF (the top panel) and the PF-MCMC (the bottom panel). Performance is quantified by NIC. Positive values show improvements made by DA. Higher values of NIC are associated with higher improvements. The x-axis shows the station number.

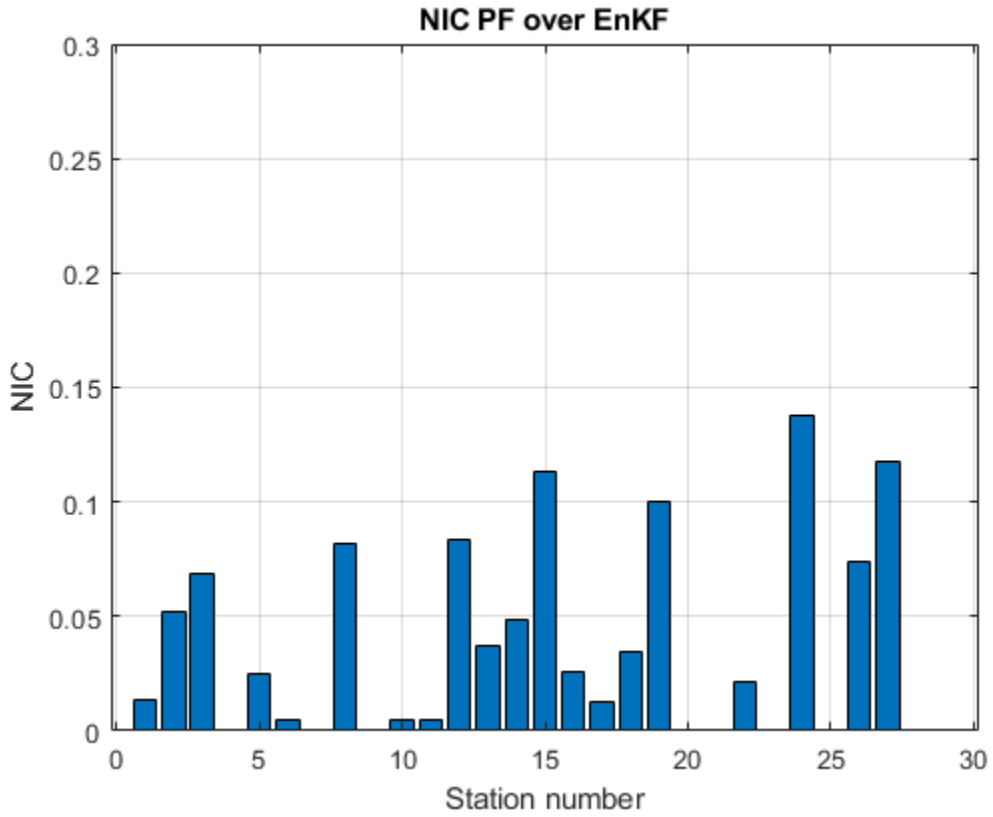

Figure 2-19: Real experiment results. Performance evaluation of PF-MCMC over the EnKF. Performance is quantified by NIC. Positive values show improvements made by PF-MCMC. Higher values of NIC are associated with higher skills of PF-MCMC to EnKF. The x-axis shows the station number.

2.9 Summary

Noah-MP is the core column land surface model in the National Water Model that has been run operationally by the National Water Center since 2016. Noah-MP is a rather new LSM and it has attracted attention because it has been coupled with atmospheric models and its inclusion into the NLDAS project has been considered. The Noah-MP model requires atmospheric variables such as rainfall and temperature as forcing inputs and the resulting outputs include runoff, evapotranspiration and soil moisture simulations. Soil moisture, in this study, is of particular interest because it is a critical variable in forecasting atmospheric variables. Additionally, it is an integral part of drought and flood prediction. Besides using a land surface model (such as Noah-MP) to simulate soil moisture, one could use satellite or gauge observations to measure soil moisture. Instead of using either observations or models, research has suggested using both. Combination of these two is possible through data assimilation techniques. Numerous data assimilation techniques have been introduced in the mathematics, atmospheric and hydrologic communities. All these techniques are comprised of two steps: estimations and update. In the estimation step, a dynamic model is run and the resulting variable of interest is compared against observations. Next, in the update step, model simulations and observations of that variable are combined and then the model is updated accordingly. Two frequently used DA techniques in hydrology are the Ensemble Kalman Filter (EnKF) and the Particle Filter (PF). Assimilation of soil moisture observations into a land surface model has been studied frequently; however, limited research has been conducted

to study the performance of DA techniques on the Noah-MP model. Successful implementation of data assimilation on this model needs to be demonstrated. Therefore, this study aims at assessing the performance of DA techniques on Noah-MP. This study presents successful implementations of EnKF and PF on Noah-MP. It was shown that the performance of Noah-MP in simulating soil moisture is further improved by DA. Moreover, comparison of two commonly used DA techniques is performed in this study and it was concluded that, in the area of interest, the PF shows a higher skill in simulating soil moisture than the EnKF. Additionally, this study proposed an algorithm for implementing any ensemble data assimilation method on the Noah-MP model. This algorithm is designed to reduce the computational time in data assimilation by using as many computational resources as possible. This algorithm is designed for supercomputers and clusters of multiple computer nodes. The results of this study are beneficial for any future research on the assimilation of observations into the Noah-MP model, for improving the current flood forecasting skills and for improving weather prediction skills. The NCEP and the NWC could particularly benefit from the results of this study for operational forecasting purposes.

2.10 Conclusion, discussion, and future work

The main highlights of this study are as follows:

(1) Assessing the performance of DA techniques on the Noah-MP model. Successful implementations of two data assimilation techniques including the Ensemble Kalman Filter and the Particle Filter Markov Chain Monte Carlo were demonstrated in this study. This could guide future implementation of DA on Noah-MP regarding estimations of errors, perturbation of forcing inputs/soil moisture simulations/ soil moisture observations, and efficiently implementing any DA through parallel computing.

Additionally, climate modelers could benefit from the results of this chapter for more accurate weather predictions resulted from a more accurate representation of soil moisture. More accurate soil moisture provides a better initial condition for climate models like WRF. The importance of improved initial conditions is also highlighted by Walker and Houser (2001). Moreover, a better representation of soil moisture provides flood forecasting models with a more accurate initial condition which ,in turn, results in more effective forecasts. This will help improve real-time flood forecasting systems such as the NWM for which Noah-MP is the core LSM.

(2) Performances of two data assimilation techniques were compared in this study and it was shown that the PF-based DA method had a higher skill in improving soil moisture simulations. Previous research on such comparisons was conducted on hydrologic models such as the VIC model and the HyMod model and this study complements them by conducting such analysis on the Noah-MP land surface model.

(3) This study proposed a parallel algorithm for ensemble data assimilation of satellite soil moisture into the Noah-MP model. This algorithm aims at decreasing the computational time by simultaneously using multiple computational nodes. The algorithm is suitable for high-performance-computing infrastructure such as supercomputers and clusters of individual CPUs. This algorithm could be used in future research on Noah-MP for assimilation of any kind of observations. Successful implementation of this algorithm was demonstrated for simulating soil moisture during a significant flood in the Colorado Front Range.

For future extensions of this study, the spatial dependence of adjacent cells could be considered. The DA is implemented on cells separately (cells are independent of each other) in this chapter. A future extension of this work can consider preserving the spatial variation of model simulations and transferring information from the assimilation of one cell to another. Also, the introduced parallel data assimilation and the error settings in this work could be used for assimilation of vegetation-related observations.

Another extension of this study could conduct similar experiments on more watersheds with various characteristics (such as low flows, high flows, and droughts) with longer durations to further support the results of this study.

3 A Multivariate Ensemble data assimilation in the WRF-Hydro: Potential DA integration to the National Water Model

3.1 Abstract

Performance of the ensemble data assimilation techniques on the community WRF-Hydro model is evaluated in this chapter. WRF-Hydro is a distributed land surface model that integrates column land surface models with the surface, subsurface, and channel routing modules. Three scenarios are defined here. First, satellite soil moisture observations are assimilated into WRF-Hydro using a univariate Ensemble Kalman Filter technique. The results of this scenario indicate that the DA improved WRF-Hydro's skill in simulating soil moisture; however, it is found that the soil moisture assimilation information is not significantly informing the outlet streamflow. Next, streamflow observations at USGS gauges are assimilated into WRF-Hydro using an Ensemble Kalman Filter algorithm. Significant improvements in streamflow simulation skill are observed; however, the model is not able to propagate the streamflow information to soil moisture. Finally, joint assimilation of soil moisture and streamflow is implemented using a multivariate EnKF and considerable improvements in both variables are achieved. The methodology could guide future research on WRF-Hydro and flood forecasting. Operational agencies such as the National Water Center, Offices of Water Prediction, and River Forecast Centers could also benefit from the outcomes of this chapter for flood modeling and forecasting.

3.2 Highlights

(1) Separate assimilations of satellite soil moisture and streamflow observations into the community WRF-Hydro model that uses Massage Passing Interface protocols are demonstrated.

(2) The ability of WRF-Hydro in transferring the assimilation information to other hydrologic variables is investigated.

(3) Improved soil moisture and streamflow simulations are achieved by employing a multivariate Ensemble Kalman Filter technique that simultaneously assimilates soil moisture and streamflow observations.

3.3 Introduction

WRF-Hydro is a hydrologic model recently developed by the National Center for Atmospheric Research (NCAR) (Gochis et al., 2015; 2018). It has been adopted by the National Weather Service (NWS), the National Water Center (NWC) and Office of Water Predictions (OWP). The model is the midst of its operational transition to River Forecast Centers (RFC). WRF-Hydro is a combination of modules for land processes. For many processes multiple options are available for the user to choose from. For example, for the core column land surface model, the user can choose the Variable Infiltration Capacity (VIC) model, the Noah LSM, The National Aeronautics and Space Administration (NASA)'s Land Information System (LIS), Community Land Model (CLM), or Noah-MP (Noah with multi parameterization option). The output variables of

the column land surface model are passed to hydrologic routing modules including the surface and subsurface routings. The results of the routing are first passed back to the column land surface model and then passed to a channel routing model. For channel routing, the user can choose between commonly used methods of Muskingum-Cunge, Muskingum, or diffusive wave. The distinct features of WRF-Hydro are as follows:

(1) It is the core land surface model in the National Water Model: The National Water Model (NWM), operated by the National Water Center, has been in operation since 2015 with the goal of delivering flood forecasts for the nation at 2,700,000 river reaches. The NWM is a specific configuration of WRF-Hydro. Once the WRF-Hydro model is run over customized watersheds of the National Hydrographic Dataset Plus[8] (NHDPlus) network with specific datasets as inputs, it is called the NWM.

(2) It can be coupled with the Weather Research and Forecast (WRF) climate model: WRF is a well-known atmospheric model used for meteorological prediction. WRF-Hydro users have the option of running the model in an online mode which means running the model coupled with WRF. In the online mode, the land surface model results will have feedback into the WRF model and vice versa. This coupling will be significant for the atmospheric community as it will allow the interactions between land surface and the atmosphere more accurately. These interactions are shown to have a significant effect on climate predictability (Niu et al., 2011).

[8] NHDPlus is national geospatial surface water framework developed and maintained by the U.S. Geological Survey (USGS) and the U.S. Environmental Protection Agency (EPA)

(3) Flexibility in modeling: WRF-Hydro users are able to choose between multiple options for different processes. These processes include the core column land surface model and the routing method. Additionally, switches are provided to turn (surface, subsurface, and channel) routing and groundwater modules on and off. Also, if Noah-MP is chosen as the column land surface model, one can choose between 1080 different schemes for modeling land surface processes.

Some output variables of WRF-Hydro include surface latent heat flux, canopy moisture content, snow depth, deep soil drainage, ground heat flux, and soil moisture. Among these variables, soil moisture is of particular interest in this study because of the following reasons: (1) The water stored in the land (as soil moisture) during a wet season will feedback to the atmosphere in the dry season through evapotranspiration (Niu et al., 2011). Soil moisture is persistent meaning that the water stored in soil needs weeks to months to evaporate. Therefore, soil moisture can provide information about the future of the atmosphere. (2) Soil moisture is a crucial variable in disastrous events. It determines onset, duration, and termination of agricultural droughts (Ahmadalipour et al., 2017b; Madadgar and Moradkhani, 2013; Yan et al., 2017; Yan et al., 2018) and it also is one of the essential predictands of (flash) floods (Cenci et al., 2017). Floods, in particular, are affected by soil moisture (Komma et al., 2008) as soil moisture is the main factor to determine if precipitation penetrates to the ground or if it flows as runoff. Therefore, improving soil moisture simulations has been the focus of several studies (Oglesby and Erickson III, 1989; Rebel et al., 2012; Sheffield et al., 2004). An accurate representation

of soil moisture would be beneficial for a variety of purposes ranging from emergency planning to resource allocation and disaster prediction.

An alternative in obtaining soil moisture is using in-situ or remotely-sensed measurements. In-situ soil moisture data are sparse and are not uniformly distributed across the CONUS. Another way of measuring soil moisture is through remote sensing (Brocca et al., 2011; Cenci et al., 2017; Entekhabi et al., 2010; Lacava et al., 2012). There are shortcomings associated with each of these procedures in measuring soil moisture. In situ measurement, although more accurate, they are limited in spatial representativeness. Remotely sensed satellite observations, although with good spatial coverage, are limited in the spatial and temporal resolution. Therefore, hydrologic models at a better resolution and coverage become essential as another source of information for soil moisture estimations. Hydrologic models, on the other hand, are subject to multiple uncertainties including uncertainties associated with parameterization, model structure, initial condition, and meteorological variables. These uncertainties lead to uncertain soil moisture simulations. Instead of using either measurements or land surface models, research has shown that their integration results in more accurate soil moisture simulations (Daescu and Navon, 2004; DeChant and Moradkhani, 2012; Moradkhani et al., 2012, 2005a; Zupanski et al., 2006). Specifically, using soil moisture observations to inform land surface models are suggested. Such integration is possible through data assimilation (DA) techniques (Pathiraja et al., 2016a, 2016b). DA helps reduce and quantify the uncertainties associated with LSMs. Commonly used DA techniques

employed in earth system modeling fall into two categories of Kalman Filter-based (KF) methods (Moradkhani et al., 2005b), Particle Filter-Based (PF) methods (Moradkhani et al., 2012), and Variation DA (Daescu and Langland, 2017; Shaw and Daescu, 2016). All these techniques are comprised of two steps: estimation and update. In the estimation step, a dynamic model is run and the resulting variable of interest is compared against observations. Next, in the update step, model simulations and observations of that variable are combined and then the model is updated accordingly. Another DA technique is Nudging (Gochis et al., 2018). Nudging is a simple method of data assimilation that inserts an observed state variable into the model. Currently, the NWM employs a simple nudging algorithm to assimilate USGS observed streamflow into the WRF-Hydro model. Although ensemble data assimilation techniques are known to be more effective, their implications on this model have not been reported yet.

In the majority of DA studies, improving the same variable that is assimilated is of interest (Yan et al., 2017, 2015). In some studies, this variable is soil moisture (Yan et al., 2017; Yan et al., 2018) and in some others, it is streamflow (Moradkhani et al., 2012, 2005b). However, research is still needed on propagating the assimilated information to other hydrologic variables. While Scipal et al. (2005) and Aubert et al. (2003) reported successful propagation of soil moisture assimilation information to other variables such as streamflow/runoff, Chen et al. (2011), Parajka et al. (2006), and Marc Etienne Ridler et al. (2014) fail to do so. Alvarez-Garreton et al. (2014) reported marginal improvements in streamflow simulations after they tested three different data assimilation methods to

assimilate soil moisture observations into a hydrologic model. Yan and Moradkhani (2016) also considered univariate and multivariate assimilating of soil moisture and streamflow to improve SAC-SMA simulations. They did not observe improvements in soil moisture simulations when they assimilated streamflow and reported improved soil moisture simulations when they assimilated both satellite soil moisture and streamflow. Aubert et al. (2003) observed a significant improvement in streamflow simulations when they assimilated station soil moisture in a lumped model. They observed the most significant improvements during flood events. They also observed improvements in the forecasting mode. They conclude that for normal conditions, streamflow assimilation is sufficient while for high-flows and extreme hydrologic conditions, multivariate assimilation of streamflow and soil moisture is required. When they increased the prediction lead-time to 1-3 days, they noticed that the effectiveness of soil moisture assimilation remains constant. Similarly, Chen et al. (2011) showed that assimilation (EnKF) of surface soil moisture into the semi-distributed SWAT model only has limited success in updating streamflow. They attributed this failure to the inability of the EnKF to correct the biases in SWAT-predicted streamflow components. Likewise, Clark et al. (2008) failed to propagate information through data assimilation to the neighboring cells in a distributed hydrologic model (the TopNet model) and they attributed this to the inability of the model in modeling spatial variability of hydrologic processes.

Therefore, with the overarching goal of further improving the current flood modeling skills, the objectives of this study are as follows:

(1) Assessing the performance of ensemble data assimilation methods in assimilating observed streamflow into the community WRF-Hydro model.

(2) Assessing the performance of ensemble data assimilation methods in assimilating satellite soil moisture into the community WRF-Hydro model.

(3) Assessing the effects of soil moisture (streamflow) assimilation on streamflow (soil moisture).

(4) Comparing the performance of univariate and multivariate data assimilation on the WRF-Hydro model.

The improved soil moisture and streamflow simulating skills of this research will benefit the hydrologic science community in flood modeling and forecasting. One of the implications of this study is improved soil moisture simulating skill which benefits the atmospheric science community in improving climate predictions. Finally, the results of this research directly benefit operational flood forecasting agencies especially the NWC. The findings and the methodologies of this study could help the NWC in planning for the future versions of the NWM. This could start the important discussion of including satellite information and ensemble data assimilation for flood forecasting in the NWM. It could also help the NWC improve their algorithms to more complicated (and more accurate) methods such as ensemble data assimilation techniques. The rest of the chapter is organized as the following. First, an introduction to the study area and data is presented which is followed by the methodology section. In the methodology section, the DA technique and the parallel DA algorithms are illustrated. Consequently, results are

presented and discussed and the chapter concludes with a discussion on the values and suggestions for future works.

3.4 Study area and data

3.4.1 Study area

This chapter has two study areas. The first study area is on Croton-on-Hudson River in New York as shown in Figure 3-1. The elevation of this area is mapped in Figure 3-2. The second study area is located in Huntsville, Alabama as shown in Figure 3-3. These areas were chosen due to multiple limiting factors: (1) since this study attempts to replicate the operational flood forecasting in the NWM, an area for which WRF-Hydro is already calibrated had to be studied. WRF-Hydro has already been calibrated by the WRF-Hydro team at NCAR for around 100 watersheds over the U.S. The calibrated domain files were acquired from NCAR. The selected area had to be calibrated with good coverage of USGS and in-situ soil moisture gauges. Additionally, lakes and reservoirs had to be avoided since reservoir information is not available to the public. Another important factor in choosing a study area was the size of the area. Examinations of the calibrated watersheds led to choosing an area in Huntsville, AL and Croton study area was adopted from WRF-Hydro's example cases.

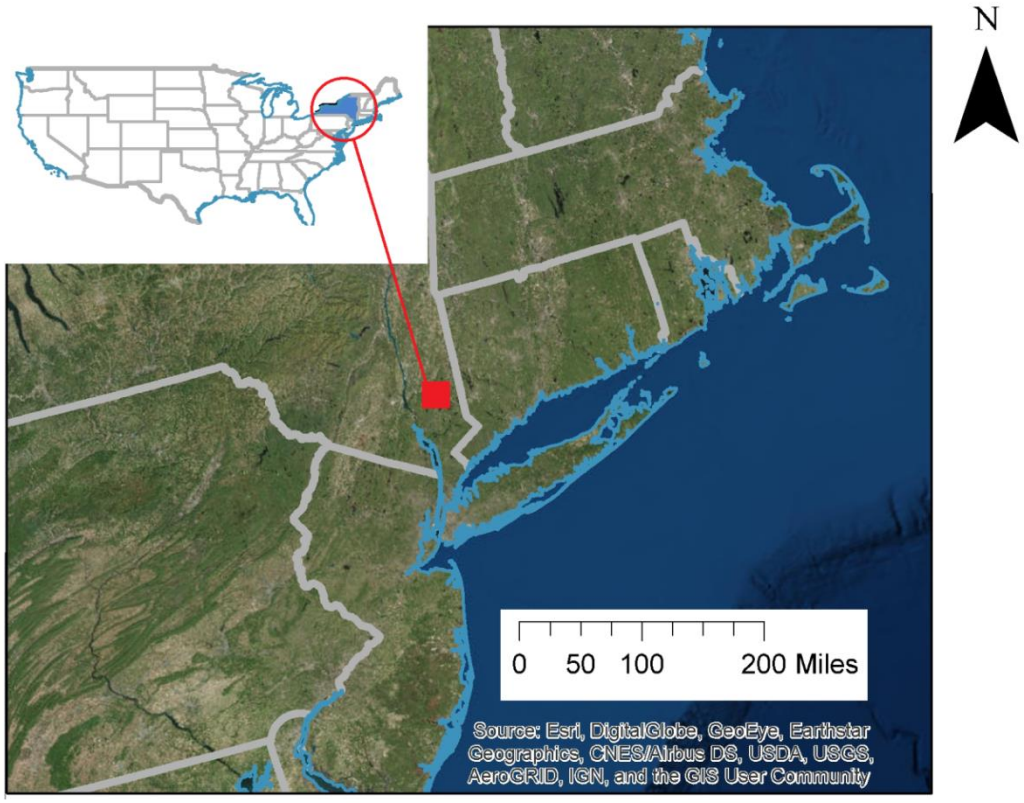

Figure 3-1: The location of the study area in Croton, NY.

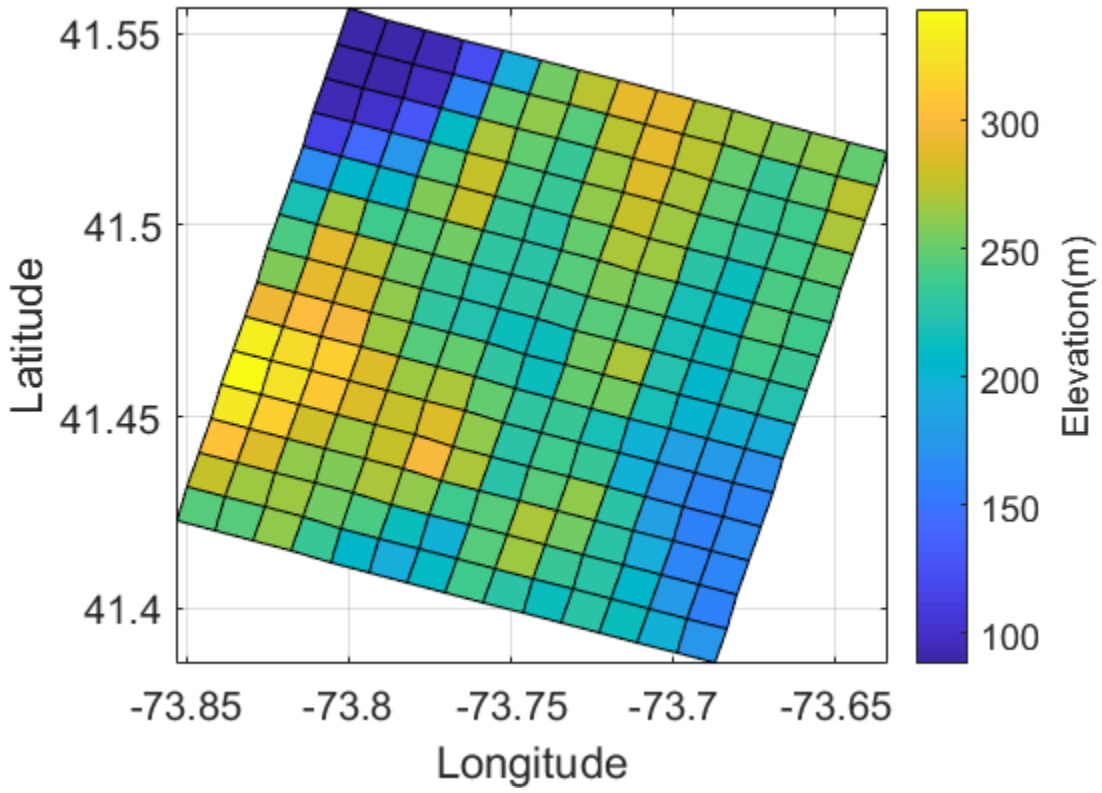

Figure 3-2: The elevation of the studied domain in Croton, NY.

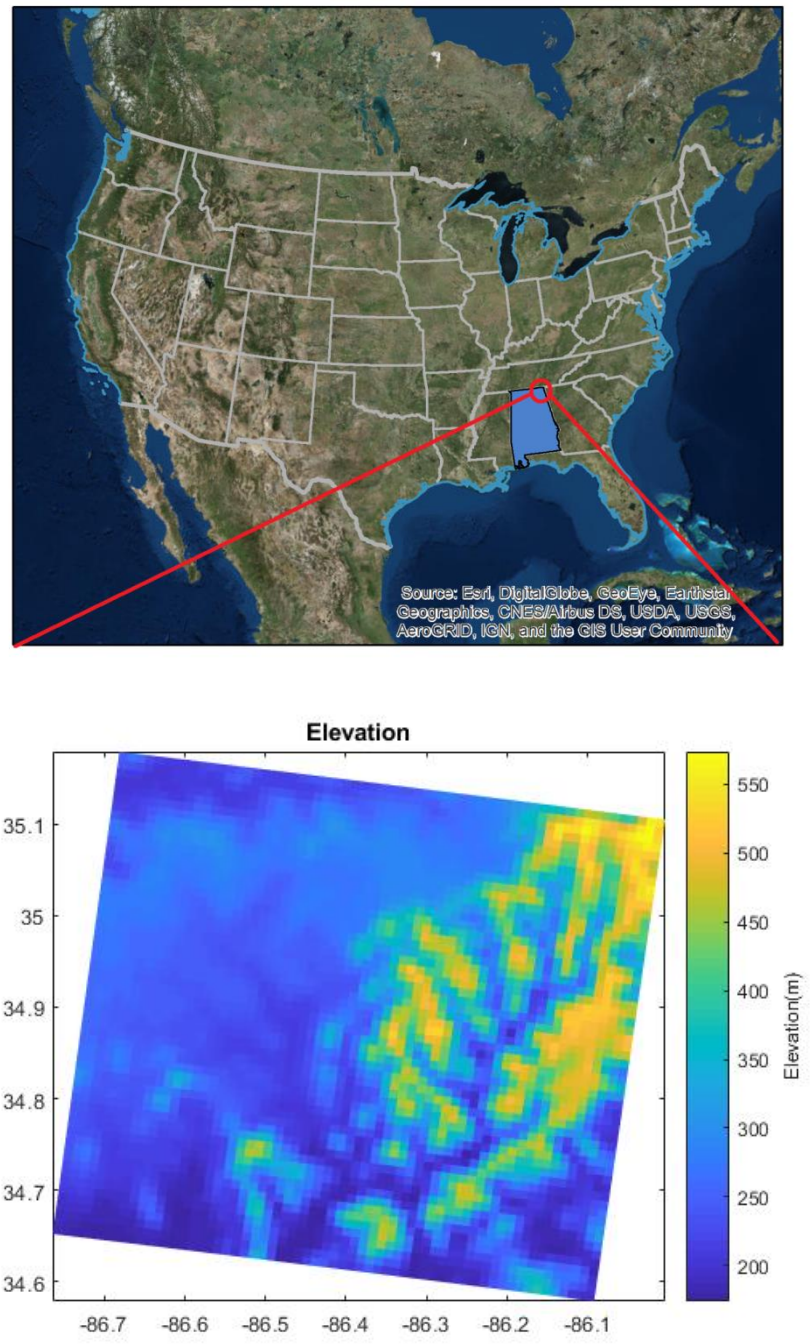

Figure 3-3: The location (the top panel) and elevation (the bottom panel) of the studied area in Huntsville, AL.

The high-resolution terrain routing file required by WRF-Hydro needs the location of streams in the area. Figure 3-4 shows the complete network of streams in the domain files of the model for the area in Huntsville. The red circle indicates the location of the outlet USGS gauge. The colors of the streams indicate their Strahler stream order (Strahler, 1952). In Strahler ordering, all reaches are assigned to integer numbers (stream order) greater than zero. The reaches that do not have any junctions in the upstream are assigned to one. At a junction of two streams, if the two upstream orders are the same, the downstream order would be that number plus one. Otherwise, if the upstream orders are not similar, the downstream order would be equal to the greater number.

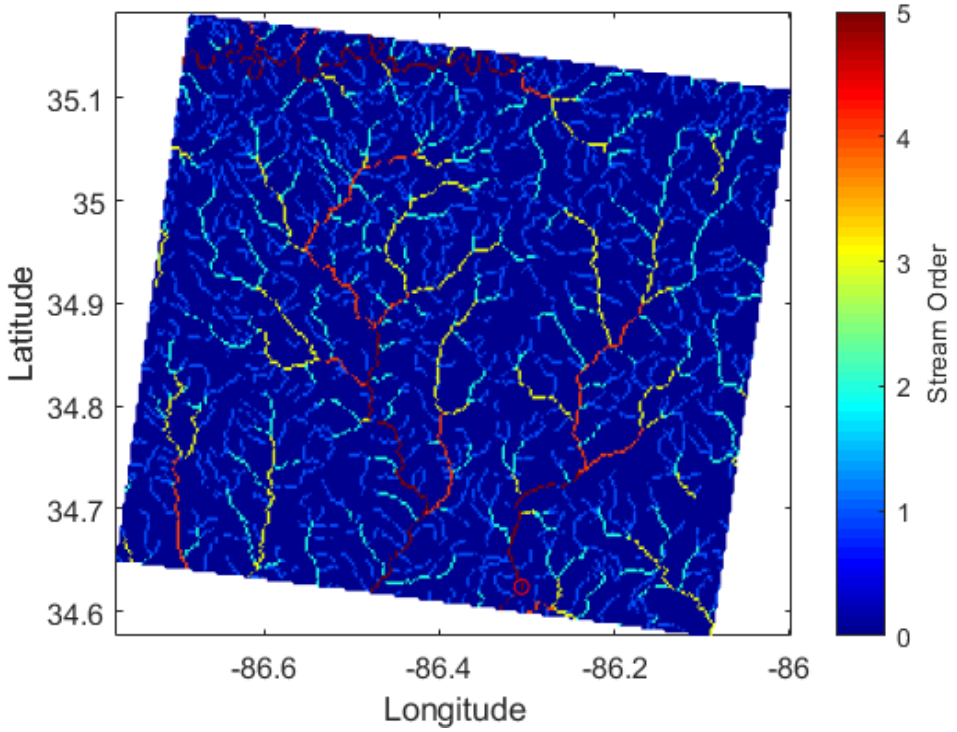

Figure 3-4: Strahler stream order in the high-resolution terrain file of WRF-Hydro model. The red circle indicates the location of the outlet point where USGS measurements are available.

3.4.2 Streamflow

Streamflow was obtained from USGS streamflow gauge database. Gauge numbers are listed in Table 3-1.

Table 3-1: USGS gauge information for two study areas in this chapter

STUDY AREA	GAUGE NUMBER
HUNTSVILLE, AL	03574100
HUNTSVILLE, AL	03574500
CROTON, NY	1374559
CROTON, NY	1374581
CROTON, NY	137462010

3.4.3 Atmospheric forcings

The atmospheric forcings for WRF-Hydro are similar to those of Noah-MP introduced in the previous chapter. The LSM model is forced with surface meteorological data including rain rate (mm/s), wind speed (m/s), surface pressure (Pa), temperature (k), and short and longwave radiation (W/m^2) obtained from the Phase II North American Land Data Assimilation System (NLDAS-2) (Xia et al., 2012b) gridded to the 1/8˚ resolution. However, a preprocessing step is required before running the model to rescale the projection and resolution of grids from NLDAS to WRF-Hydro domain files. This preprocessing is conducted using WRF-Hydro re-gridding tools available on their website. The required fields and units are similar to the Noah-MP model input requirements discussed in the previous chapter.

3.5 Methodology

3.5.1 WRF-Hydro

The land surface model used in this chapter is the community WRF-Hydro model (Gochis et al., 2015, 2018). For this chapter, the latest version of the model, version 5, released on April 13, 2018 was utilized. WRF-Hydro (Weather Research and Forecast-Hydrological modeling system) has been developed by NCAR with the goal of facilitating improved terrestrial hydrologic processes modeling and is an extension of NCAR Weather Research and Forecast (WRF). WRF-Hydro is a modeling architecture facilitating coupling of various hydrological processes (Gochis et al., 2018). The model is in FORTRAN90 and allows users to make modifications into the model. The initial version of the WRF-Hydro model was introduced to the community as "Noah-distributed" (Gochis and Chen, 2003). Gochis and Chen (2003) discussed mapping land surface condition from a coarse resolution to a terrain routing grid at a finer resolution. WRF-Hydro is now evolved to version 5 and is capable of coupling multiple land surface models to various routing options and parameters. An important feature about WRF-Hydro, that highlights the importance of more research around it, is that National Oceanic and Atmospheric Administration (NOAA), in pursuit of increasing the nation's water prediction skill, uses the WRF-Hydro model to predict stream flooding over the Continental United States. NOAA operationally uses the National Water Model (NWM) which is a specific configuration of WRF-Hydro with specific forcing datasets and methodologies. Multiple atmospheric models such as CAM/CESM or WRF are capable

of being coupled with land surface models (such as VIC, Noah, Noah-MP), groundwater models (such as HsB, ParFlow, VIC), and hillslope/routing models (such as VIC, TOPOFLOW). At the current version, WRF-Hydro can be coupled with WRF atmospheric model. For LSM, Noah and Noah-MP options are provided. For groundwater model, DHSVM is provided. For hillslope/channel routing, CASC2D is provided, and for water management, the linear reservoir is provided. Figure 3-5 illustrates the steps inside the model. After the LSM is run, the output variables are passed to routing modules such as surface routing and subsurface routing. The results of the routing processes (depending on the user choice) may be passed back to the column land surface model (two-way coupling). Then, the results are delivered to a channel routing model. For channel routing, the user can choose between commonly used methods of Muskingum-Cunge, Muskingum, or diffusive wave. Figure 3-6 is a simple representation of the model's required files, outputs, and procedure. Domain files are required by any WRF-Hydro run. The files can be obtained from WRF-Hydro's preprocessing tools. Restart files are required in case of "warm start" which means that the initial states are known. When the initial states are not known, the run is called "cold start".

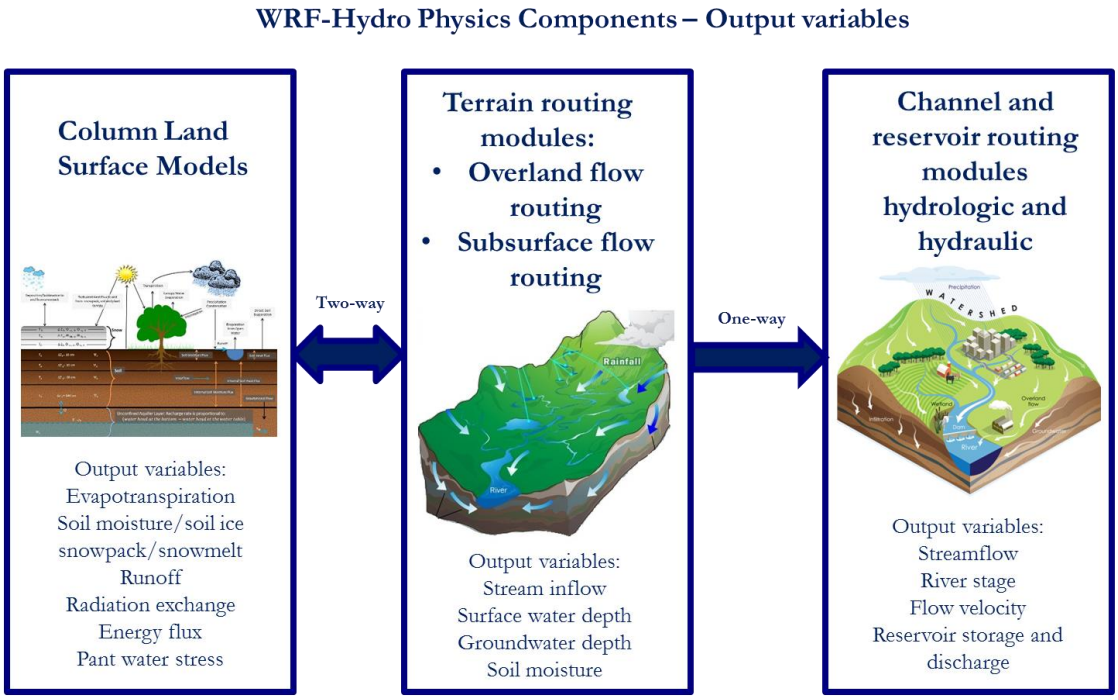

Figure 3-5: Schematic of WRF-Hydro structure (Gochis et al., 2018)

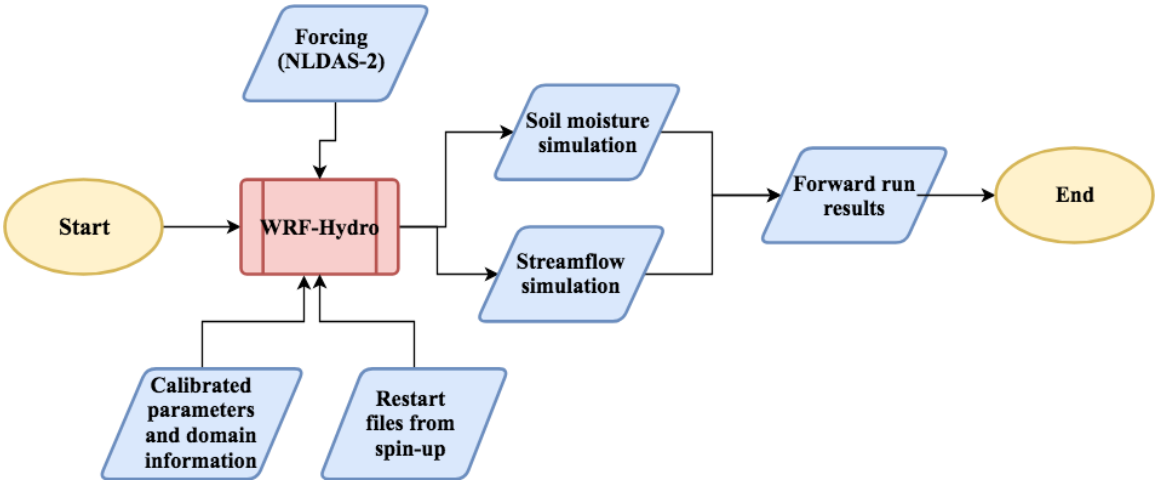

Figure 3-6: The procedure and required files to run the WRF-Hydro model

3.5.2 Data Assimilation

Two DA methods are discussed in this study including EnKF and PF. In this chapter, Ensemble Kalman Filter (EnKF) is employed. For details of the EnKF, please see section 2.6.1.2 in the previous chapter. When a hydrologic model is integrated with soil moisture observations another hydrologic variable such as streamflow can be updated. Both methods have been successfully implemented in hydrologic modeling. For example, Clark et al. (2008) discussed the application of the EnKF for assimilating streamflow observations and updating model states. They proposed transforming streamflow into a log space before computing the error covariance. Yan and Moradkhani (2016) used PF, assimilated streamflow and updated state variables.

3.5.3 High-performance computing

Parallel Computing or Parallel Processing is an integral part of analyses with WRF-Hydro and the NWM, especially if used for data assimilation. Implementing sequential data assimilation in WRF-Hydro is very expensive. The computational burden becomes even more severe in operational flood forecasting in the NWM where WRF-Hydro is being run in more than 2,000,000 reaches every hour. Thus, many agencies such as NWC, NOAA, NWS, and NCAR are using parallel computing for their analyses. The parallel computing algorithm used in this chapter is similar to the algorithm introduced in the previous chapter. Figure 3-7 shows a schematic of this algorithm. For more information about the detail of this algorithm, readers are referred to 2.6.2 in the previous Chapter.

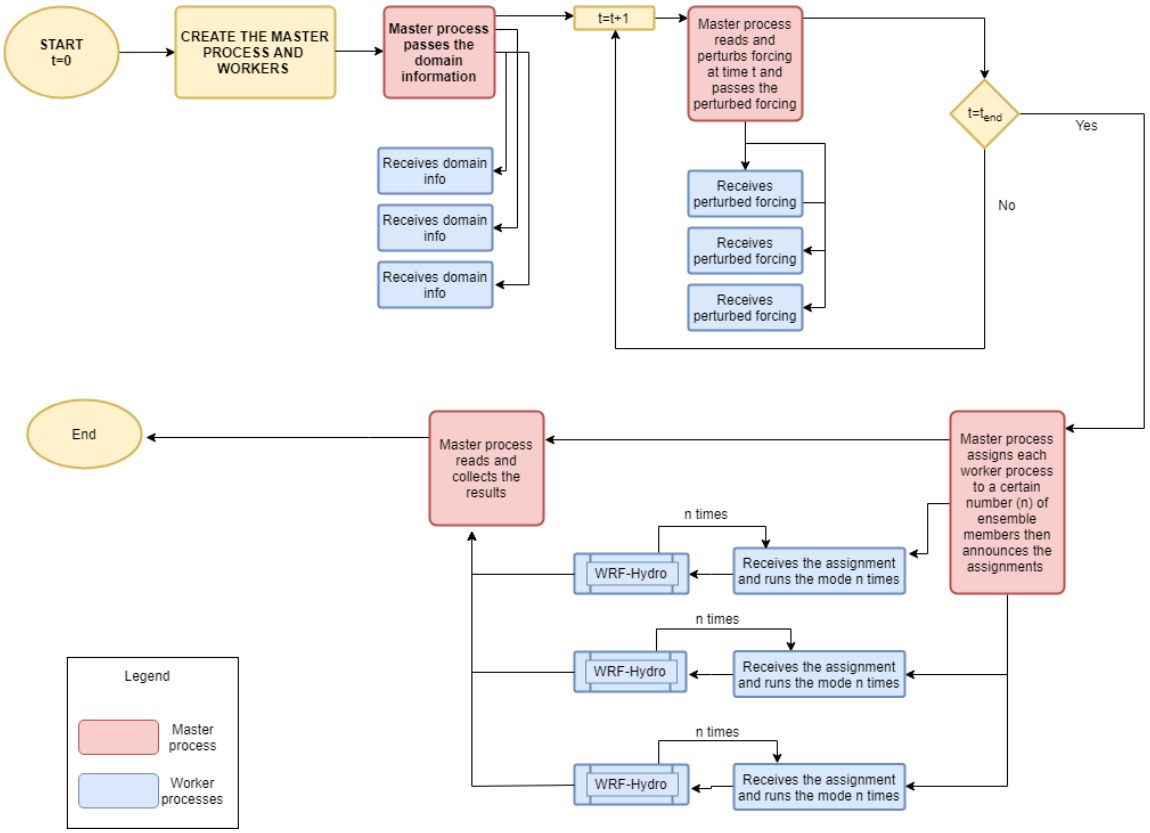

Figure 3-7: The algorithm of the parallel data assimilation methodology applied in this chapter.

3.5.4 Performance measures

In this chapter, five commonly used performance measures (Gupta et al., 2009) including Root Mean Square Error (RMSE), Normalized Information Contribution (NIC), Nash-Sutcliff Efficiency criterion (NSE), Kling-Gupta Efficiency (KGE), and Bias are employed. These measures are defined as the following.

$$RMSE = \sqrt{\sum_{i=1}^{n}(y_{oi} - y_{pi})^2 / N} \tag{14}$$

$$Bias = \sum_{i=1}^{n} |y_{oi} - y_{pi}| \quad (15)$$

$$NIC = RMSE_{ol} - RMSE_{da})/RMSE_{ol} \quad (16)$$

$$NSE = 1 - \frac{\sum_{i=1}^{n}(y_{ot} - y_{pt})^2}{\sum_{i=1}^{n}(y_{ot} - \overline{y_o})^2} \quad (17)$$

$$KGE = 1 - \sqrt{(r-1)^2 + (\alpha - 1)^2 + (\beta - 1)^2} \quad (18)$$

Where y indicates the variable of interest (soil moisture or streamflow in this dissertation), o indicates "observed" and p indicates "predicted". N is the length of the dataset, r is the linear correlation coefficient, α is the measure of variability in observed and simulated values, and β is the ratio between mean simulated and mean observed values. For more information about the performance measures specially KGE, readers are referred to Gupta et al. (2009)

3.6 Results

The model is capable of running at a daily time step; however, the author's initial research showed that WRF-Hydro sometimes fails to close the water balance if it is run at a daily time step. In addition, it is noticed that model simulations are more accurate at an hourly time step. Therefore, a time step of one hour was chosen for the entire analysis. To assess the effects of ignoring the groundwater, the model was tested with and without the groundwater module. It was observed that ignoring the groundwater interactions results

in a dry bias in soil moisture simulations. However, due to the added computational complexity of the model, and the long spin-up time required for the groundwater module, this bias is acknowledged and ignored for the analyses.

The results of both synthetic and real experiment are presented in this section. First, the results of running the model forward for the period of interest are discussed. Next, assimilation scenarios are explained. Finally, the real study results are presented and discussed.

3.6.1 LSM setup and preprocessing

NCAR has calibrated WRF-Hydro (for the NWM) for multiple watersheds in the United States. The subject areas in this study are from two of the calibrated watersheds obtained from NCAR by request. For the spin-up, while 8 years is suggested for soil moisture (Cai et al., 2014b), 10 years were left in this study. The schemas used for the Noah-MP model are similar to those of the previous chapter except that for the vegetation dynamic, option 4 is chosen (it is the default for WRF-Hydro V5) which means that vegetation dynamic is off and it uses Leaf Area Index (LAI) but maximum vegetation fraction is considered.

Domain files were acquired from the NCAR team by request. It should be noted that a cutout of the NWM was requested which includes all the required files for the model run. Users that are interested to run the model outside the framework of the NWM need to generate the DOMAIN files through available pre-processing tools(Gochis et al., 2018).

It should be noted that the spatial resolution of the simulations is 1 (km) and the temporal resolution is 1 hour. The simulation in the Huntsville domain is conducted for the period of January 1, 2018 to February 28, 2018. For the Croton, NY domain, the model is run with similar resolutions for August 2011.

3.6.2 Characterizing the uncertainties

Characterization of uncertainty in this chapter is similar to the previous chapter. Precipitation is assumed to follow a lognormal distribution with mean zero and coefficient of variation of 25%. Temperature errors are assumed homoscedastic with mean zero and standard deviation of 3 degrees as considered in the previous data assimilation studies (Ahmadalipour et al., 2017b; Yan et al., 2017). For the synthetic experiment, it is considered that the model is perfect and that there is no model error. For the real study, model error is 10%. Finally, the observation error for soil moisture is 0.04 (m^3/m^3) and it is 15% for streamflow observations, assuming heteroscedasticity in errors.

3.7 Synthetic study

Three scenarios for the synthetic experiment are studied. In all scenarios, the effects of DA on both soil moisture and streamflow are assessed. First, only synthetic soil moisture observations are assimilated using a univariate EnKF. Second, streamflow is assimilated using a multivariate EnKF. Finally, both soil moisture and streamflow are assimilated employed a multivariate EnKF. A schematic of the synthetic study steps is shown in Figure 3-8.

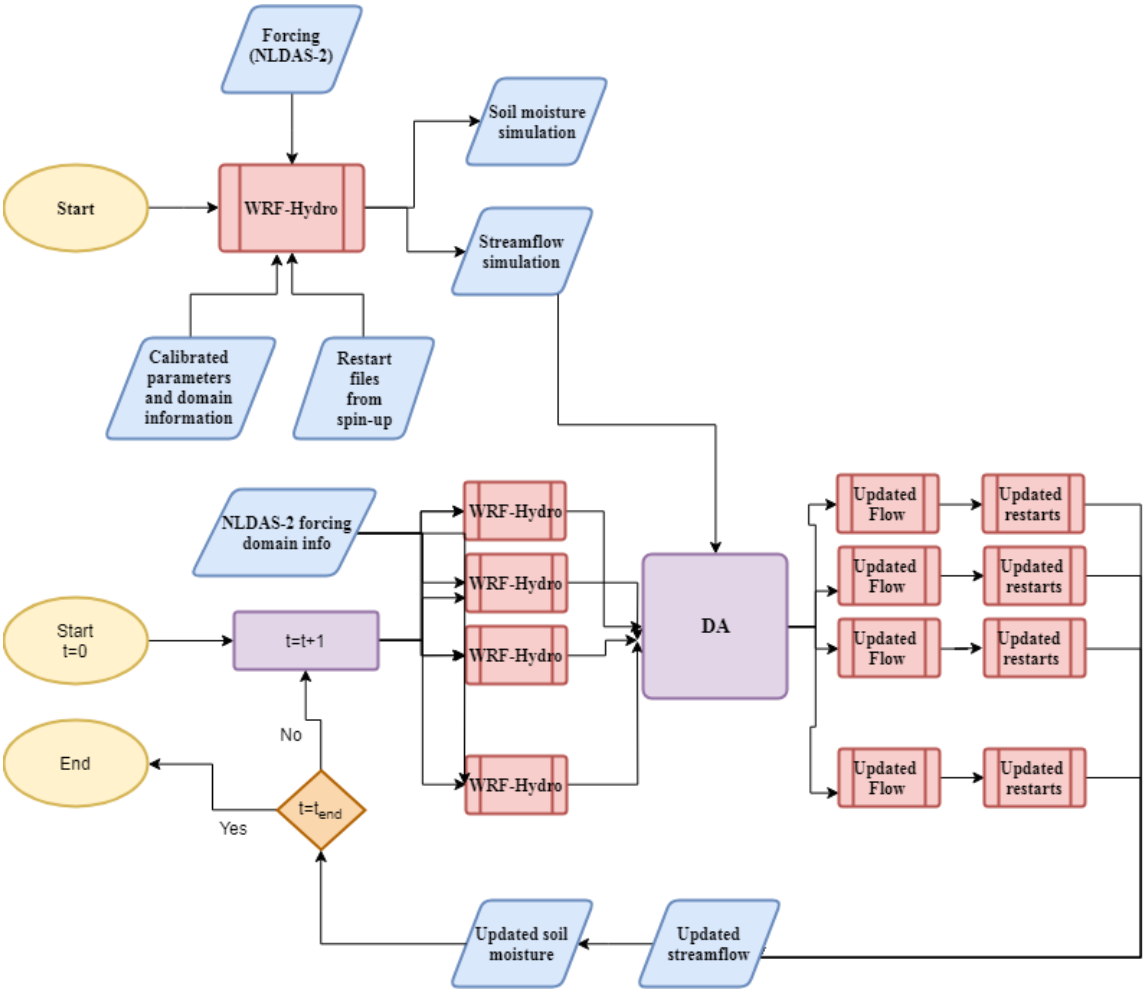

Figure 3-8: A schematic of the synthetic study algorithm. In this case, synthetic discharge is assimilated into the model. The other version of this figure, Figure 2-10, shows assimilation of synthetic soil moisture.

3.7.1 Univariate soil moisture assimilation

This section explains the assimilation of gridded soil moisture simulations in the WRF-Hydro model. Soil moisture observations are derived from the model forward run (synthetic observations) with an assumed error of 0.04 (m^3/m^3). First, the effects of

assimilation on soil moisture simulations are assessed and then the effects on streamflow are evaluated. Univariate EnKF is used with an ensemble size of 100.

Area-averaged DA soil moisture simulations are compared against the true soil moisture in Figure 3-9. RMSE, NSE, KGE, and BIAS are calculated. The results of the RMSE shows that the DA decreases the error by 0.02 (mm) and the BIAS in DA is lower by 15 (mm). The NSE and KGE of DA are also marginally higher than those of DA.

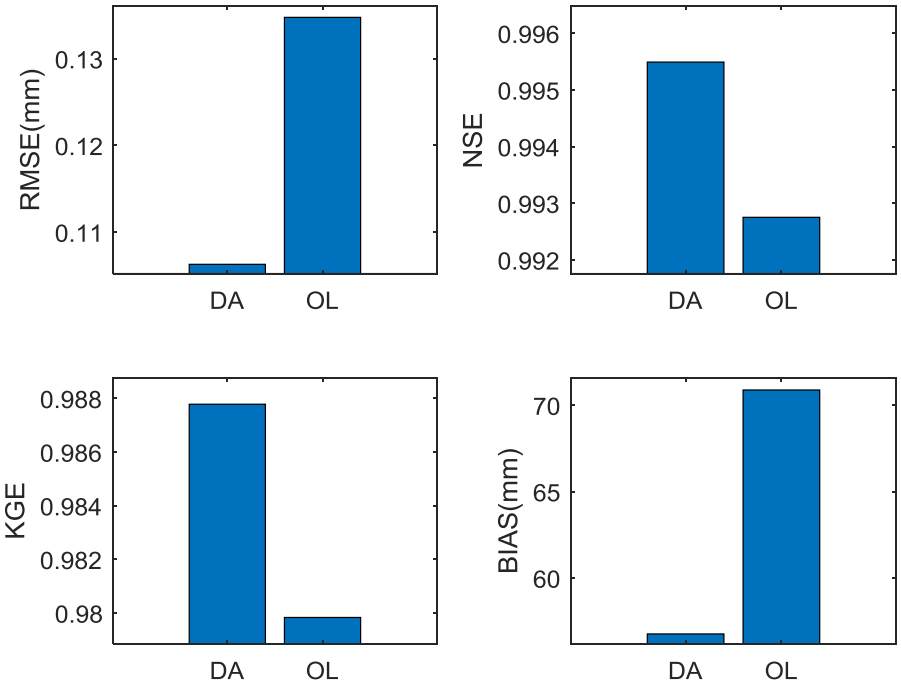

Figure 3-9: Univariate synthetic soil moisture assimilation results. Performance of OL and DA in simulating soil moisture in the Huntsville domain. Performance is measured by RMSE, NSE, KGE, and BIAS.

Cell-wise comparisons of the performance of DA over OL are shown in the following. Figure 3-10 shows the spatial variation of RMSE in the area. It is observed that RMSE of the OL is significantly higher than the RMSE of DA in the south of the domain. Also, in the main watershed, the DA RMSE map is darker blue which indicates lower values of RMSE. This confirms that the DA outperforms the OL, especially in the northeast and south part of the area. In the same figure, a scatter plot is presented where cells are indicated by points. OL and DA RMSEs are compared in this plot. Departure from the 1:1 (gray) line shows the difference in RMSEs. Points that fall above the 1:1 line, indicate that in those cells, DA is outperforming OL. Points below the 1:1 line indicate that the OL outperforms the DA. It is noted in this plot that all points are located above the 1:1 line and highlight the superiority of the DA. Figure 3-11, Figure 3-12, and Figure 3-13 show the same but for NSE, BIAS, and KGE, respectively. As confirmed by all these figures, the DA is outperforming the OL in all cells of the area.

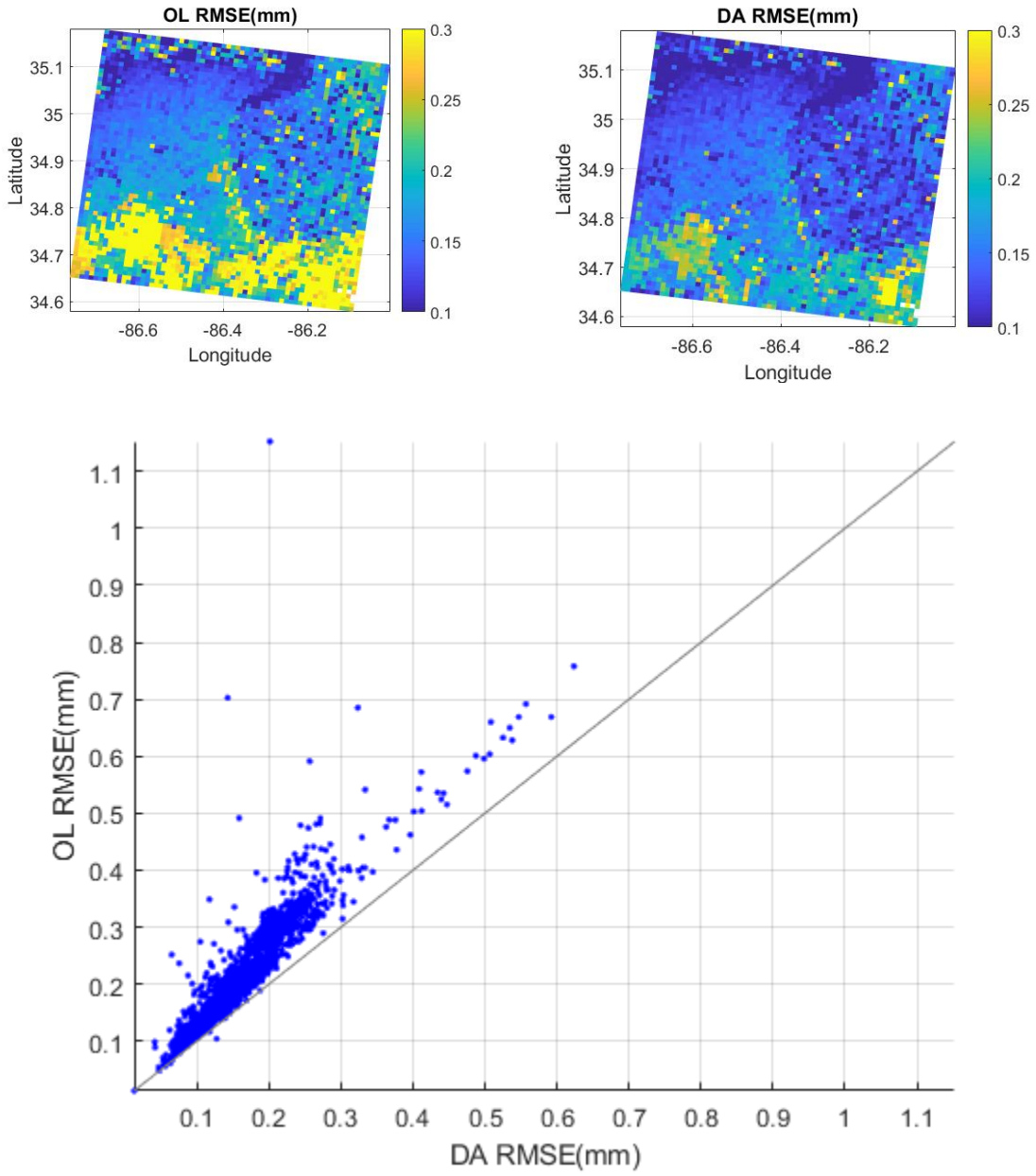

Figure 3-10: Univariate synthetic soil moisture assimilation results. Spatial variation of RMSE in Huntsville, AL from the OL run (upper left panel) and from the DA run (upper right panel). In the scatter plot, cells are indicated by points. The 1:1 gray line indicates equal RMSE of OL and DA. The area above the 1:1 line shows the outperformance of DA and the area below the 1:1 line shows the outperformance of OL.

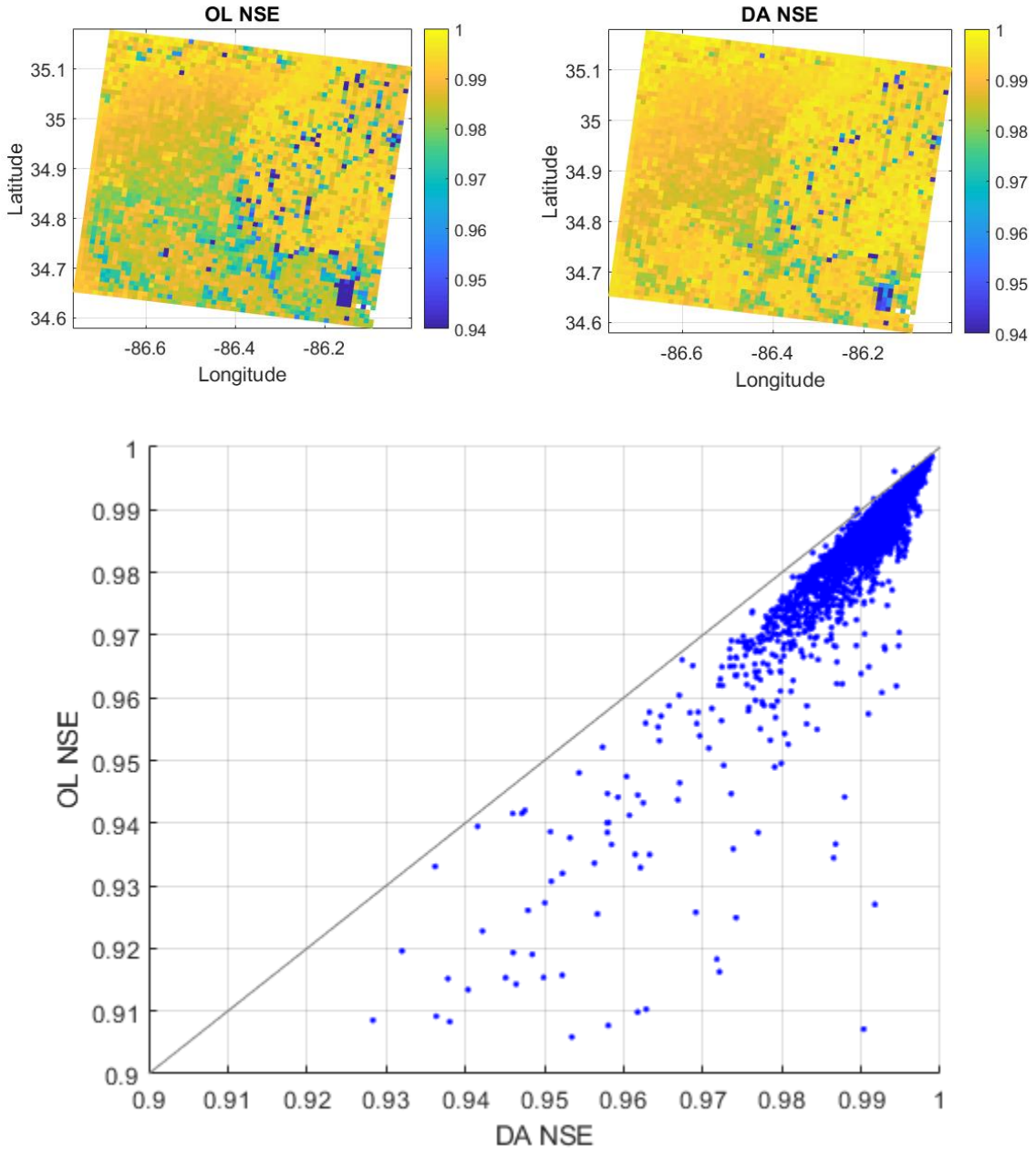

Figure 3-11: Univariate synthetic soil moisture assimilation results. Spatial variation of NSE in Huntsville, AL from the OL run (upper left panel) and from the DA run (upper right panel). In the scatter plot, cells are indicated by points. The 1:1 gray line indicates equal RMSE of OL and DA. The area above the 1:1 line shows the outperformance of OL and the area below the 1:1 line shows the outperformance of DA.

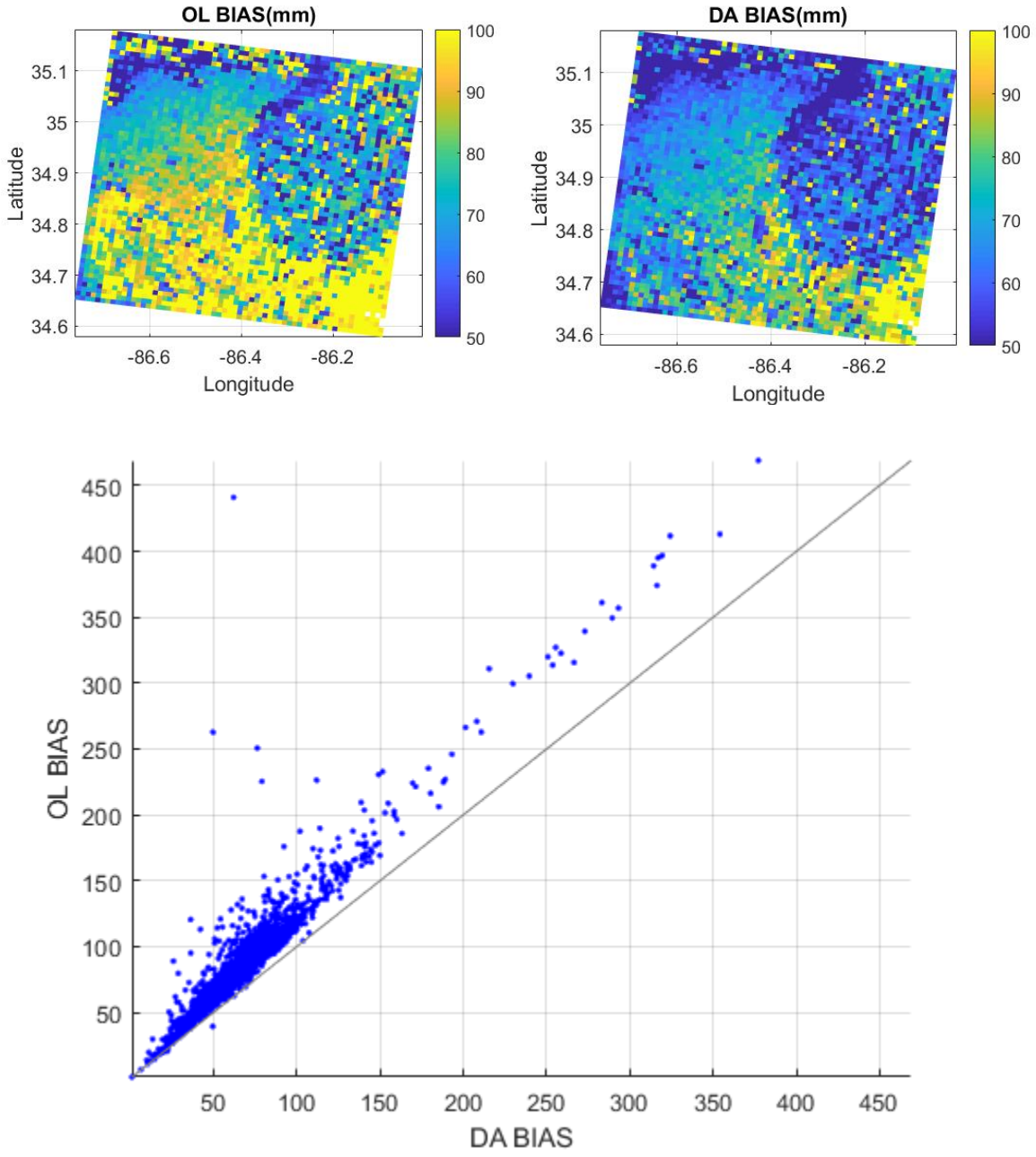

Figure 3-12: Univariate synthetic soil moisture assimilation results. Spatial variation of BIAS in Huntsville, AL from the OL run (upper left panel) and from the DA run (upper right panel). In the scatter plot, cells are indicated by points. The 1:1 gray line indicates equal RMSE of OL and DA. The area above the 1:1 line shows the outperformance of DA and the area below the 1:1 line shows the outperformance of OL.

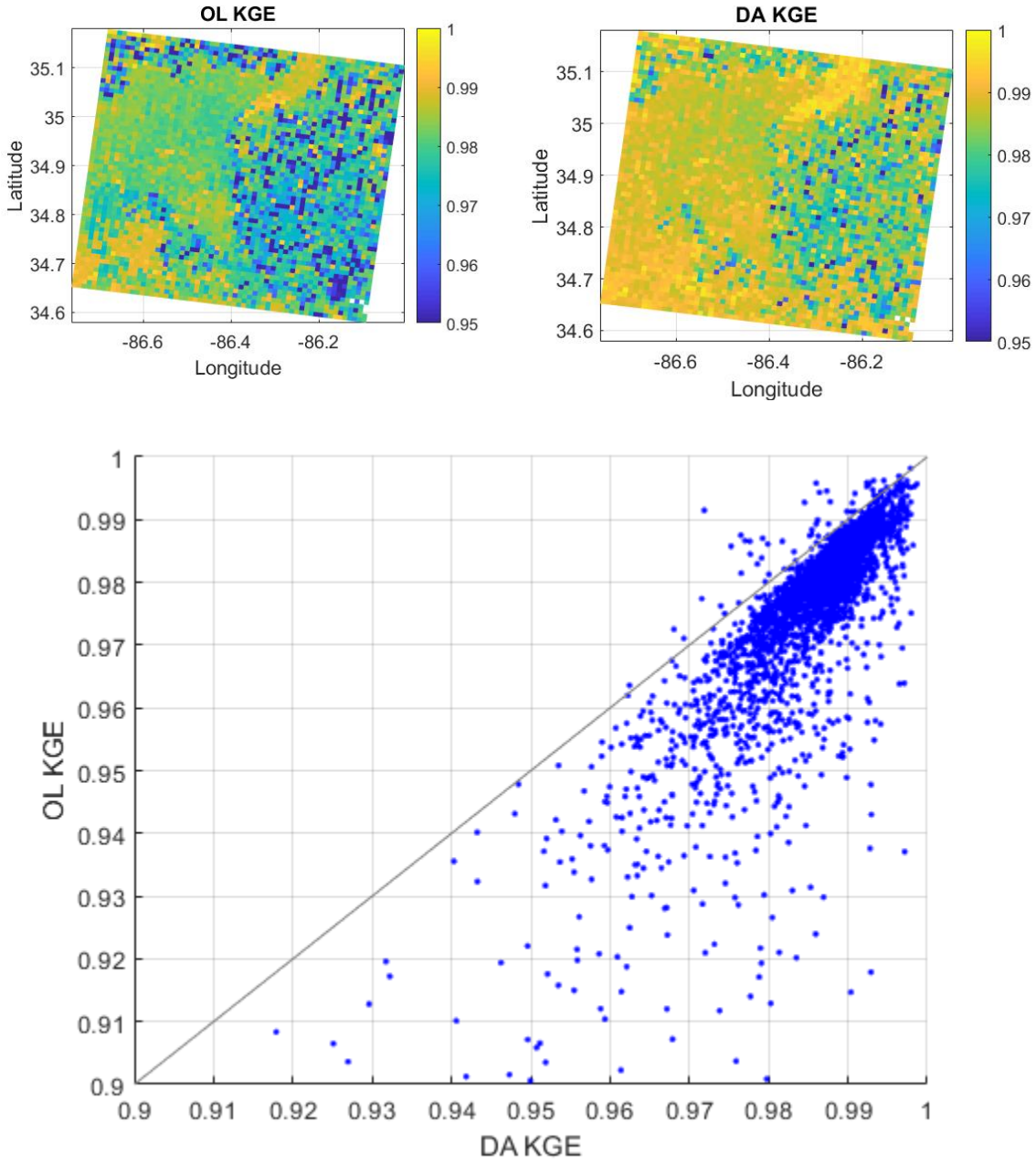

Figure 3-13: Univariate synthetic soil moisture assimilation results. Spatial variation of KGE in Huntsville, AL from the OL run (upper left panel) and from the DA run (upper right panel). In the scatter plot, cells are indicated by points. The 1:1 gray line indicates equal RMSE of OL and DA. The area above the 1:1 line shows the outperformance of OL and the area below the 1:1 line shows the outperformance of DA.

The degree of improvement by DA over OL is indicated by NIC. The spatial distribution of NIC is shown in Figure 3-14, the upper panel. Positive (up to 1) NIC values indicate DA improvement over OL and negative values indicate that DA degrades the OL. Higher values of NIC indicate a better performance. As noted in Figure 3-14, in 99.89% of the area, the NIC is positive showing improvement and only 0.11% of the area shows degradation. As shown by the histogram in the lower panel, the average improvement is about 20%. It reaches 80%. The west part of the area shows around 10% improvement. The lower improvements in this area can be attributed to the urbanization effect since Huntsville is located in that area. This may imply poor model performance in urban areas.

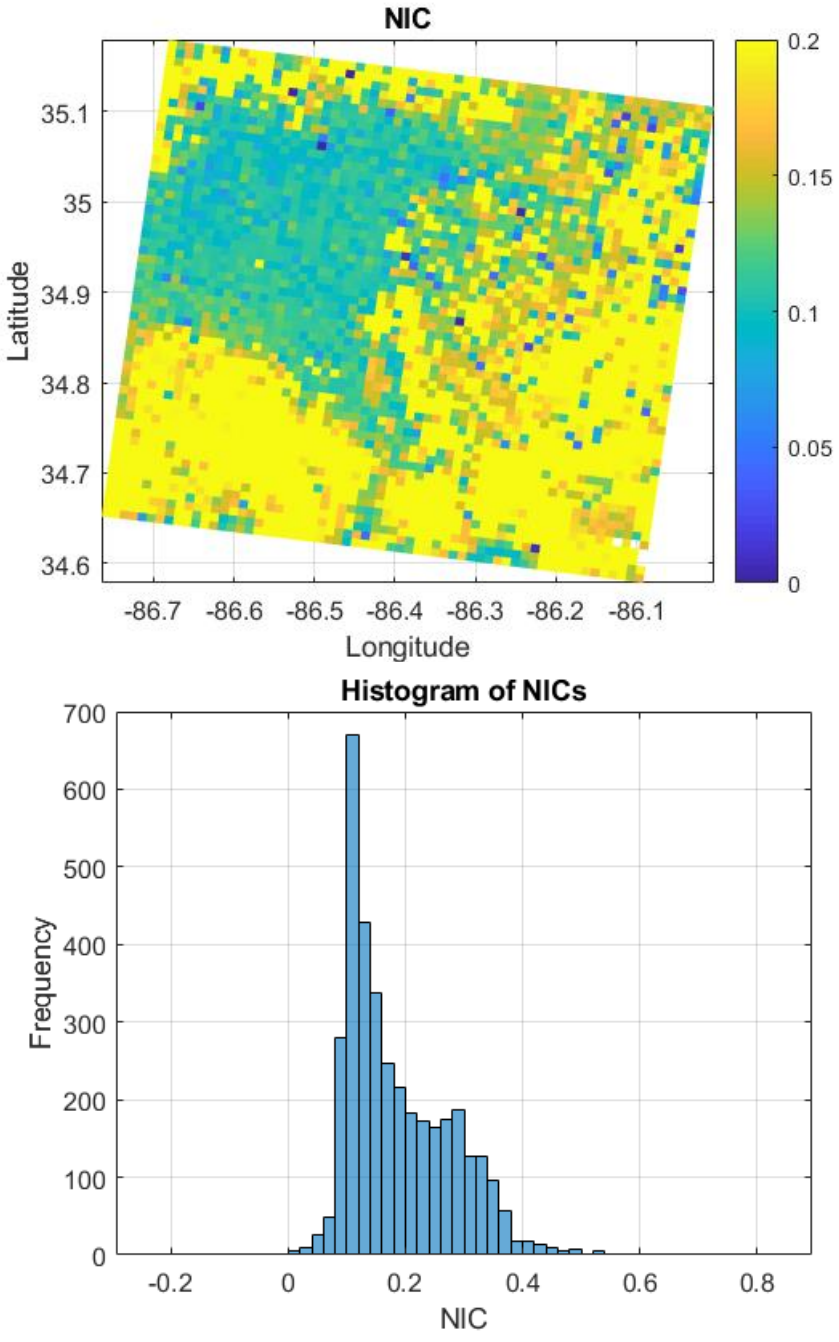

Figure 3-14: Univariate synthetic soil moisture assimilation results. Level of improvement by the DA over OL is indicated by NIC. NIC for the Huntsville, AL domain is mapped in the top panel. The histogram of all cells is plotted in the bottom panel.

A similar methodology was used to evaluate the performance of EnKF DA in the Croton area. OL and DA RMSE, NSE, KGE, and BIAS are compared in Figure 3-15. In this figure, scatter plots are presented. Cells are shown as points in these plots. The gray lines indicate the 1:1 line where the measure in OL equals that of DA. For RMSE and BIAS, the area above the line shows that the DA is outperforming the OL and the area below the line shows that the OL is outperforming the DA. For NSE and KGE plots, the points that fall above the 1:1 line indicate the outperformance of OL while the points that fall below the line indicate the opt performance of DA.

The degree of improvements by DA over OL is further assessed by NIC, as mapped in Figure 3-16 and summarized in Table 3-2. Positive NIC confirms that DA improves the model simulations while negative NICs indicate that DA degrades the model simulations. Higher values of NIC show a higher degree of improvement. It is noted that NIC is positive over the area which indicates that the DA outperforms the OL in the majority of the grid cells. The degree of improvement by DA over OL in this area is lower than the degree of improvement in the Huntsville area. Improvements in this area reach up to 20%. In 94.5% of the area, improvement was observed and in the remaining 5.4% of the grid cells, 0 to 10% degradation by DA was observed. This indicates that in those cells, DA does not improve the model simulations. An analysis of the temporal variation of biases (not shown) indicated that the OL has higher bias around the peak of the flood and early in the recession limb. This confirms the effectiveness of the DA in modeling the extremes.

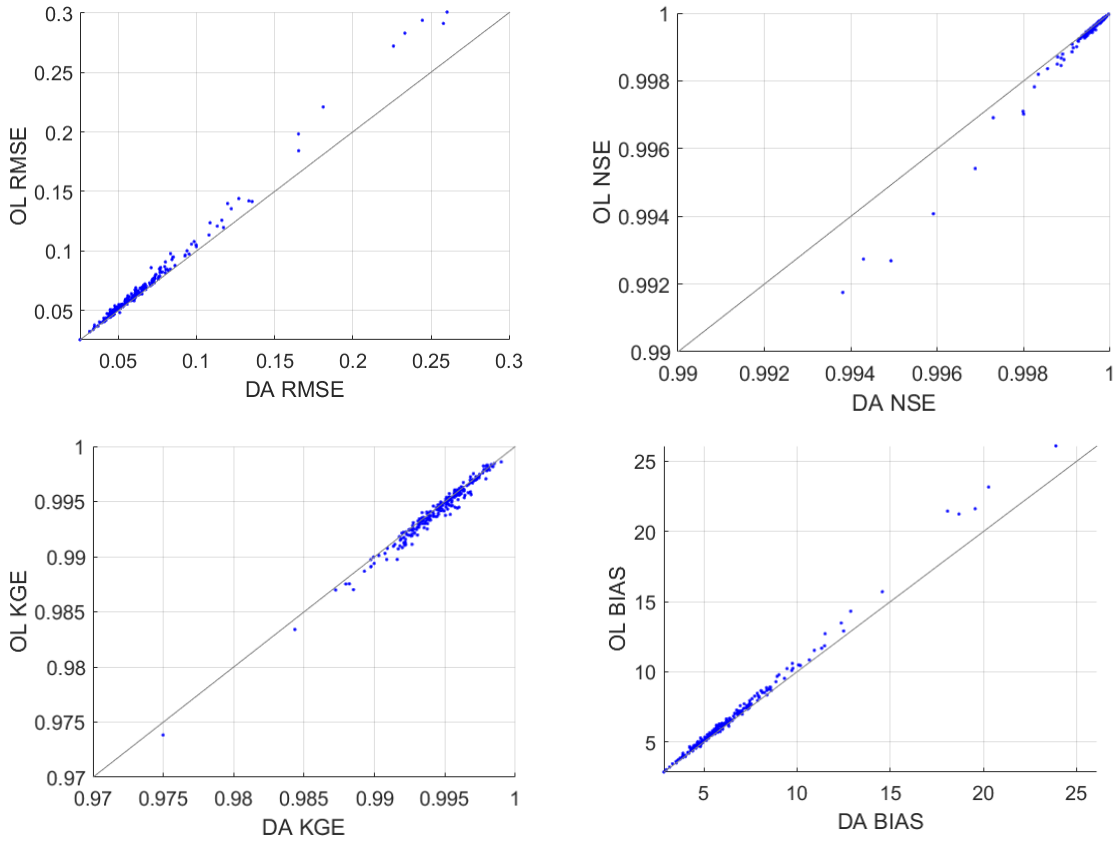

Figure 3-15: Univariate synthetic soil moisture assimilation results. Comparisons of OL and DA RMSE (upper left), NSE (upper left), KGE (lower left), and BIAS (lower right) in the Croton, NY area are presented in the scatter plots.

Table 3-2: Univariate synthetic soil moisture assimilation results. The spatial mean of performance measures of OL and DA over the domain in Croton, NY.

	RMSE	*NSE*	*KGE*	*BIAS*
OL	0.0704	0.9995	0.9945	6.7165
DA	0.0662	0.9996	0.9942	6.4511

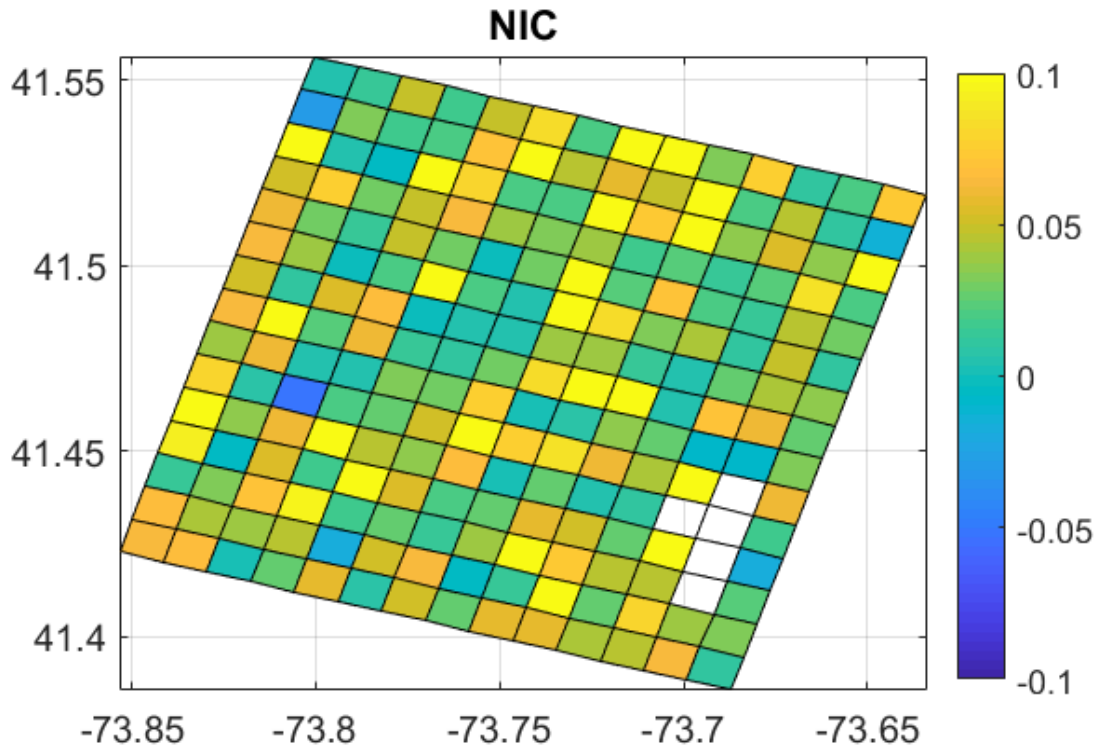

Figure 3-16: Univariate synthetic soil moisture assimilation results. The degree of improvement made by DA in the Croton, NY area is mapped. In 94.5% of the cells, the NIC is positive (improvements by DA) and in 5.4% of the area, the NIC is negative (degradation from DA).

3.7.1.1 Effect of univariate soil moisture assimilation on discharge

Since the DA adjusts the soil moisture state variable, it is expected that the updated states will transfer to streamflow through the routing component of the WRF-Hydro model. In this section, the effect of soil moisture DA on streamflow is discussed. Similar to the previous results, synthetic soil moisture is assimilated into the model. The adjustment made by DA to soil moisture at every time step is expected to change the

streamflow values at the next time steps. Therefore, during the DA run streamflow was also recorded. The resulting streamflow simulations were then compared with true streamflow. The performance measures are presented in Table 3-3. The first two rows indicate the Huntsville domain the rest of the rows indicate the Croton area.

Table 3-3: Univariate synthetic soil moisture assimilation results. The effects of soil moisture assimilation on streamflow are presented. The first two rows indicate the measures for the Huntsville domain and the lower three rows show the measures for the Croton area. OL and DA RMSE, NSE, BIAS, and KGE are shown in the columns. The last column shows NIC, the improvement made by DA over OL.

Station	$RMSE_{OL}$	$RMSE_{DA}$	NSE_{OL}	NSE_{DA}	$BIAS_{OL}$	$BIAS_{DA}$	KGE_{OL}	KGE_{DA}	*NIC*
Huntsville-1	0.8727	3.4169	0.9979	0.9974	0.0220	0.0164	0.9464	0.9698	-0.24
Huntsville-2	3.4188	24.4122	0.9970	0.9953	0.1176	0.1288	0.9503	0.9746	-0.09
Croton-1	0.24	0.24	0.99	0.99	12.93	12.93	0.97	0.97	0
Croton-2	0.59	0.59	0.99	0.99	27.13	27.13	0.96	0.96	0
Croton-3	0.88	0.88	0.99	0.99	42.93	42.93	0.96	0.96	0

It is observed that the discharge performance is not improved when soil moisture is assimilated. This complements on the previous studies, as discussed in the introduction, with SAC-SMA and other land surface models.

3.7.2 Univariate streamflow assimilation

In this scenario, synthetic streamflow observations at USGS gauges are assimilated into the WRF-Hydro model using a univariate EnKF algorithm. The effects of DA on both soil moisture and streamflow are assessed. In the Huntsville area, observations at two USGS gauges are assimilated. For the Croton domain, observations at three USGS locations are assimilated. The resulting streamflow from OL and DA runs

are recorded and compared against the true streamflow. The performance measures are presented in Table 3-4.

Table 3-4: Univariate synthetic streamflow assimilation results. The performances of OL and DA in simulating streamflow are measured by RMSE, BIAS, KGE, and NSE. The first three rows indicate the measures for the Croton domain and the lower two rows show the measures for the Huntsville area. The last column shows NIC, the improvement made by DA over OL.

	$RMSE_{OL}$	$RMSE_{DA}$	$BIAS_{OL}$	$BIAS_{DA}$	KGE_{OL}	KGE_{DA}	NSE_{OL}	NSE_{DA}	NIC
Croton-1	0.24	0.15	12.93	9.67	0.97	0.98	0.99	0.99	0.35
Croton-2	0.59	0.25	27.13	14.05	0.96	0.98	0.99	0.99	0.56
Croton-3	0.88	0.43	42.93	24.76	0.96	0.98	0.99	0.99	0.51
Huntsvill-1	0.40	0.38	0.02	0.01	0.94	0.97	0.99	0.99	0.05
Huntsville-2	2.11	0.88	0.11	0.04	0.95	0.98	0.99	0.99	0.58

It is noted that the DA is significant in improving streamflow simulations as indicated by NIC (in the last column of Table 3-4). All NIC values are positive. This indicates that the DA outperforms the OL. The lowest degree of improvement is observed in the internal gauge of the Huntsville domain. The highest degree of improvement is observed at the outlet of the Huntsville area. In the Croton domain, the upper gauge has the lowest improvements (similar to the upper gauge in the Huntsville). The highest improvements (56%) are observed at the middle gauge of the domain. The outlet is expected to have the highest degree of improvements. The lower performance at the outlet than the middle gauge in the Croton area is attributed to the lake just upstream of the outlet and downstream of the middle gauge.

3.7.2.2 Effect of univariate streamflow assimilation on soil moisture

The influence of streamflow DA on soil moisture is assessed in this section. Observed streamflow is assimilated into the WRF-Hydro model at USGS gauge locations. In the assimilation process, soil moisture is also recorded. The resulting soil moisture is then compared with the true soil moisture and the performance measures are calculated accordingly. Spatially-averaged performance measures (RMSE, NSE, KGE, and BIAS) are shown in bar plots in Figure 3-17. The upper left plot compares RMSE. It is observed that the RMSE of DA is lower than the RMSE of OL. Similar results are observed for NSE, KGE, and BIAS. In all the plots, the outperformance of DA over OL is confirmed. A similar analysis is presented for the Croton, NY area in Figure 3-18.

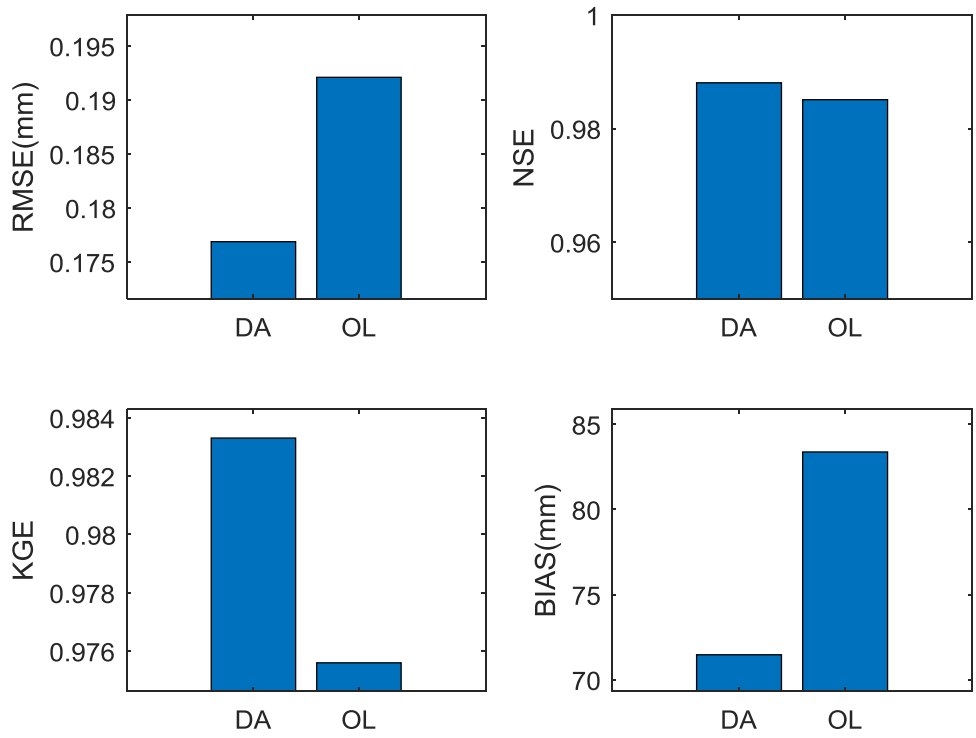

Figure 3-17: Univariate synthetic streamflow assimilation results. The effect of streamflow assimilation on soil moisture is evaluated. RMSE (upper left panel), NSE (upper right panel), KGE (lower left panel), and BIAS (lower right panel) are plotted for OL and DA. The bars show the spatially averaged. The study area is Huntsville, AL.

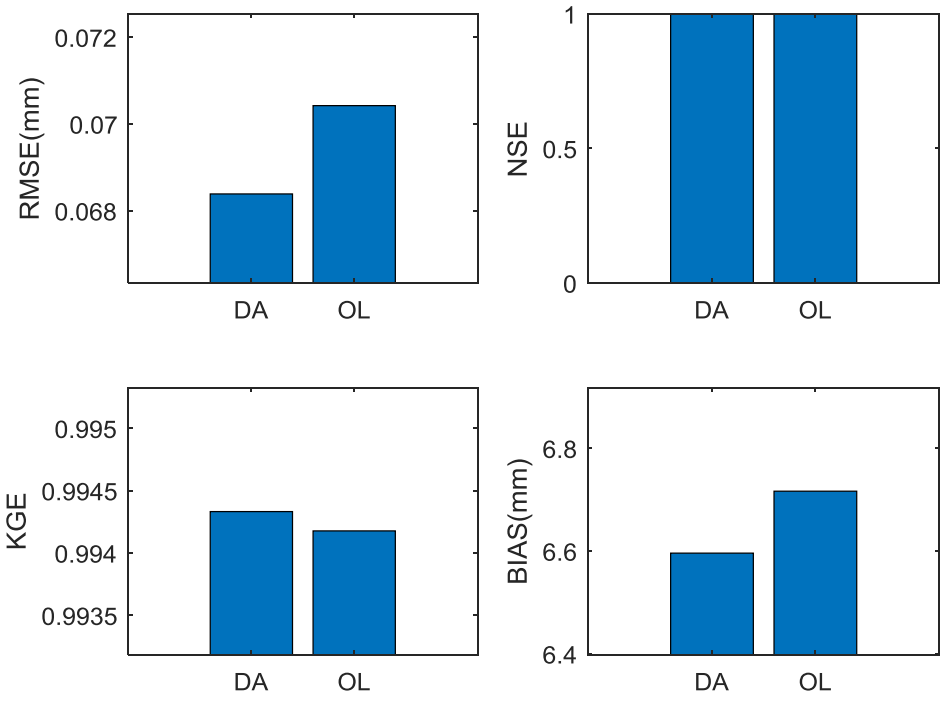

Figure 3-18: Univariate synthetic streamflow assimilation results. Same as Figure 3-17 but for the Croton, NY area.

A more detailed comparison is presented in Figure 3-19. Scatter plots are used. Points indicate domain grid cells. The lower left panel of this figure compares the BIAS in OL and DA. The gray line indicates the 1:1 line. If a point falls on this line, it means that the OL and DA have equal performance. If it falls above the line, it means that the BIAS in OL is higher than the BIAS in DA which indicates the outperformance of DA over OL. If a point falls below this line, it means that the OL outperforms the DA. It is noted that all points in this plot are above the 1:1 line; indicating the outperformance of DA over OL. This result is confirmed by other scatter plots of the figure. RMSE of DA in

all points is lower than the RMSE of OL. The DA NSEs of all points are higher than OL NSEs. Similarly, the DA KGEs of all points are higher than the OL KGE.

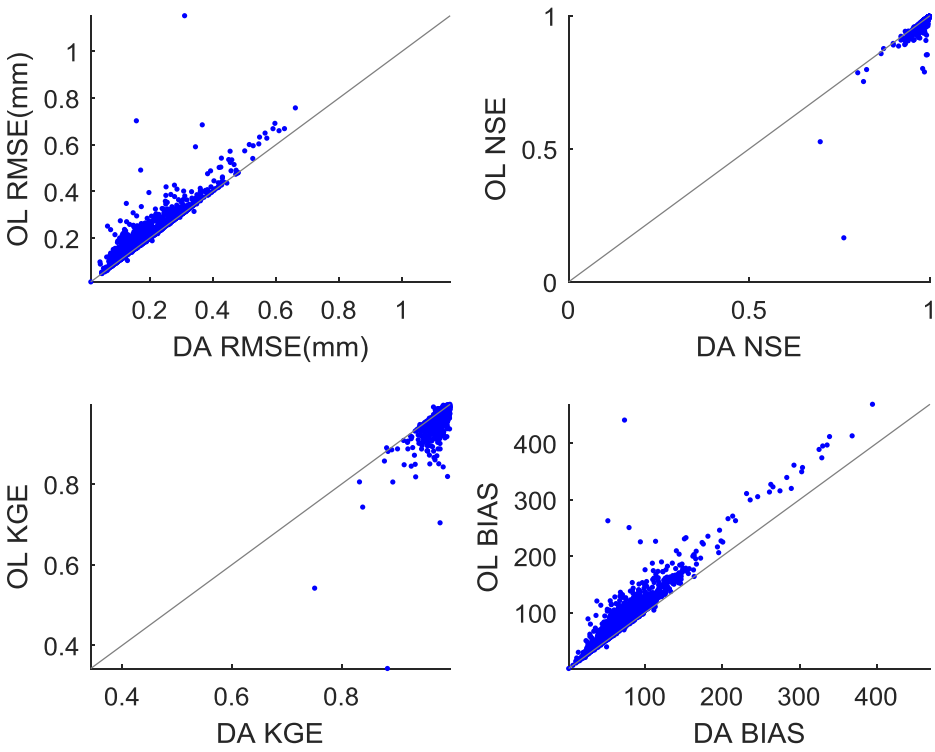

Figure 3-19: Univariate synthetic streamflow assimilation results. The effect of streamflow assimilation on soil moisture is evaluated. RMSE (upper left panel), NSE (upper right panel), KGE (lower left panel), and BIAS (lower right panel) are plotted for OL and DA. Points represent grid cells in the area. The gray line is the 1:1 line that indicates the equal performance of OL and DA. The study area is Huntsville, AL.

Finally, the degree of outperformance of DA over OL is directly measured by NIC. Positive values of NIC show that DA performs better than OL. Higher values of NIC indicated higher improvements. Negative values, on the other hand, indicate degradation by DA over OL. The spatial variation on NIC in the Huntsville area is mapped in Figure 3-20, the upper panel. It is observed that the NIC values are positive for all grid cells. The histogram of the NICs shown in the lower panel of the figure indicates that the improvements are as high as 40%. For the majority of the cells, the improvements are less than 10%.

Comparing these results with the results of the previous scenario indicates that the improvements here are lower. This means that higher improvements in soil moisture are achieved in the univariate soil moisture DA. Therefore, while both DAs are capable of improving soil moisture, direct assimilation of soil moisture is suggested. However, in cases where both soil moisture and streamflow improvements are of interest, multivariate EnKF is used, as shown in the next section.

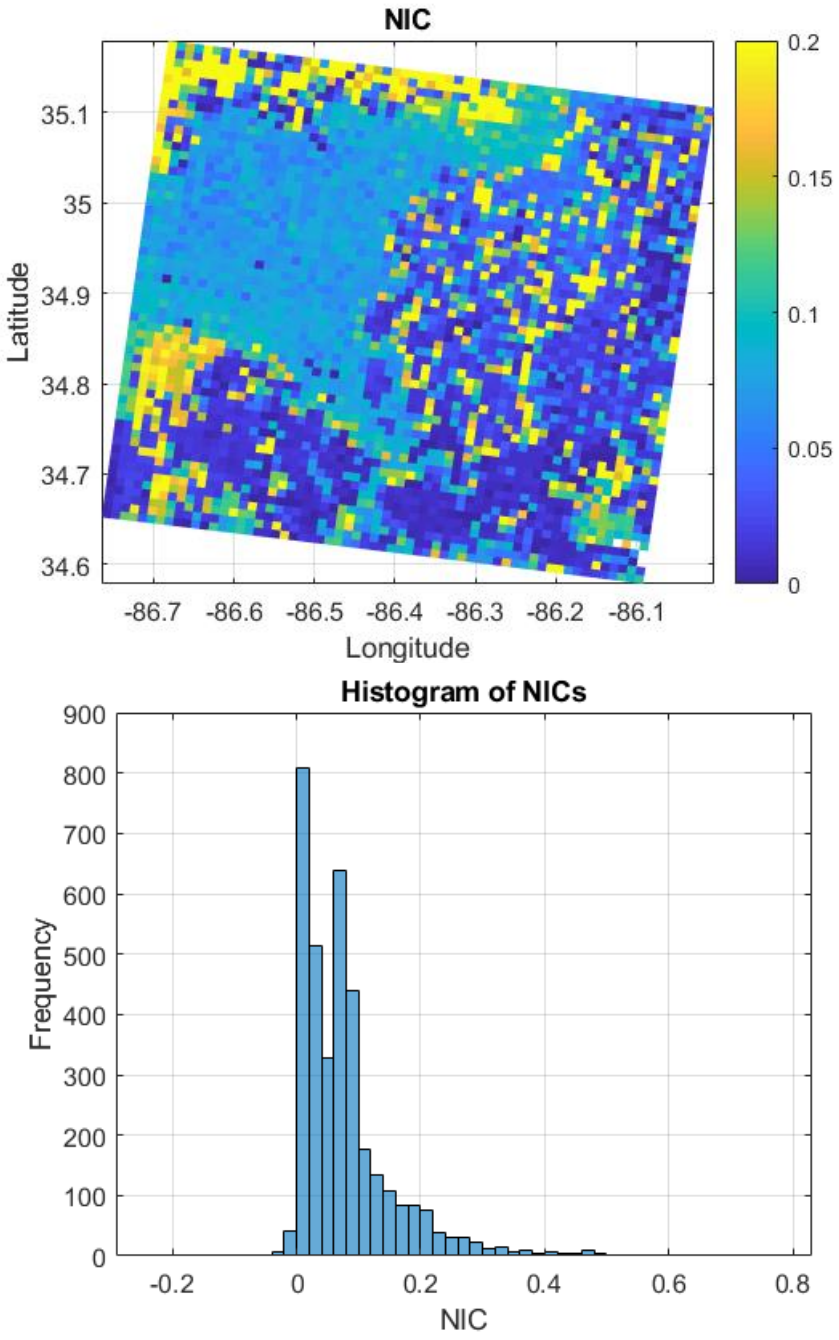

Figure 3-20: Univariate synthetic streamflow assimilation results. Improvements of DA over OL in soil moisture simulations in the scenario that univariate streamflow is assimilated at USGS gauges. The study area is Huntsville, AL. The spatial variation of NIC is mapped in the upper panel and the histogram of grid cell NICs is plotted in the bottom.

3.7.3 Multivariate assimilation of soil moisture and streamflow

In this section, the results of assimilating both soil moisture and streamflow using a multivariate EnKF are explained. Synthetic streamflow is assimilated at USGS gauges and synthetic soil moisture is assimilated in every grid cell over the LSM terrain with a resolution of 1 (km) in WRF-Hydro. The effects of assimilation on soil moisture are discussed first followed by the effects on streamflow.

3.7.3.3 Effect of multivariate streamflow/soil moisture assimilation on soil moisture

Soil moisture simulations were compared with the true soil moisture and the performance measures were computed. The spatially averaged performance measures for OL and DA are presented in Figure 3-21. In the RMSE and BIAS charts, the DA is lower and in the NSE and KGE charts, the OL is higher. All four plots indicate the outperformance of DA over OL.

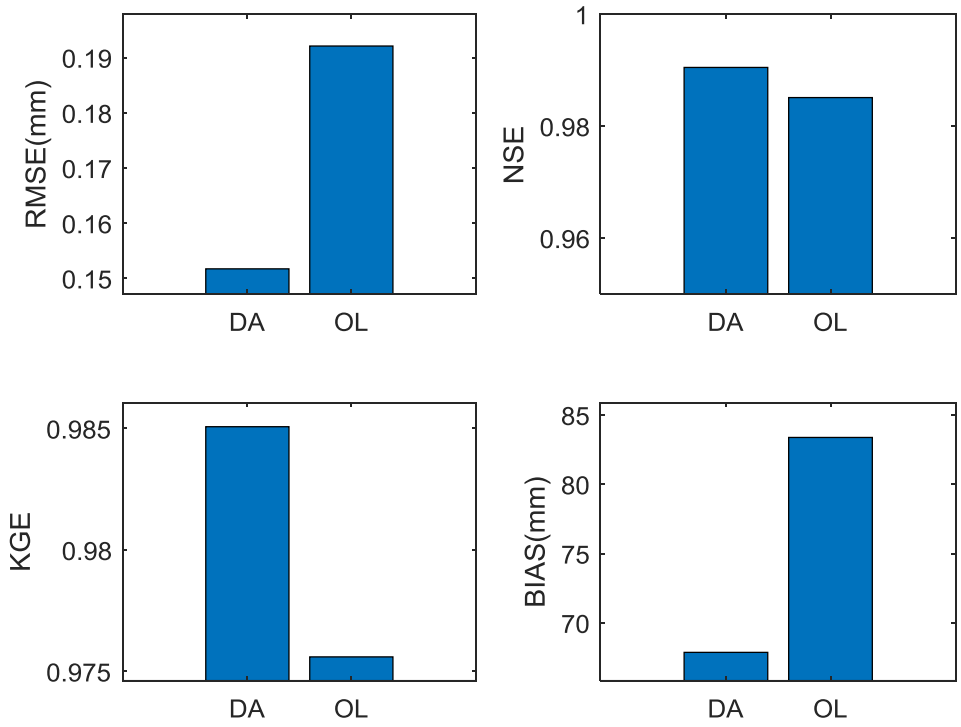

Figure 3-21: Multivariate synthetic streamflow and soil moisture assimilation results. OL and DA performance measures for soil moisture simulations in Huntsville, AL.

The spatial distributions of these measures are shown in Figure 3-22. Maps are provided for RMSE, NSE, KGE, and BIAS in this figure. The left column shows the OL results and the right column shows the DA results. From BIAS and RMSE, it is observed that OL has a high error in the western part of the domain which is the urban Huntsville area. DA shows lower biases in these areas. Similar results are confirmed by the NSE and KGE maps.

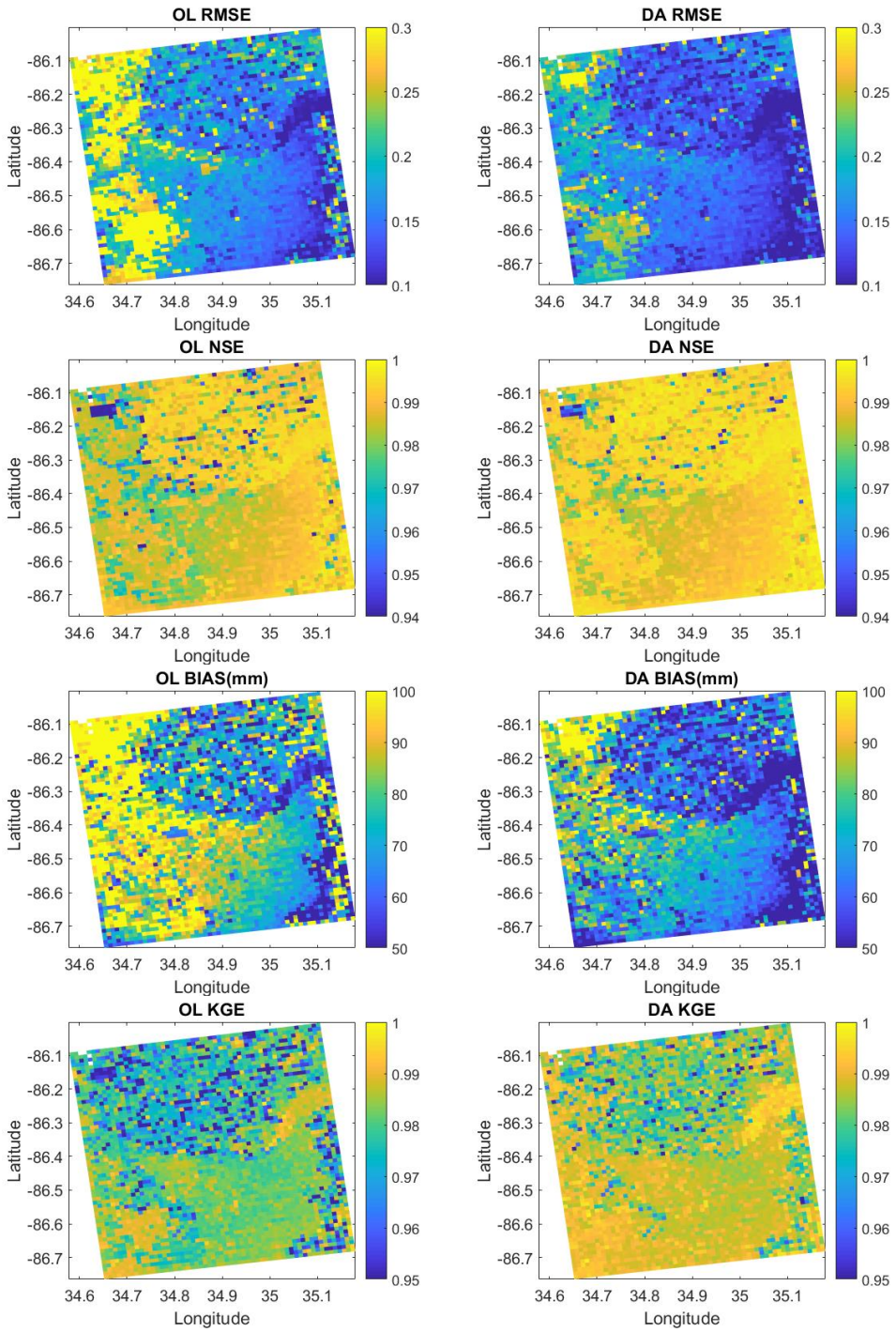

Figure 3-22: Multivariate synthetic streamflow and soil moisture assimilation results. Spatial distributions of RMSE, NSE, BIAS, and KGE measures are provided in row 1, 2, 3, and 4, respectively. The left column shows OL and the right column shows the DA. The study area is Huntsville, AL.

Cell-wise comparisons are presented in Figure 3-23. Scatter plots are provided to compare OL and DA RMSE, NSE, KGE, and BIAS. Dots in these plots indicate the grid cells in the domain. The gray lines are 1:1 lines. Points that fall on this line indicate a similar performance of OL and DA. In RMSE and NSE the points that fall above this line show a better performance of DA and in NSE and KGE, the points that are below the line show a better performance of DA. In all of the figures, the distributions of the dots show the outperformance of DA over OL which confirms the results of the previous figures.

Finally, the improvements made by DA over OL are quantified by NIC, as discussed in the methodology section. Positive values of NIC indicate the outperformance of the DA. Higher values indicate better performances. The spatial distribution of NIC is shown in Figure 3-24, the upper panel. It is observed that in the urban area, the outperformance is lower (about 12%). In the main watershed, the outperformance increases to more than 20%. The histogram of the NICs is shown in the second panel of this figure. It is noted that in the majority of cells, the NIC is between 0 to 10%. The improvements are as high as 50%.

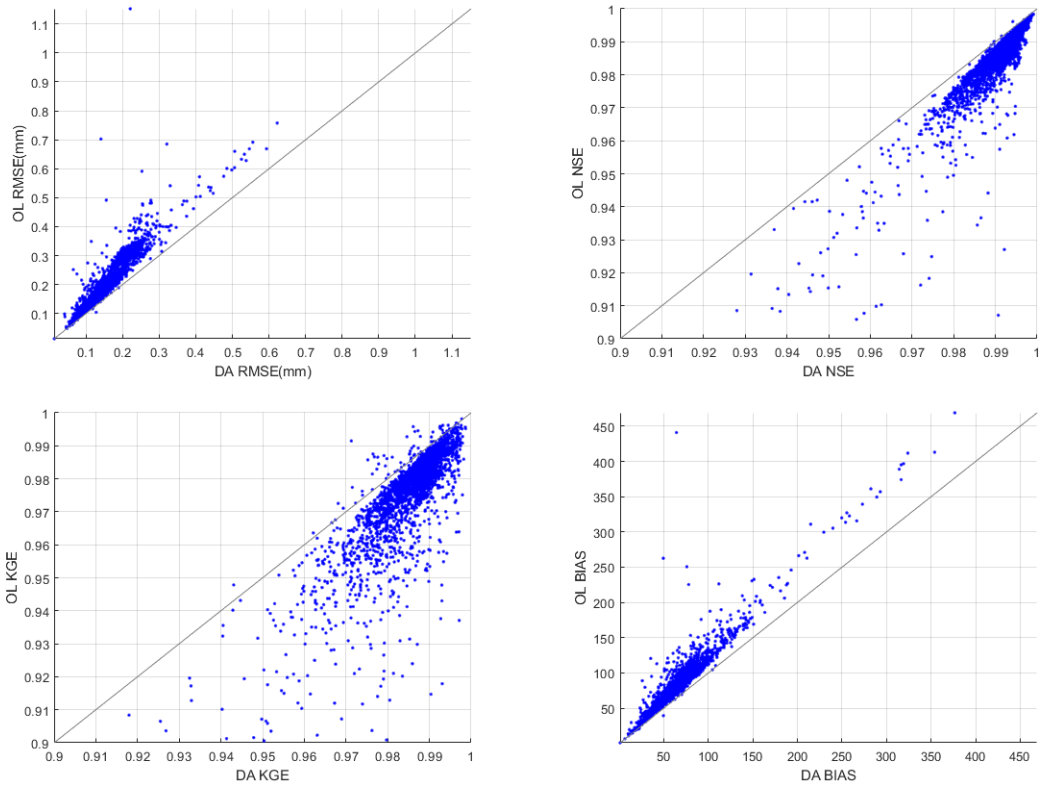

Figure 3-23: Multivariate synthetic streamflow and soil moisture assimilation results. Cell-wise comparisons of OL and DA performance in Huntsville, AL. Dots represent cells in the domain. The gray line is the 1:1 line.

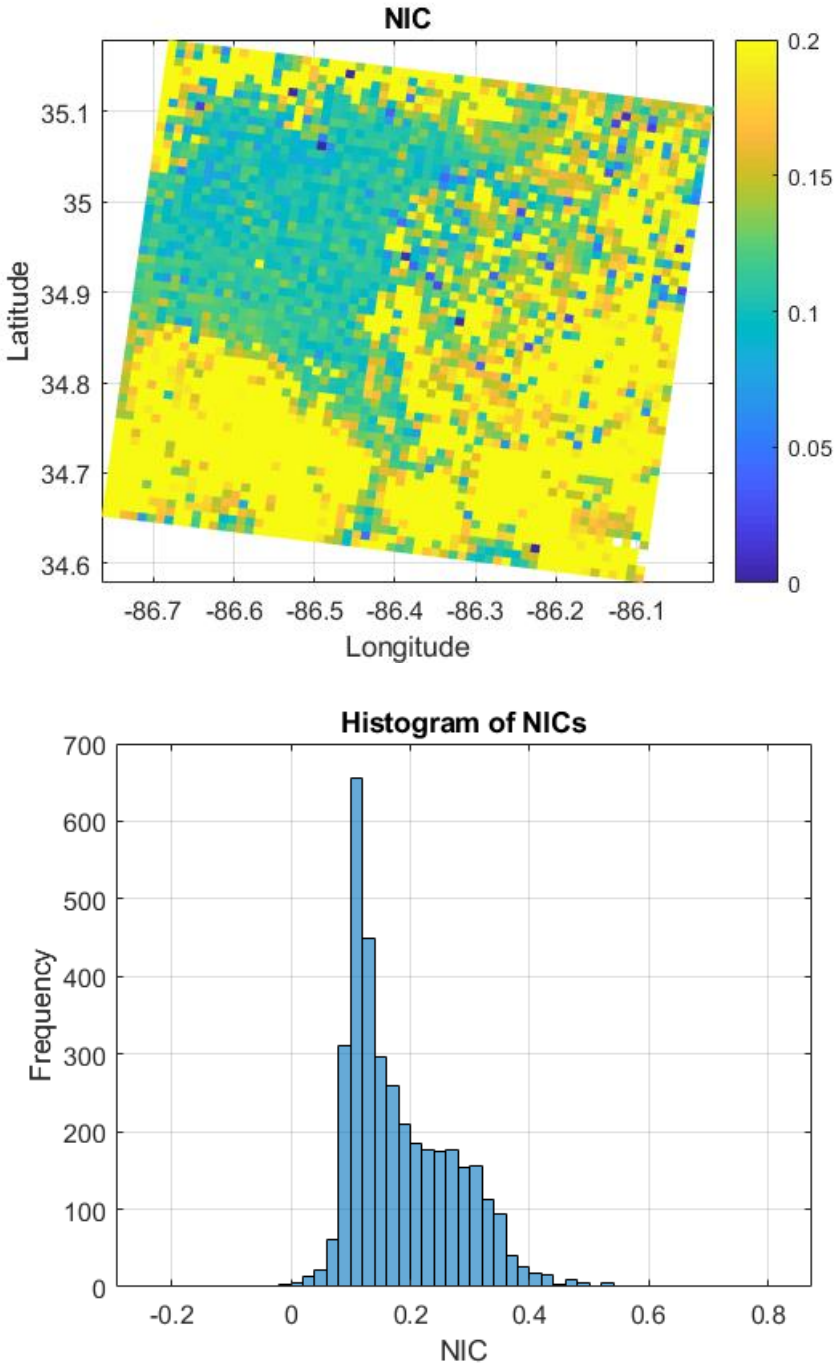

Figure 3-24: Multivariate synthetic streamflow and soil moisture assimilation results. The degree of improvement of DA over OL for soil moisture simulations as indicated by NIC for Huntsville, AL. The spatial distribution of the improvements is shown on the upper panel. The histogram of the values is shown in the lower panel.

Next, similar results are provided for the Croton, NY area. The NICs are mapped in Figure 3-25. NIC is positive in 71% of the cells and it is negative in 29% of the area. The improvements are as high as 15%. The spatially averaged performance measures are also shown in Table 3-5. KGE and NSE are not different in OL and DA while RMSE and BIAS indicate a marginally lower error in DA.

Table 3-5: Multivariate synthetic streamflow and soil moisture assimilation results. Comparison of spatially-averaged performance of OL and DA in simulating soil moisture in Croton, NY is performed.

	RMSE	*NSE*	*BIAS*	*KGE*
OL	0.07	0.99	6.71	0.99
DA	0.06	0.99	6.59	0.99

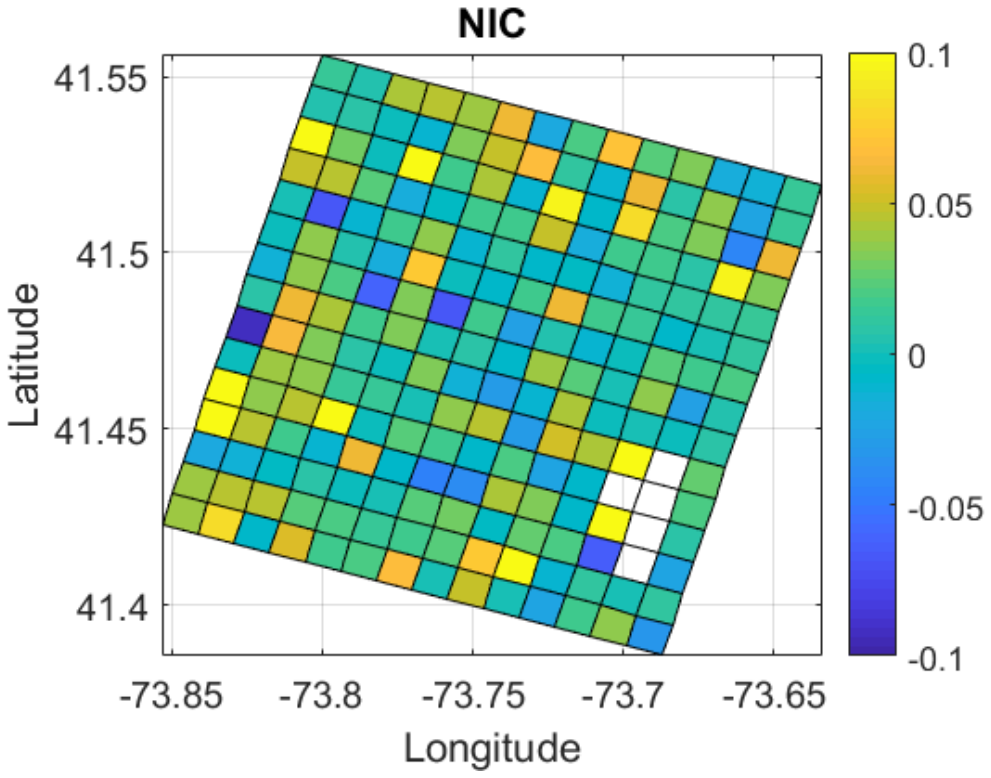

Figure 3-25: Multivariate synthetic streamflow and soil moisture assimilation results. The spatial distribution of NIC as an indication of improvements by DA over OL in simulating soil moisture is mapped. The white cells indicate the water bodies.

3.7.3.4 Effect of univariate streamflow assimilation on streamflow

The effects of dual soil moisture and streamflow assimilation on streamflow are presented in the following. Table 3-6 shows the performance measures in both areas at USGS gauge locations. It is noted that streamflow in all the USGS gauges is improved by DA. These improvements are as high as 49% in the middle gauge of the Croton area. For the Huntsville area, the improvements are as high as 58% at the outlet. The upstream gage is not improved significantly by the DA.

Table 3-6: Multivariate synthetic streamflow and soil moisture assimilation results. Comparison of performance measures of OL and DA in simulating streamflow in all gages in both watersheds. A better performance is shown in bold.

	$RMSE_{OL}$	$RMSE_{DA}$	$BIAS_{OL}$	$BIAS_{DA}$	KGE_{OL}	KGE_{DA}	NSE_{OL}	NSE_{DA}	*NIC*
Croton-1	0.24	**0.12**	12.93	**8.42**	0.97	**0.99**	0.99	0.99	0.48
Croton-2	0.59	**0.30**	27.13	**16.12**	0.96	**0.98**	0.99	0.99	0.49
Croton-3	0.88	**0.57**	42.93	**30.21**	0.96	**0.98**	0.99	.99	0.34
Huntsvill-1	0.40	**0.38**	0.02	**0.01**	0.95	**0.98**	0.99	0.99	0.05
Huntsville-2	2.11	**0.88**	0.11	**0.04**	0.94	**0.97**	0.99	0.99	0.58

3.7.4 Summary of the performance measures

A summary of the performance measures is provided in Table 3-7. It is noted that highest soil moisture improvements are achieved when a univariate EnKF is used to assimilate soil moisture into the WRF-Hydro model. Next high improvements in soil moisture are achieved by dual assimilation of soil moisture and streamflow. Finally, when discharge is assimilated using a univariate EnKF, soil moisture improvements are observed; however, the improvements are not as high as other scenarios.

The highest degree of improvements is achieved by direct univariate assimilation of streamflow. Dual assimilation results in improved streamflow, too (with lower improvements, though). However, streamflow simulations are not improved in the case of univariate soil moisture assimilation.

Table 3-7: Summary of performance measures in all scenarios. NI indicates no improvement, P_{25}, μ, and P_{75} indicate the 25th, average, and the 75th spatial percentile. The first column from left is associated with the scenario of univariate assimilation of soil moisture. The middle column results are related to the univariate assimilation of streamflow, and the third column (on the right) indicates the result of multivariate assimilation of both soil moisture and streamflow. Numbers are in percent.

		Soil Moisture			Discharge			Soil moisture and discharge		
Huntsville	SM	P_{25}	μ	P_{75}	P_{25}	μ	P_{75}	P_{25}	μ	P_{75}
		11.56	16.14	25.42	2	6	9	11.54	16.05	25.15
	Q-upstream	NI			5.06			5.25		
	Q-outlet	NI			58.19			58.0		
Croton	SM	P_{25}	μ	P_{75}	P_{25}	μ	P_{75}	P_{25}	μ	P_{75}
		2	3	6	NI			0	1.57	3.86
	Q-upstream	NI			35			48		
	Q-middle	NI			56			49		
	Q-outlet	NI			51%			34%		

The results indicate the added value of multivariate data assimilation. This DA leads to improved soil moisture and streamflow. The next scenario that improves both variables is streamflow assimilation. Even though the soil moisture improvements in this scenario are not as high, it is recommended as no degradation is observed. Soil moisture

assimilation is recommended in cases where the focus is on soil moisture. If streamflow is not of interest, this scenario is recommended.

3.8 Real study

To be consistent with the current implementation of the National Water Model, for the real case study, streamflow is assimilated. Streamflow with an assumed coefficient of variation of 15% is assimilated into the WRF-Hydro using EnKF and the model states and outputs are updated. This has been done for three gauges in the Croton area and at the outlet of the Huntsville area. The streamflow observations are acquired from the USGS observations. Results indicate that DA is capable of improving flow simulations up to 80%. As shown in Table 3-8, the highest improvements are observed in the outlet of the Huntsville area followed by the middle gauge of Croton, NY. The lower performance improvement in the middle gauge compared to the outlet is attributed to the lake that is just upstream of the outlet. Other performance measures including BIAS, RMSE, NSE, and KGE are shown in Figure 3-26 and Figure 3-27. Figure 3-28 compares flow simulations with regards to observations. In all gauges, the intensified performance of the DA is an indication of its effectiveness.

Table 3-8: OL and DA root mean square errors and the degree of improvements by DA for the real case study.

	$RMSE_{OL}$	$RMSE_{DA}$	*NIC*
Croton, NY-Gage1	5.807	1.936	0.666
Croton, NY-Gage2	11.867	2.464	0.792
Croton, NY-Gage3	21.299	5.320	0.750
Huntsville, AL	52.332	8.435	0.838

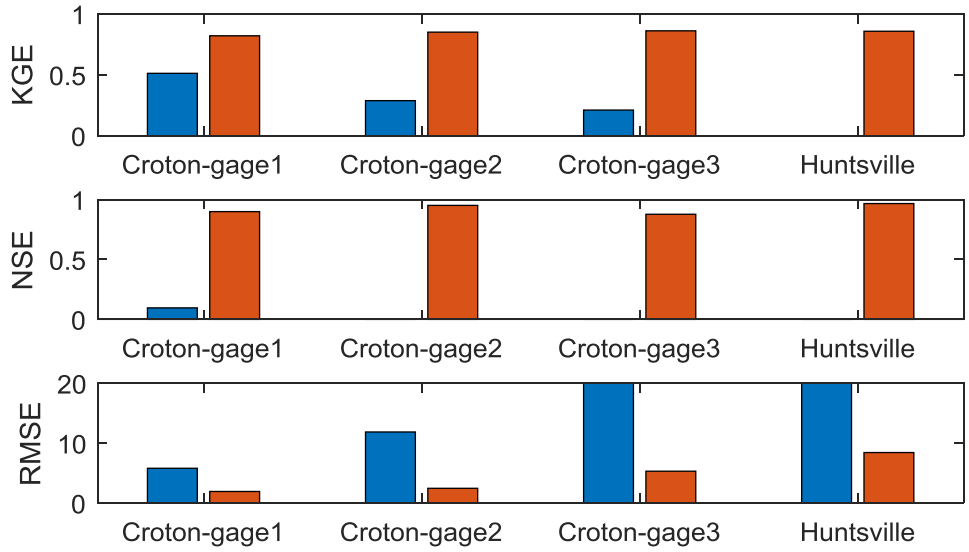

Figure 3-26: Streamflow performance measures of the OL and DA. The blue bars indicate OL and the orange bars indicate DA. KGE and NSE are dimensionless and RMSE is in m^3/s

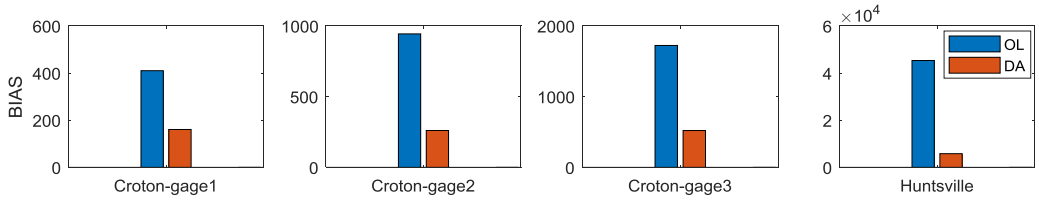

Figure 3-27: BIAS (in m^3/s) in the studied gauges. The DA technique is a univariate EnKF to assimilate streamflow observations.

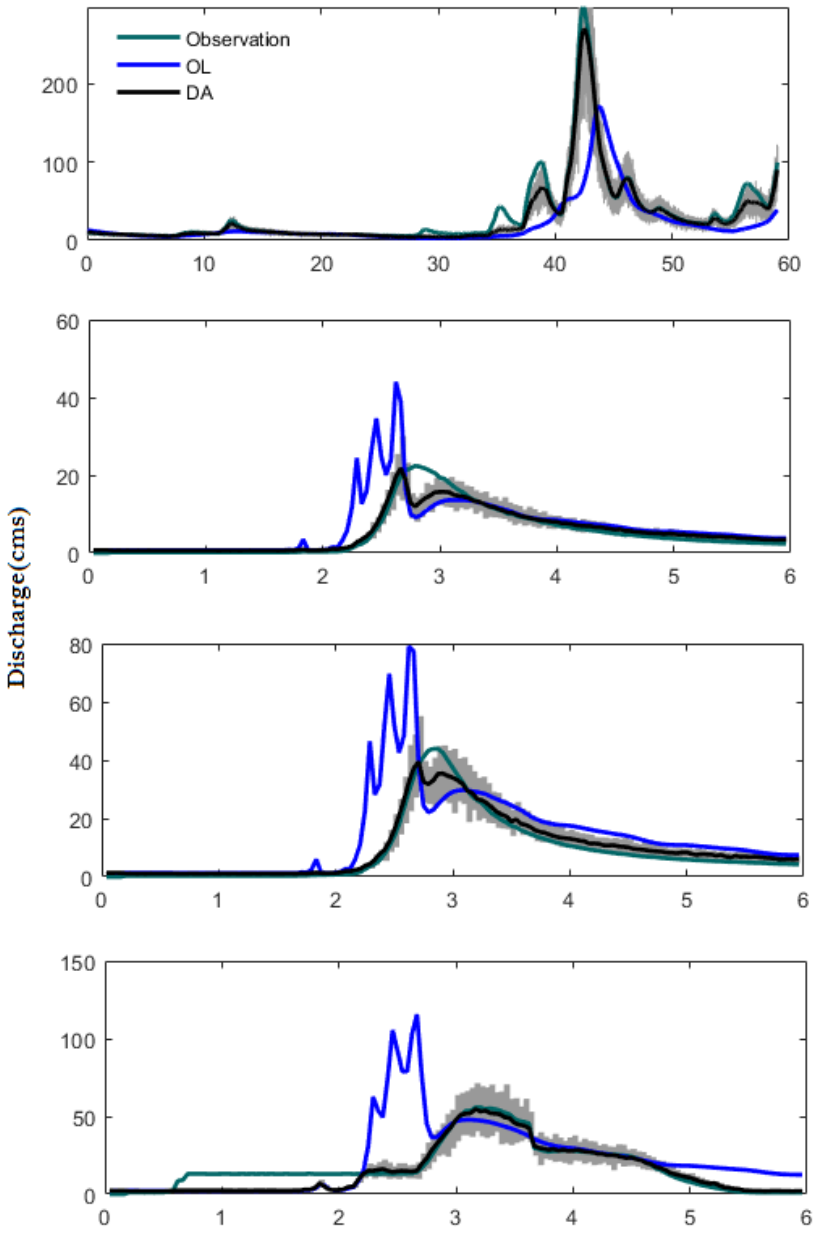

Figure 3-28: Comparison of OL, DA and observed streamflow in (1) Huntsville outlet, (2) upstream gauge of Croton, (3) middle gauge of Croton, and (4) outlet gauge in Croton.

3.9 Conclusion and discussion

With an overarching goal of improved flood modeling skill, this study focused on two critical variables in the hydrologic cycle including soil moisture and streamflow. The added value of ensemble data assimilation into the community WRF-Hydro model was assessed in three steps:

First, univariate Ensemble Kalman Filter was employed to assimilate satellite soil moisture observations in WRF-Hydro. This assimilation resulted in improved soil moisture simulation and demonstrated successful data assimilation into the model. The employed errors and the parallel computing methodology could be used for any future data assimilation study. Moreover, the effects of this assimilation on streamflow were investigated. It was observed that improvements in outlet streamflow were limited. This implies the inability of the model in propagating soil moisture assimilation information to streamflow. Similar results were reported by studies on less complex land surface models, which indicates that even with such a complex model as WRF-Hydro, it is hard to update other variables.

Next, univariate Ensemble Kalman Filter was employed to assimilate USGS streamflow observations in WRF-Hydro. Significant improvements were observed in streamflow simulations; however, no significant improvement in soil moisture simulations was observed.

Finally, multivariate Ensemble Kalman Filter was employed for simultaneously assimilating soil moisture over the area and streamflow at the outlet. Significant

improvements in both soil moisture and streamflow simulations were observed. The highest degree of improvements (20% to 80%) was observed in non-urban areas of the study area while the improvements decreased in urban areas (~10%). This could be an indication of model inadequacy in urbanized watersheds. Moreover, the most significant improvements were observed around the peak of the flood and the least significant improvements were at low-flows.

Therefore, the main findings of this study are as the following.

The choice of the variable to be assimilated in ensemble data assimilation depends on the goal of the assimilation. If an atmospheric scientist, for example, aims at coupling WRF-Hydro with WRF and cares about the outputted atmospheric variables, univariate assimilation of soil moisture is adequate and there is no need for assimilation of streamflow. However if a hydrologist, for example, seeks improved flood forecasting at the outlet of a watershed, assimilating streamflow using univariate ensemble data assimilation is suggested. Finally, the author suggests that operational agencies such as the NWC, that need to improve both soil moisture and streamflow, consider dual assimilation of soil moisture and streamflow using a multivariate ensemble data assimilation technique. The employed parallel algorithm explained in the previous chapter can be used for an efficient implementation of such data assimilation with less computational demand.

It is acknowledged that running ensemble data assimilation continuously at a large scale such as the Continental United States could result in delay in delivering the

forecasts or a too high computational demand, and a framework with less frequent assimilation might be more favorable. In this case, the author suggests using ensemble data assimilation only in cases that a flood is expected. The fact that the ensemble data assimilation had the most significant improvements around the peak of the flood supports this suggestion. A reasonable strategy would be starting the Ensemble Kalman Filter DA (with initial conditions from the nudging algorithm) once the streamflow magnitude passes a certain percentile of the climatology (75%, for example). This way, the computational burden of ensemble data assimilation is not imposed all the time and at the same time, the forecasts benefit from the advantages that ensemble data assimilation offers, those that the nudging algorithm does not have.

A future extension of this study may conduct the same analysis for various seasons. There is a high possibility that in some seasons, DA is more crucial than other seasons or the variable of interest may vary depending on the season. This can save significant computational power and time in an operational setting.

Similar to the referred studies, this work does not consider the time lag between the updated soil moisture information and streamflow in the outlet. This is also highlighted by Clark et al. (2008) and a future extension of this paper can investigate a suitable time lag with regard to the time of concentration of the watershed. The second chapter of this dissertation focused on the core column LSM in the NWM; the Noah-MP model, This chapter expanded on the previous chapter by studying the WRF-Hydro model which adds routing components to Noah-MP, and unlike Noah-MP that does not

transfer information from one cell to another and ignores the lateral movement of water, WRF-Hydro accounts for the lateral movements too. This chapter will be followed by a study where the NWM and uncertainties in flood forecasting are investigated. In the next chapter, the potential improvements that DA and satellite remote sensing can have on flood forecasting will be assessed.

.

4 Improved National Water Model forecasts based on Ensemble data assimilation

4.1 Abstract

Quantification of uncertainty in flood forecasting systems is studied in the current chapter. A frequently studied source of uncertainty in flood forecasting systems comes from the atmospheric forcing inputs. This study moves toward full uncertainty quantification by simultaneously accounting for both atmospheric forcings and initial condition uncertainties. Initial condition uncertainty is quantified by ensemble data assimilation where a hydrologic model is run up to the forecast initial date with the assimilation of USGS streamflow observations. Ultimately, the updated model states in the forecast date are considered to represent the initial condition uncertainty. The benefits of initial condition uncertainty quantification are underscored in this study. The results show improvements up to 80%. Improvements in short-, medium-, and long-range forecasts are evaluated and it is observed that short-range forecasts are significantly sensitive to initial conditions. It is observed that the effects of an updated initial condition last for two days. After that, the system forgets about the initial condition and atmospheric forcings become dominant. The results of this study highlight the importance of initial condition uncertainty and encourage more attention to this source of uncertainty. Besides, this work can help operational flood forecasting agencies such as the National

Water Center to improve flood forecasts. Uncertainty quantification and ensemble runs are particularly suggested.

4.2 Introduction

A reservoir manager has to decide whether to release water or not. Such decision is based on upstream soil moisture condition and snowpack, precipitation forecast, and anticipated streamflow. The manager needs to evaluate the trade-off between alternatives including releasing water before a storm begins to avoid overtopping or retaining water for customers in downstream. In the former case, if the precipitation is less than expected, the water is lost and in the latter case, if the precipitation is more than expected, the reservoir can be topped which is followed by catastrophic flooding in the downstream (Schaake et al., 2007). Remarkable uncertainties are inherent in similar examples mainly because weather forecasts are imperfect. A natural approach to tackle these myriad uncertainties is probabilistic weather forecasts in the form of an ensemble of possible weather conditions. The manager in the above example can benefit from a probabilistic forecast by weighing the costs of reduced storage from a dam release against the probability of flooding and hazards in case of not releasing water (Schaake et al., 2007).

Rather than single deterministic forecasts, the flood forecasting community (in both operation and research) is moving towards forcing hydrological models with multiple weather forecasts for the same location and time in the form of an ensemble. The forecasts come from numerical weather prediction (NWP) models. Such system is also known as Ensemble Prediction System (EPS) (Cloke and Pappenberger, 2009). NWPs

are the results of sophisticated computer runs on supercomputers to solve numerical atmospheric equations and predict variables such as rainfall, temperature, pressure, and wind speed and are well known for forecasting day-to-day changes of weather states (Bowler et al., 2008; Shutts, 2005; Wei et al., 2006). An ensemble of NWPs accounts for the uncertainties associated with the atmosphere resulting from the inability to determine the exact state of the system due to its non-linearity and complexity, spatiotemporal resolution of the simulations, etc. The North American Multi-Model Ensemble (NMME) (Khajehei et al., 2018; Kirtman et al., 2014) that uses an ensemble of NWPs is a recent example.

Currently, several flood-forecasting centers are considering the adoption of NWP-EPS and many others are already using it. For example, NOAA Advanced Hydrological Prediction Services (AHPS) uses National Weather Services (NWS) weather predictions for their EPS. Similarly, European forecast centers such as Finnish Hydrological Services, Royal Meteorological Institute of Belgium (Roulin and Vannitsem, 2005; Roulin, 2006), and Swedish Hydro-Meteorological Services (Johnell et al., 2007) use European Center for Medium-Range Weather Forecasts (ECMWF) data as their NWP input. Moreover, several international bodies support the use of ensemble prediction systems such as Hydrologic Ensemble Prediction Experiment (HEPEX) (Schaake et al., 2007), an open participatory project with the goal of bringing scientists with different backgrounds together and improving hydrologic forecast techniques through interdisciplinary collaborations. Other examples include the International Commission

for the Hydrology of the Rhine Basin (CHR), World Meteorological Organization (WMO), and the International Commission for the Protection of the Danube River (ICPDR).

Numerous studies have focused their attention on enhancing flood forecasting skill by improving weather forecasts. Often, they assume that increasing the spatial resolution of weather simulations removes some of the large errors; however, the improvement in the forecast skill is restricted by computing power and storage limits. As a compromise, clustering ensemble members is proposed (Cloke and Pappenberger, 2009; Thirel et al., 2008) where depending on the purpose of the EPS, some ensemble members are prioritized (Molteni et al., 2001; Verbunt et al., 2007). Another attempt to improve the weather forecasts includes building an ensemble of predictions from different forecast centers and forming a grand ensemble by combining different ensembles (Park et al., 2008).

While the meteorologists explore the opportunities of upgrading the weather forecasts, hydrologists are after advancing the flood forecasting systems by, for instance, downscaling NWPs, and correcting for bias or dispersion. Main challenges for hydrologic modeling are (1) identifying the sources of uncertainty, (2) identifying the implications of an imperfect hydrologic model, and (3) addressing all sources of uncertainty in the final hydrologic ensemble prediction (Schaake et al., 2006). In most cases, errors in meteorological forcings are considered as the greatest source of uncertainty in the flood forecasting procedure (Cloke and Pappenberger, 2009). Such errors cascade through the

model and thus produce uncertain flood forecasts; however, there is no mutual agreement on the sensitivity of flood forecasts on the input uncertainty, and the results vary case by case. For example, some studies conclude that uncertainty in precipitation is amplified through the flood forecasting system (Komma et al., 2007) while others conclude that it is neither amplified nor dampened (Cloke and Pappenberger, 2009; Olsson and Lindstrom, 2008). Cloke and Pappenberger (2009) demonstrated that input uncertainty could be augmented or shrunk (or neither) depending on the watershed characteristics such as the size, resolution of forcing data, and the dominant surface runoff process. In addition, they highlight that a watershed's sensitivity to meteorological forcings is not static and it changes in space and time. Such investigations have been discussed frequently in the literature (Dodov and Foufoula-Georgiou, 2005; Smith et al., 2004; Woods and Sivapalan, 1999). Other sources of uncertainty, however, need more attention. These uncertainty sources include but are not limited to the initial condition, imperfect hydrologic models, and parameterization.

Full uncertainty quantification requires representing all sources of uncertainty. A notable source of uncertainty that is often ignored is initial condition uncertainty. Initial conditions provide the foundation for the hydrologic processes within the hydrologic model and erroneous initiation of the model results in a deviation from the true states. A study by Wood and Lettenmaier (2008) underscores the importance of quantifying initial condition uncertainties. They assess the importance of initial condition versus boundary forcing uncertainties and conclude that depending on space and season, one could be

more critical than the other. They also highlight that the currently used flood forecasting methods lack a mechanism for representing initial condition errors. Moreover, it is shown that more accurate uncertainty quantification in initial condition leads to more reliable hydrologic forecasts. For example, DeChant and Moradkhani (2011) aimed at investigating the effects of quantifying initial condition uncertainty in the SAC-SMA (Sacramento Soil Moisture Accounting) hydrologic model. They quantified the input data uncertainty by creating an ensemble of meteorological forcings resampled from historical series, which is called Ensemble Streamflow Prediction (ESP) (Twedt et al., 1977). In addition, they quantified the initial condition uncertainty via data assimilation (DA) methods and concluded that quantification of initial condition uncertainty improved the ESP's seasonal flood forecasting skill. Similarly, Yan et al. (2017) reported improved drought forecasting skill after they used DA to quantify the initial condition uncertainty.

Data assimilation methods have proved beneficial in the estimation of the Earth system states. Being defined as (Liu and Gupta, 2007) "*procedures that aim to produce physically consistent representations or estimates of the dynamical behavior of a system by merging the information present in imperfect models and uncertain data in an optimal way to achieve uncertainty quantification and reduction*", data assimilation methods have been occasionally employed to update a hydrologic variable which is then used to initialize a flood/drought prediction framework. For example, Dechant and Moradkhani (2011) used ensemble data assimilation to assimilate SNOTEL data into the SNOW-17 model and improve the estimation of snow quantities. They subsequently use the updated

snow quantities to initialize ESP flood forecasting method. Similarly, Yan et al. (2017) assimilate satellite data to update root zone soil moisture.

This chapter aims at enhancing the flood forecasting skill by advancing toward full uncertainty quantification. Short-, medium-, and long-term forecast skills are investigated with and without uncertainty quantification. Uncertainty quantification occurs by simultaneously accounting for the initial condition as well as weather forecast uncertainties. Initial condition uncertainty is explained by the updated model initial condition, and forcings uncertainty is explained through an ensemble. Updated initial conditions are adopted from a separate data assimilation run up to the forecast date. In this DA run, USGS streamflow observation (at the outlet) is assimilated to the hydrologic model. The sensitivity of forecasting skill to initial condition uncertainty is assessed by comparing short-, medium-, and long-term responses.

Therefore, the overarching objectives of this chapter are as the following:

(1) Assessing the sensitivity of flood forecasts to initial conditions. Answering the question of "how long does it take for a land surface model to forget about an updated/improved initial condition?" is of particular interest in this chapter.

(2) Evaluating the added value of quantification of initial condition uncertainty in flood forecasting.

The results of this chapter will help improve the current flood forecasting approaches. Currently, quantification of uncertainty in atmospheric forcing inputs are

considered and this chapter may aid in attracting more attention to other sources of uncertainty such as the initial condition.

Particularly, operational agencies such as the National Water Center can benefit from this research. This study can be the start of discussions on probabilistic flood forecasting and uncertainty quantification in their model, the National Water Model.

4.3 Study area and data

In this chapter, the studied area is Huntsville, AL. For more information about this study area and data, readers are referred to the previous chapter.

Similar to the previous chapters, the NLDAS-2 data are used for atmospheric forcings.

4.4 Methodology

4.4.1 National Water Model

The National Water Model (NWM) is a mathematical representation of the water cycle that simulates complex processes such as rainfall, infiltration, evapotranspiration, etc. and builds upon the current operational river forecasting routine by increasing the spatial and temporal resolution as well as increasing the river forecasting locations from 4,000 to 2,700,000. As depicted in Figure 4-1, the NWM outputs fall into four categories including analysis and assimilation, short-term forecasts, medium-term forecasts, and long-term forecasts. Short-term forecasts are issued hourly, medium-range forecasts are issued four times a day, and long-term forecasts are issued daily for the next 30 days.

Ultimate variables include streamflow at 2,700,000 points and other hydrologic variables such as soil moisture and runoff over a 1km×1km and 250m×250m grid. The following figure provides a detailed description of the NWM outputs and frequencies.

Figure 4-1: Four configurations of the NWM, the data used, and the associated frequencies (adopted from the NWM website at http://water.noaa.gov/about/nwm)

The NWM is a specific configuration of the community WRF-Hydro Land Surface Model (LSM) which has recently been introduced to the hydrologic community. The WRF-Hydro model, itself, uses another newly-developed column LSM called Noah-MP as the core hydrologic model. In WRF-Hydro, Noah-MP results (such as soil moisture and runoff) are passed to routing modules. Riverine water level and discharge,

among other variables, are outputted by WRF-Hydro. Figure 4-2 depicts a schematic of this process.

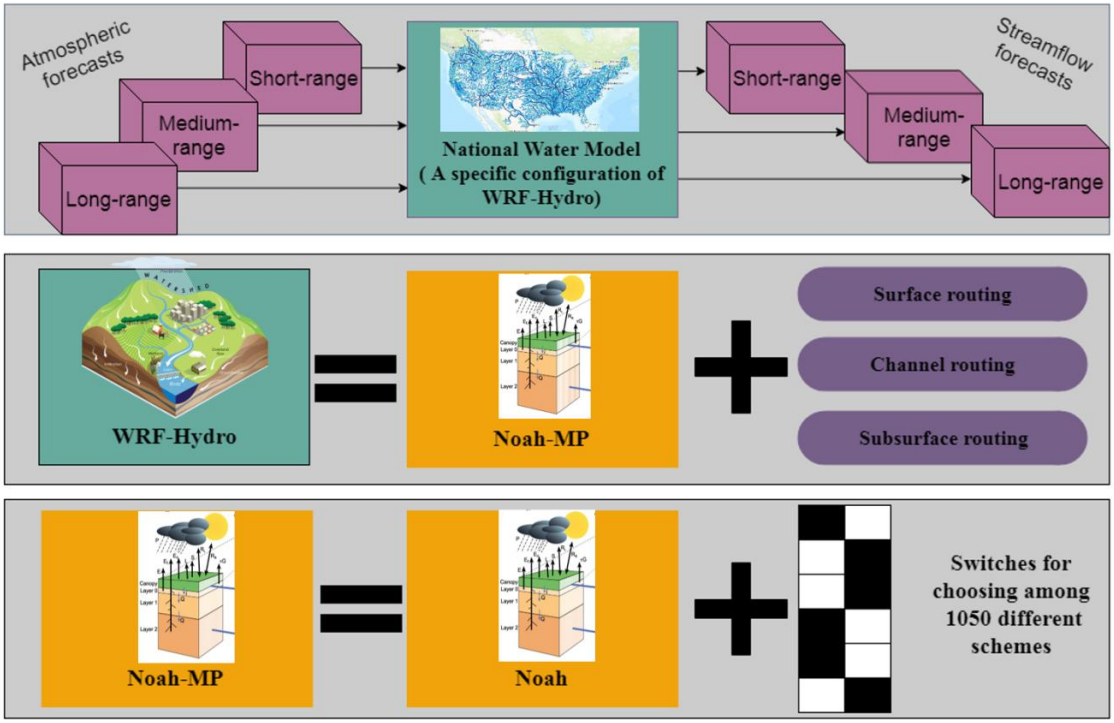

Figure 4-2: A Schematic of the NWM modules and procedures.

4.4.2 Data assimilation

In this chapter, similar to the previous chapter, Ensemble Kalman Filter is used. For more information about the formulation and the background of this method, readers are referred to section 2.6.1.2.

4.4.3 High-Performance Computing

The high-performance algorithm for this chapter is similar to the steps explained in section 2.6.2. Readers are referred to this section for more information.

4.4.4 Performance measures

NIC and RMSE are used for assessing the performance in this chapter. Please see section 2.6.3 for details of calculating NIC.

4.5 Results

4.5.1 Synthetic study

To evaluate the forecast performance, a synthetic study that was mentioned in the previous chapters was designed. In the synthetic study, the model was run forward and the simulated streamflow was considered truth. For more information on building the synthetic experiment, please see section 2.8.2. OL and DA were run for 1/1/2018 to 2/10/2018 at an hourly time step and initiated the forecasts on 2/10/2018 based on their states. Two ensembles of model forecasts were initiated. In both ensembles, the forcing inputs were perturbed as described in the methodology section. Next, short-range, medium-range, and long-range forecast skills are assessed.

4.5.1.1 Short-range forecasts

Forecasts are initialized on 2/10/2018 for the next 18 hours (similar to the NWM) and the results show that the DA improves the forecasts at the outlet by approximately 54% and in the internal gauge by about 50% as shown in Figure 4-3. Other measures such as RMSE, NSE, BIAS, and KGE are shown in Figure 4-4 and Figure 4-5.

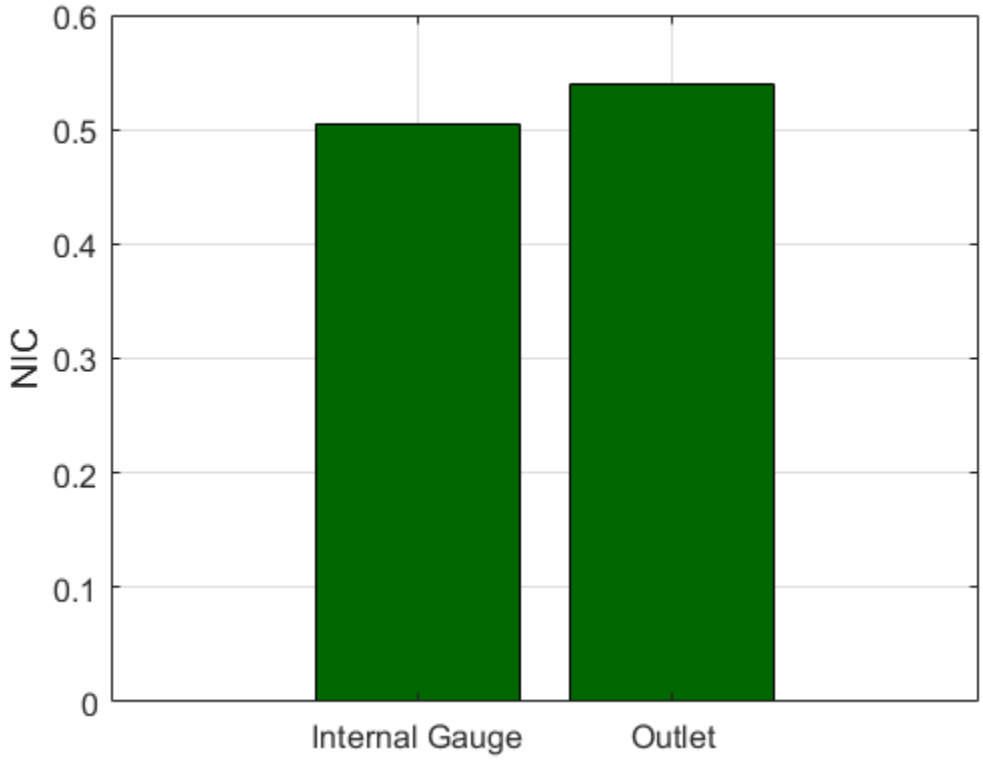

Figure 4-3: Improvements (as indicated by NIC) by DA as compared to the OL for short-term streamflow forecasts in Huntsville, AL.

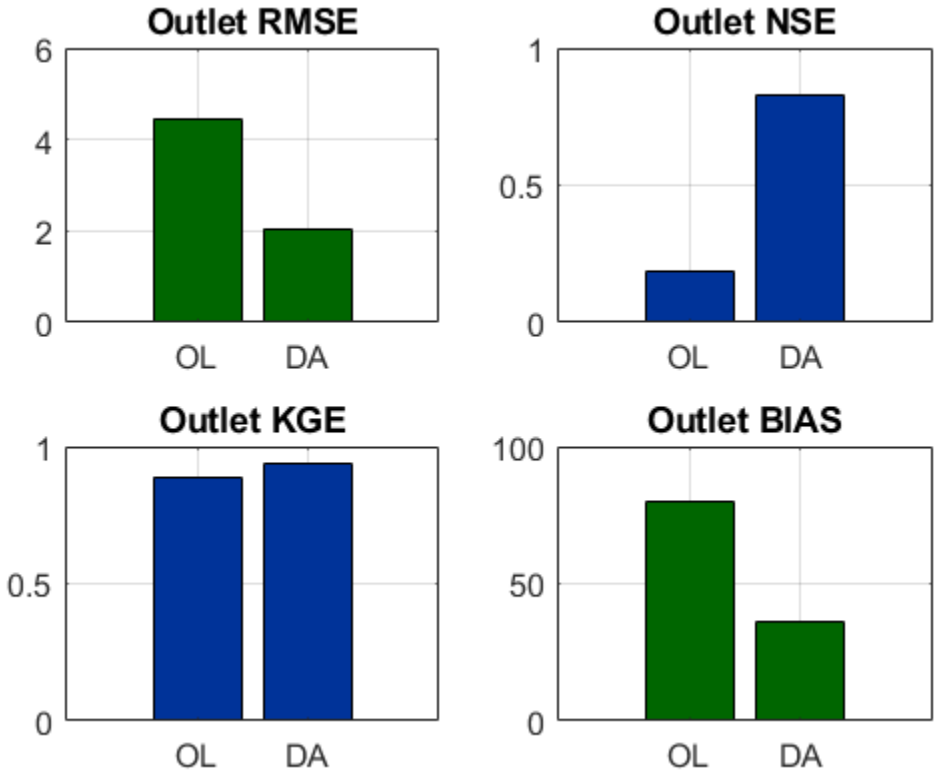

Figure 4-4: Performance measures of the OL and DA short-range predictions at the outlet of the Huntsville, AL area. Forecasts are initialized on 2/10/2018.

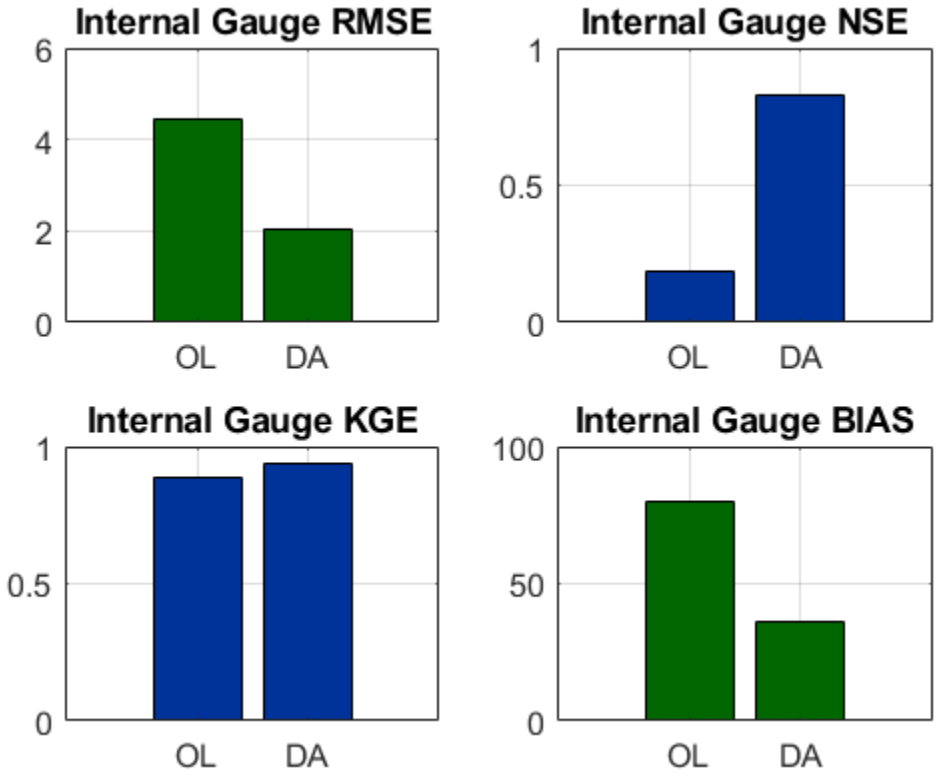

Figure 4-5: Same as Figure 4-4 but for the internal gauge of the same area (short-term forecasts initialized on 2/10/2018.

4.5.1.2 Medium-range forecasts

For testing the effectiveness of medium-range forecasts, the model was initiated on 2/10/2018 and the results were saved for the next 10 days. Comparison of OL and DA results is presented in the following figures. It was observed that the improvements decreased as compared to the short-range forecasts. The improvements of DA over OL at the internal gauge and at the outlet decreased to about 4% and 12%, respectively.

Figure 4-6 compares the improvements and Figure 4-7 compares other performance measures.

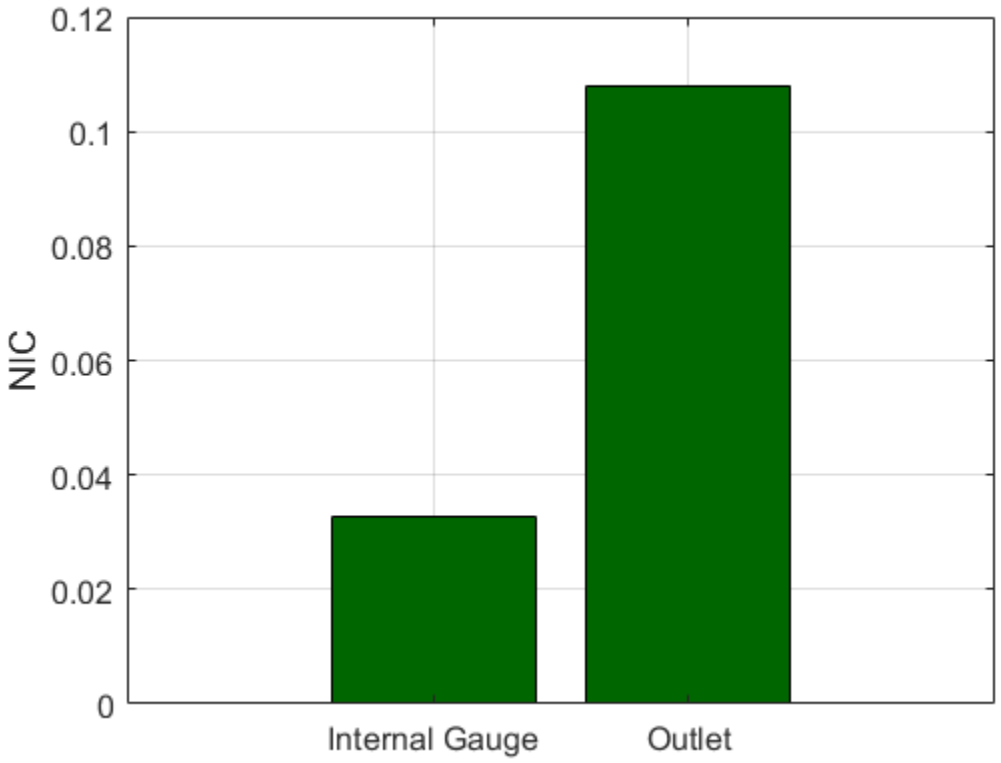

Figure 4-6: Medium-range forecast performance of DA as compared to OL indicated by NIC for the Huntsville, AL area.

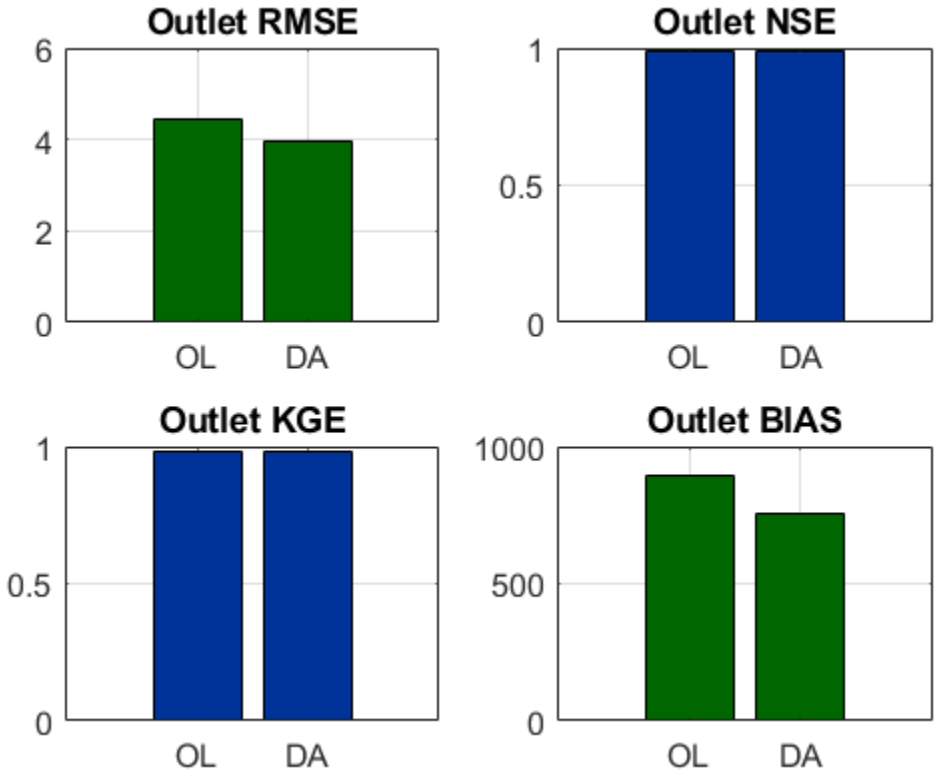

Figure 4-7: Performance measures of OL and DA for medium-range forecasts in Huntsville, AL.

4.5.1.3 Long-range forecasts

Similarly, long-range forecast performance was assessed and it was observed that the DA improved OL performance by 10% at the outlet and by 2% at the internal gauge. This means that as the lead-time increases, the performance decreases and that generally, the DA made higher improvements at the outlet than the internal gauge. A performance comparison of OL and DA and the associated NICs are shown in Figure 4-8.

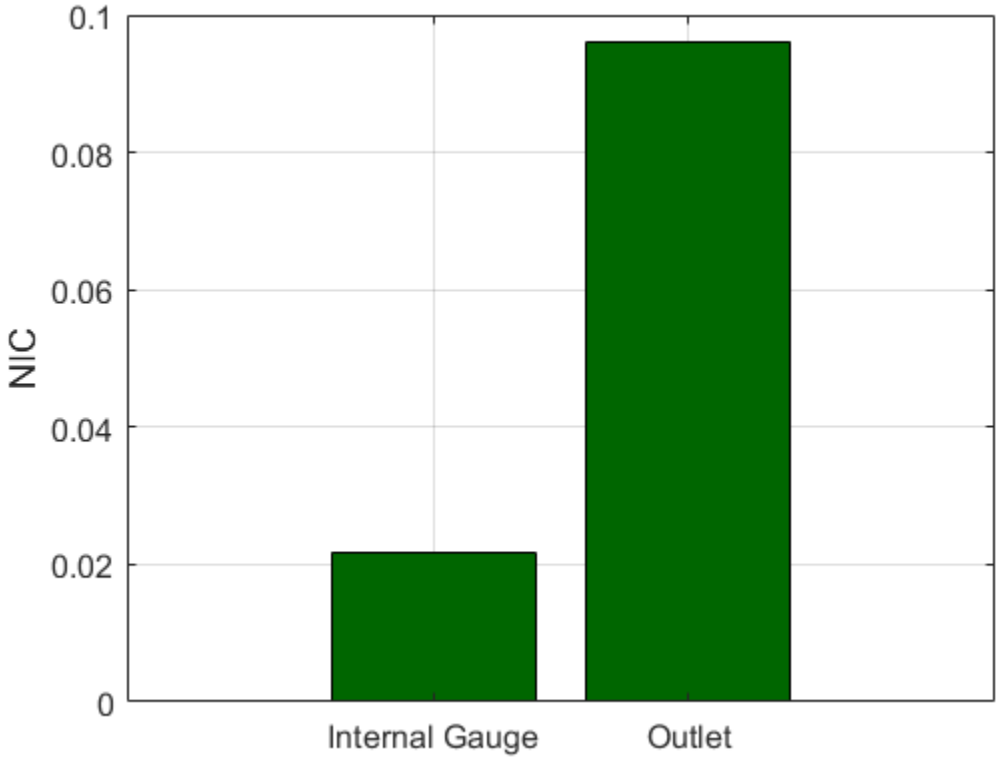

Figure 4-8: Degree of improvements by DA over OL at the outlet and the internal gauges for long-range forecasts in Huntsville, AL area.

4.5.2 Real study

Subsequent to the synthetic study, an analysis was performed using the real USGS gauge observations. OL and DA were run for the period of 1/1/2018 to 2/5/2018 at an hourly time step. Then, the states on 2/5/2018 were saved. Next, the model was initialized with the updated initial states for 2/5/2018 to 2/28/2018. Figure 4-9 shows the variation of the performance with lead-time. As the lead-time increases, the forecast skill decreases which agrees with previous research by Yan et al. (2017). Similarly, in Figure 4-10, the

performance of short-, medium-, and long-range forecasts as defined by the NWM are demonstrated. Short-term (18 hours) predictions are improved by about 35% while medium (10 days) range and long range (1 month) forecasts are improved by around 10%. It is observed that ensemble data assimilation is capable of improving the forecasts by up to 90% for the next hour. The degree of improvement is dependent on the time of initialization and the location of the gauge. In general, more improvements were observed at the outlet than the internal gauge. The time series of the forward run, the OL, and the DA are presented in Figure 4-11.

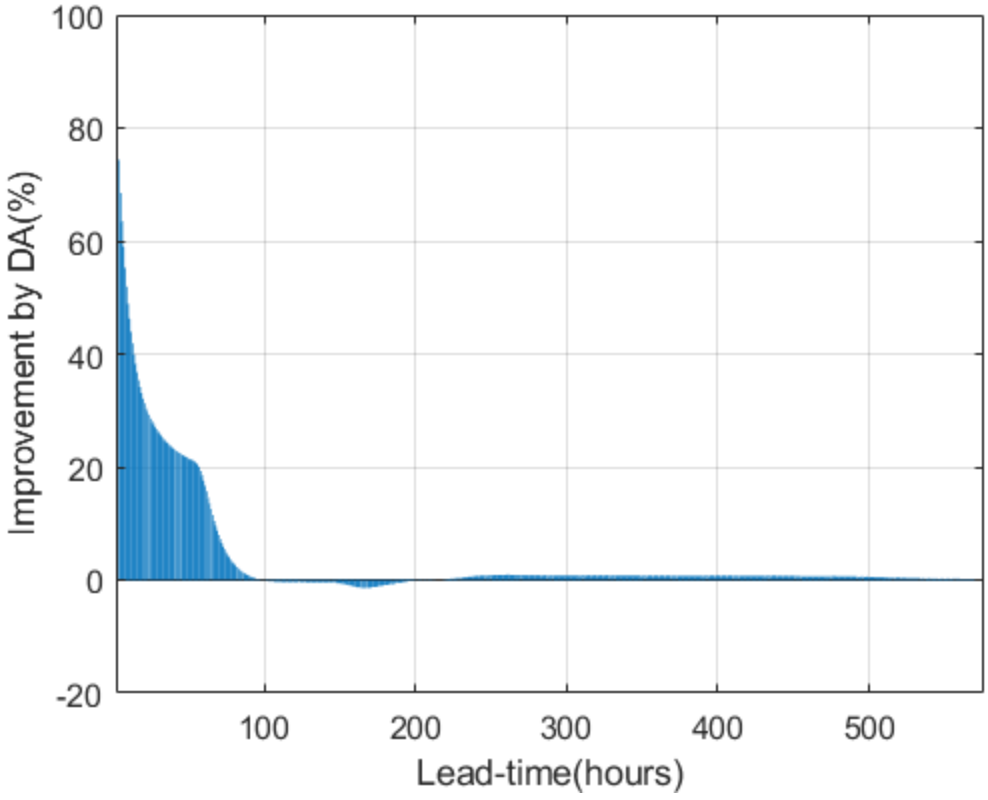

Figure 4-9: Variation of improvements by DA as opposed to OL with lead-time. Forecasts are initiated on 2/5/2018 before the flood peak at the rising limb of the hydrograph

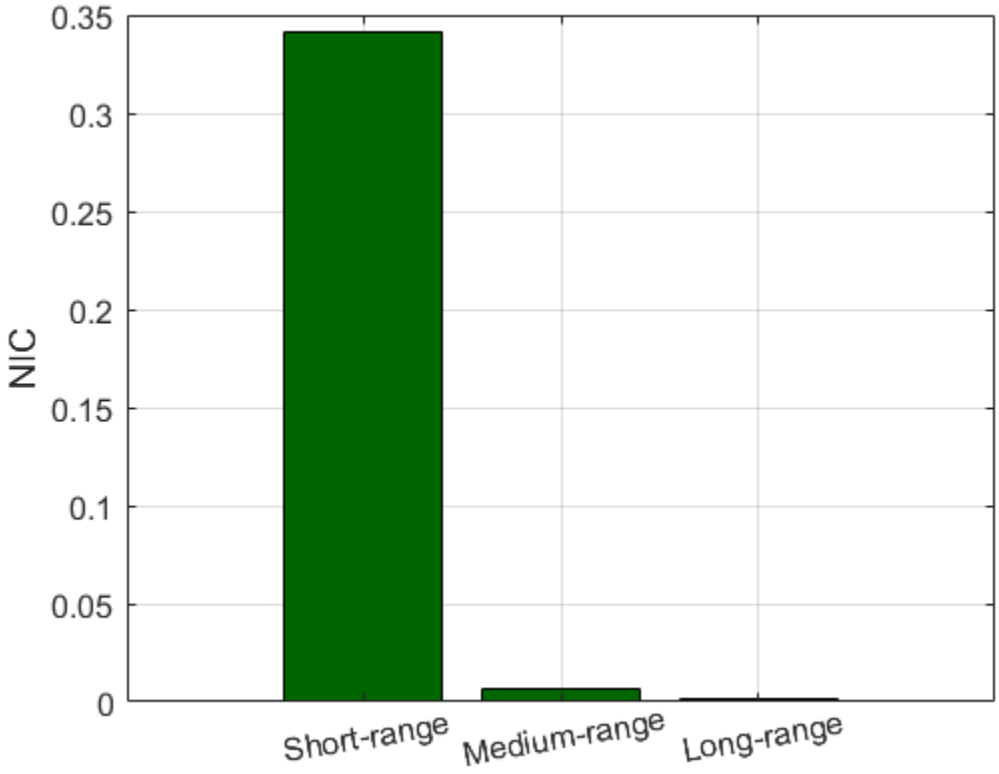

Figure 4-10: DA improvements in short-, medium-, and long-range forecasts. Forecasts are initiated on 2/5/2018 before the flood starts. The lead times are defined in a similar way as the NWM.

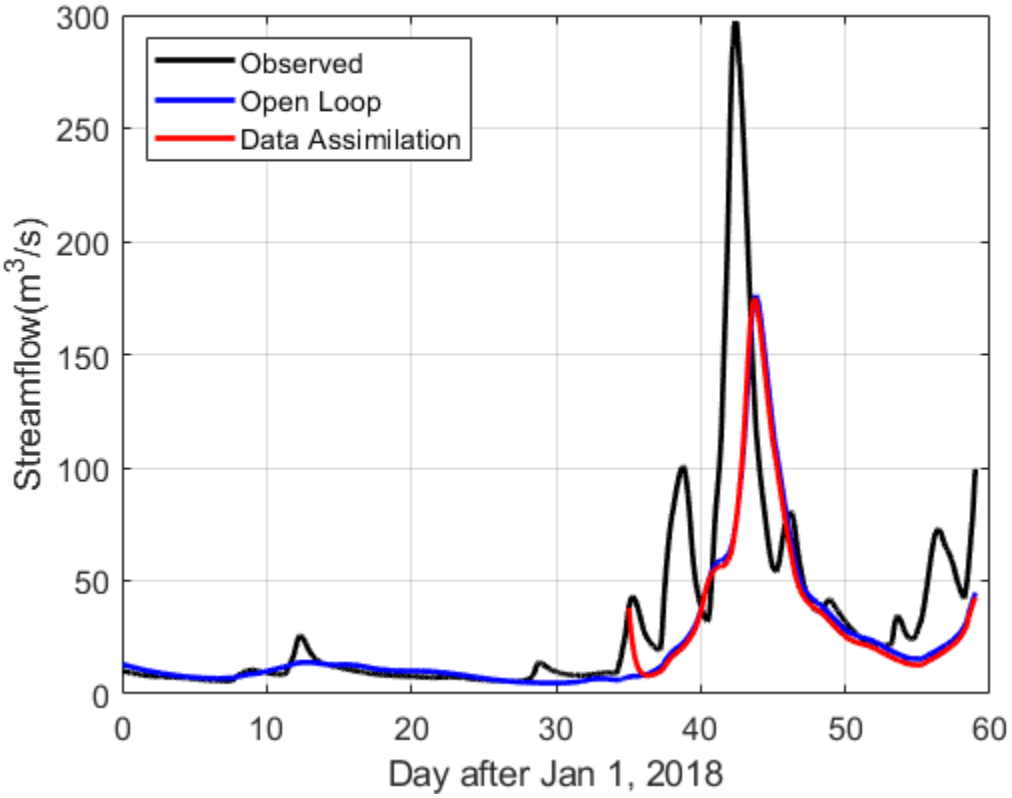

Figure 4-11: Time series of forecasted streamflow in OL and DA initial condition. DA Forecast (the red line) is initiated on 2/5/2018. The blue line indicates the OL forecasts and the black line indicates the observation.

4.6 Conclusion and discussion

Avoiding flood-induced economic damages demands an early and effective flood warning system. Such a system is affected by uncertainties from different sources including forcing data (weather forecasts), initial land surface condition, model representation (structural uncertainty), and model parameters. In this chapter, uncertainties associated with the atmospheric forcings are characterized by using an ensemble of possible conditions, instead of a single deterministic forecast. While other

sources of uncertainty (mainly from the initial condition) are acknowledged in the literature, a full quantification of uncertainties including both initial condition and meteorological forcings needs more attention. This study moves toward a more complete characterization of uncertainty by simultaneously accounting for both atmospheric forcings and initial condition uncertainties. Initial condition uncertainty is quantified by ensemble data assimilation where a hydrologic model is run up to the forecast initial date with the assimilation of USGS streamflow observations. Ultimately, the updated model states in the forecast date are considered to represent the initial condition uncertainty. Regarding the atmospheric forcings uncertainty, an ensemble is utilized. The added value of initial condition uncertainty quantification was demonstrated in this study. It was observed that quantification of initial condition uncertainty in addition to quantification of meteorological forcing inputs is able to improve the forecasts from a forward model run. Improvements in short-, medium-, and long-range forecasts were assessed and it was observed that updated initial condition uncertainty affects the short-range forecasts the most. Medium- and long-range forecasts were not much affected by the initial conditions. Therefore, the main findings of this chapter are as follows:

(1) Short-range forecasts are significantly sensitive to initial conditions. Medium and long-range forecasts are not sensitive to initial conditions.

(2) The effects of an updated initial condition last for two days. After that, the system forgets the initial condition and atmospheric forcings become dominant.

These findings highlight the importance of initial condition uncertainty for flood forecasting. The results of this chapter suggest more research is necessary on the value of initial condition uncertainty. This chapter can also start a discussion in the National Water Center on the values of uncertainty quantification for operational flood forecasting (the current forecasts are deterministic and uncertainty is not quantified).

The author's initial investigations on the forecasts quality show that improvements in the forecasts are significantly sensitive to the time of initializing the forecast. In this chapter, the forecasts are initialized at the rising limb of the peak. The results might vary if the model was initialized at the time of the peak or at the falling limb. Future extensions of this study may consider initializing the forecasts in different parts of the hydrograph and quantifying the sensitivity of forecasts at the time of the initiation.

Additionally, in the DA run before initializing the forecasts, only streamflow observations are assimilated in the model. Future extensions of this work may consider assimilation of satellite observations including remotely-sensed soil moisture and/or snow water equivalent (SWE) in snow dominated regions.

5 Conclusion

The key findings of this dissertation are as the following.

(1) Performances of two DA techniques (EnKF and PF-MCMC) were assessed on the Noah-MP model. In both DAs, CCI satellite soil moisture observations were assimilated into the model. Both DAs were successful in improving Noah-MP's ability in simulating soil moisture. PF-MCMC demonstrated a better performance than the EnKF.

(2) A parallel algorithm based on Massage Passing Interface protocols was introduced in this dissertation. A successful implementation of this algorithm was demonstrated for simulating soil moisture during a significant flood in Colorado Front Range.

(3) Performance of DA (EnKF) on WRF-Hydro was assessed. Successful assimilation of remotely-sensed soil moisture and USGS streamflow observations were provided. Improvements of up to 50% were observed.

(4) Assimilation of soil moisture into the WRF-Hydro model does not improve outlet streamflow. Similarly, assimilation of USGS streamflow observations into WRF-Hydro does not improve soil moisture simulation skill.

(5) Forecasts are sensitive to initial conditions. Short-range forecasts are the most sensitive. Medium-range forecasts showed less sensitivity and long-range forecasts showed no sensitivity to initial conditions. It was estimated that the effects of an updated

initial condition last for about 50 hours. After that, the system forgets about the initial condition and atmospheric forcings become dominant.

These findings could be beneficial for flood forecasting in research and practice. The findings suggest that more attention needs to be given to initial condition uncertainties and DA can help quantify this source of uncertainty. Moreover, these findings highlight the importance of DA for flood forecasting. Currently, USGS streamflow gauge observations are incorporated into the WRF-Hydro model using a nudging algorithm. This method, even though easy and quick, is not as effective as the ensemble data assimilation techniques elaborated in this dissertation. The results of this dissertation suggest that besides improving soil moisture and streamflow simulation skills, ensemble data assimilation is capable of improving short-range flood forecasts (up to two days). Moreover, uncertainty quantification and probabilistic forecasts are easier to communicate through an ensemble. Since such assimilation could become too expensive, DA is recommended to be initialized once a flood is expected (or in cases where more accurate forecasts are needed). Another way of decreasing the computational burden by DA is customizing the initiation of DA. The author suggests using ensemble data assimilation only in cases that a flood is expected. A reasonable strategy is starting the DA (with initial condition from the nudging algorithm) once the streamflow magnitude passes a certain percentile of the climatology (e.g., 75%). This way, the computational burden of the ensemble data assimilation is not imposed all the time.

Employing the proposed algorithm for a more efficient implementation of DA is also suggested.

Some future extensions of this work are as follows:

(1) Investigating the effects of the routing methodology on the result of data assimilation. Given that the diffusive method has been proved to be more effective than the reach-based Muskingum-Cunge method, it might be more effective in passing the updated information from soil moisture data assimilation to the neighboring cells and finally to streamflow. It would be interesting to compare the performance of data assimilation under different routing schemes.

(2) Investigating the advantages of ensemble data assimilation on more study areas with various sizes and elevations.

(3) Investigate the time lag between updated soil moisture and streamflow: it was observed in the second chapter that updated soil moisture does not significantly affect the streamflow simulations. One interesting question to answer is if considering a time lag between streamflow and soil moister assimilation would lead to improvements that are more significant. Another solution could be in updating soil moisture in all soil layers (not only surface soil moisture).

(4) The groundwater effect: In this dissertation, the groundwater effect was ignored mainly due to the long spin-up time that is needed for groundwater modeling. A

future extension of this study can consider the effect of water table. This is particularly important because the water table directly affects the soil moisture simulations.

(5) Another critical problem to address in implementing data assimilation is maintaining the spatial coherence. If each grid cell is updated separately from the adjacent grid cells, the mass balance might be violated, as the spatial distribution of water is not maintained. Therefore, an interesting extension to this dissertation could consider passing information from one cell to adjacent cells during data assimilation.

References

Abbaszadeh, P., Moradkhani, H., Yan, H., 2018. Enhancing hydrologic data assimilation by evolutionary Particle Filter and Markov Chain Monte Carlo. Adv. Water Resour. 111, 192–204. https://doi.org/10.1016/j.advwatres.2017.11.011

Afshari, S., Omranian, E., Feng, D., 2016. Relative Sensitivity of Flood Inundation Extent by Different Physical and Semi-Empirical Models, in: Maidment, D.R., Rajib, A., Lin, P., Clark, E.P. (Eds.), NATIONAL WATER CENTER INNOVATORS PROGRAM SUMMER INSTITUTE REPORT 2016. https://doi.org/DOI: 10.4211/technical.20161019

Ahmadalipour, A., Moradkhani, H., Rana, A., 2017a. Accounting for downscaling and model uncertainty in fine-resolution seasonal climate projections over the Columbia River Basin. Clim. Dyn. 1–17. https://doi.org/10.1007/s00382-017-3639-4

Ahmadalipour, A., Moradkhani, H., Yan, H., Zarekarizi, M., 2017b. Remote Sensing of Drought: Vegetation, Soil Moisture, and Data Assimilation, in: Remote Sensing of Hydrological Extremes. Springer, Cham, pp. 121–149. https://doi.org/10.1007/978-3-319-43744-6_7

Ahmadalipour, A., Rana, A., Moradkhani, H., Sharma, A., 2017c. Multi-criteria evaluation of CMIP5 GCMs for climate change impact analysis. Theor. Appl. Climatol. 128, 71–87. https://doi.org/10.1007/s00704-015-1695-4

Alvarez-Garreton, C., Ryu, D., Western, A.W., Crow, W.T., Robertson, D.E., 2014. The impacts of assimilating satellite soil moisture into a rainfall-runoff model in a semi-arid catchment. J. Hydrol. 519, 2763–2774. https://doi.org/10.1016/j.jhydrol.2014.07.041

Andrieu, C., Doucet, A., Holenstein, R., 2010. Particle Markov chain Monte Carlo methods. J. R. Stat. Soc. Ser. B (Statistical Methodol. 72, 269–342. https://doi.org/10.1111/j.1467-9868.2009.00736.x

Arsenault, K.R., Nearing, G.S., Wang, S., Yatheendradas, S., Peters-Lidard, C.D., 2018. Parameter Sensitivity of the Noah-MP Land Surface Model with Dynamic Vegetation. J. Hydrometeorol. 19, 815–830. https://doi.org/10.1175/jhm-d-17-0205.1

Aubert, D., Loumagne, C., Oudin, L., 2003. Sequential assimilation of soil moisture and streamflow data in a conceptual rainfall - Runoff model. J. Hydrol. 280, 145–161. https://doi.org/10.1016/S0022-1694(03)00229-4

Barlage, M., Tewari, M., Chen, F., Miguez-Macho, G., Yang, Z.L., Niu, G.Y., 2015. The effect of groundwater interaction in North American regional climate simulations with WRF/Noah-MP. Clim. Change 129, 485–498. https://doi.org/10.1007/s10584-014-1308-8

Bowler, N.E., Arribas, A., Mylne, K.R., Robertson, K.B., Beare, S.E., 2008. The MOGREPS short-range ensemble prediction system. Q. J. R. Meteorol. Soc. 134, 703–722. https://doi.org/10.1002/qj.234

Bowling, L.C., Lettenmaier, D.P., Nijssen, B., Graham, L.P., Clark, D.B., El Maayar, M., Essery, R., Goers, S., Gusev, Y.M., Habets, F., Van Den Hurk, B., Jin, J., Kahan, D., Lohmann, D., Ma, X., Mahanama, S., Mocko, D., Nasonova, O., Niu, G.Y., Samuelsson, P., Shmakin, A.B., Takata, K., Verseghy, D., Viterbo, P., Xia, Y., Xue, Y., Yang, Z.L., 2003. Simulation of high-latitude hydrological processes in the Torne-Kalix basin: PILPS Phase 2(e) 1: Experiment description and summary intercomparisons. Glob. Planet. Change 38, 1–30. https://doi.org/10.1016/S0921-8181(03)00003-1

Brazil, L., 2018. CUAHSI Summer Institute Report. https://doi.org/http://dx.doi.org/10.4211/hs.c7ee150767114d3a927b67a94f0edc04

Brocca, L., Hasenauer, S., Lacava, T., Melone, F., Moramarco, T., Wagner, W., Dorigo, W., Matgen, P., Martínez-Fernández, J., Llorens, P., Latron, J., Martin, C., Bittelli, M., 2011. Soil moisture estimation through ASCAT and AMSR-E sensors: An intercomparison and validation study across Europe. Remote Sens. Environ. 115, 3390–3408. https://doi.org/10.1016/j.rse.2011.08.003

Brutsaert, W., 1982. The Surface Roughness Parameterization, in: Evaporation into the Atmosphere. pp. 113–127. https://doi.org/10.1007/978-94-017-1497-6_5

Burakowski, E.A., Ollinger, S. V., Bonan, G.B., Wake, C.P., Dibb, J.E., Hollinger, D.Y., 2016. Evaluating the climate effects of reforestation in new england using a weather research and forecasting (WRF) model multiphysics ensemble. J. Clim. 29, 5141–5156. https://doi.org/10.1175/JCLI-D-15-0286.1

Cai, X., Yang, Z.L., David, C.H., Niu, G.Y., Rodell, M., 2014a. Hydrological evaluation of the noah-MP land surface model for the Mississippi River Basin. J. Geophys. Res. 119, 23–38. https://doi.org/10.1002/2013JD020792

Cai, X., Yang, Z.L., Xia, Y., Huang, M., Wei, H., Leung, L.R., Ek, M.B., 2014b. Assessment of simulated water balance from Noah, Noah-MP, CLM, and VIC over CONUS using the NLDAS test bed. J. Geophys. Res. 119, 13751–13771. https://doi.org/10.1002/2014JD022113

Cenci, L., Pulvirenti, L., Boni, G., Chini, M., Matgen, P., Gabellani, S., Squicciarino, G., Basso, V., Pignone, F., Pierdicca, N., 2017. Exploiting Sentinel 1 data for improving (flash) flood modelling via data assimilation techniques. 2017 IEEE Int. Geosci. Remote Sens. Symp. 4939–4942.

Chen, F., Crow, W.T., Starks, P.J., Moriasi, D.N., 2011. Improving hydrologic predictions of a catchment model via assimilation of surface soil moisture. Adv. Water Resour. 34, 526–536. https://doi.org/10.1016/j.advwatres.2011.01.011

Chen, H., Yang, D., Hong, Y., Gourley, J.J., Zhang, Y., 2013. Hydrological data assimilation with the Ensemble Square-Root-Filter: Use of streamflow observations to update model states for real-time flash flood forecasting. Adv. Water Resour. 59, 209–220. https://doi.org/10.1016/j.advwatres.2013.06.010

Cigler, B.A., 2017. U.S. Floods. State Local Gov. Rev. 49, 0160323X1773189. https://doi.org/10.1177/0160323X17731890

Clark, M.P., Rupp, D.E., Woods, R.A., Zheng, X., Ibbitt, R.P., Slater, A.G., Schmidt, J., Uddstrom, M.J., 2008. Hydrological data assimilation with the ensemble Kalman filter: Use of streamflow observations to update states in a distributed hydrological model. Adv. Water Resour. 31, 1309–1324. https://doi.org/10.1016/j.advwatres.2008.06.005

Cloke, H.L., Pappenberger, F., 2009. Ensemble flood forecasting: A review. J. Hydrol. 375, 613–626. https://doi.org/10.1016/j.jhydrol.2009.06.005

Cuntz, M., Mai, J., Samaniego, L., Clark, M., Wulfmeyer, V., Branch, O., Attinger, S., Thober, S., 2016. The impact of standard and hard-coded parameters on the hydrologic fluxes in the Noah-MP land surface model. J. Geophys. Res. 121, 10,676–10,700. https://doi.org/10.1002/2016JD025097

Daescu, D.N., Langland, R.H., 2017. Toward New Applications of the Adjoint Sensitivity Tools in Data Assimilation, in: Data Assimilation for Atmospheric, Oceanic and Hydrologic Applications (Vol. III). pp. 361–382. https://doi.org/10.1007/978-3-319-43415-5_16

Daescu, D.N., Navon, I.M., 2004. Adaptive observations in the context of 4D-Var data assimilation. Meteorol. Atmos. Phys. 85, 205–226. https://doi.org/10.1007/s00703-003-0011-5

Dalcín, L., Paz, R., Storti, M., 2005. MPI for Python. J. Parallel Distrib. Comput. 65, 1108–1115. https://doi.org/10.1016/j.jpdc.2005.03.010

Dalcín, L., Paz, R., Storti, M., D'Elía, J., 2008. MPI for Python: Performance improvements and MPI-2 extensions. J. Parallel Distrib. Comput. 68, 655–662. https://doi.org/10.1016/j.jpdc.2007.09.005

Dalcin, L.D., Paz, R.R., Kler, P.A., Cosimo, A., 2011. Parallel distributed computing using Python. Adv. Water Resour. 34, 1124–1139. https://doi.org/10.1016/j.advwatres.2011.04.013

DeChant, C.M., Moradkhani, H., 2014a. Hydrologic prediction and uncertainty quantification, in: Eslamian, S. (Ed.), Handbook of Engineering Hydrology. CRC press, pp. 387–414.

DeChant, C.M., Moradkhani, H., 2014b. Toward a reliable prediction of seasonal forecast uncertainty: Addressing model and initial condition uncertainty with ensemble data assimilation and sequential Bayesian combination. J. Hydrol. 519, 2967–2977. https://doi.org/10.1016/j.jhydrol.2014.05.045

Dechant, C.M., Moradkhani, H., 2014. Analyzing the sensitivity of drought recovery forecasts to land surface initial conditions. J. Hydrol. https://doi.org/10.1016/j.jhydrol.2014.10.021

DeChant, C.M., Moradkhani, H., 2012. Examining the effectiveness and robustness of sequential data assimilation methods for quantification of uncertainty in hydrologic forecasting. Water Resour. Res. 48, W04518. https://doi.org/10.1029/2011WR011011

Dechant, C.M., Moradkhani, H., 2011. Improving the characterization of initial condition for ensemble streamflow prediction using data assimilation. Hydrol. Earth Syst. Sci. 15, 3399–3410. https://doi.org/10.5194/hess-15-3399-2011

Deo, I., Modi, P., Zarekarizi, M., Valle, J., 2018. Sensitivity of Urban Flooding to Presence of Subsurface Storm Drainage Systems in Hydrologic Models for Low-Gradient Watersheds, in: Aristizabal, F., Grimley, L.E., Bales, J., Tijerina, D., Flowers, T., Clark, E.P. (Eds.), National Water Center Innovators Program Summer Institute Report 2018. https://doi.org/http://doi.org/10.4211/hs.c7ee150767114d3a927b67a94f0edc04

Dodov, B., Foufoula-Georgiou, E., 2005. Fluvial processes and streamflow variability: Interplay in the scale-frequency continuum and implications for scaling. Water Resour. Res. 41, 1–18. https://doi.org/10.1029/2004WR003408

Dongarra, J., Sullivan, F., 2000. Guest Editors Introduction to the top 10 algorithms. Comput. Sci. Eng. 2, 22–23. https://doi.org/10.1109/MCISE.2000.814652

Dorigo, W., Wagner, W., Albergel, C., Albrecht, F., Balsamo, G., Brocca, L., Chung, D., Ertl, M., Forkel, M., Gruber, A., Haas, E., Hamer, P.D., Hirschi, M., Ikonen, J., de Jeu, R., Kidd, R., Lahoz, W., Liu, Y.Y., Miralles, D., Mistelbauer, T., Nicolai-Shaw, N., Parinussa, R., Pratola, C., Reimer, C., van der Schalie, R., Seneviratne, S.I., Smolander, T., Lecomte, P., 2017. ESA CCI Soil Moisture for improved Earth system understanding: State-of-the art and future directions. Remote Sens. Environ. 203, 185–215. https://doi.org/10.1016/j.rse.2017.07.001

Ek, M.B., 2003. Implementation of Noah land surface model advances in the National Centers for Environmental Prediction operational mesoscale Eta model. J. Geophys. Res. 108, 8851. https://doi.org/10.1029/2002JD003296

Entekhabi, D., Njoku, E.G., O'Neill, P.E., Kellogg, K.H., Crow, W.T., Edelstein, W.N., Entin, J.K., Goodman, S.D., Jackson, T.J., Johnson, J., Kimball, J., Piepmeier, J.R., Koster, R.D., Martin, N., McDonald, K.C., Moghaddam, M., Moran, S., Reichle, R., Shi, J.C., Spencer, M.W., Thurman, S.W., Tsang, L., Van Zyl, J., 2010. The soil moisture active passive (SMAP) mission. Proc. IEEE 98, 704–716. https://doi.org/10.1109/JPROC.2010.2043918

Evensen, G., 1994. Sequential data assimilation with a nonlinear quasi-geostrophic model using Monte Carlo methods to forecast error statistics. J. Geophys. Res. 99, 10143–10162. https://doi.org/10.1029/94JC00572

Gao, Y., Li, K., Chen, F., Jiang, Y., Lu, C., 2015. Assessing and improving Noah-MP land model simulations for the central Tibetan Plateau. J. Geophys. Res. Atmos. 120, 9258–9278. https://doi.org/10.1002/2015JD023404

Gochis, D., Chen, F., 2003. Hydrological Enhancements to the Community Noah Land Surface Model. NCAR Sci. Tech. Rep. 77. https://doi.org/10.5065/D60P0X00

Gochis, D., Schumacher, R., Friedrich, K., Doesken, N., Kelsch, M., Sun, J., Ikeda, K., Lindsey, D., Wood, A., Dolan, B., Matrosov, S., Newman, A., Mahoney, K., Rutledge, S., Johnson, R., Kucera, P., Kennedy, P., Sempere-Torres, D., Steiner, M., Roberts, R., Wilson, J., Yu, W., Chandrasekar, V., Rasmussen, R., Anderson, A., Brown, B., 2015. The great Colorado flood of September 2013. Bull. Am. Meteorol. Soc. 96, 1461–1487. https://doi.org/10.1175/BAMS-D-13-00241.1

Gochis, D.J., Barlage, M., Dugger, A., Fitzgerald, K., Karsten, L., Mcallister, M., Mccreight, J., Mills, J., Rafieeinasab, A., Read, L., Sampson, K., Yates, D., Yu, W., 2018. WRF-Hydro V5 Technical Description Originally Created : Updated : WRF-Hydro V5 Technical Description. NCAR Tech. Note.

Gochis, D.J., Yu, W., Yates, D., 2015. The WRF-Hydro model technical description and user's guide, version 3.0. NCAR Tech. Doc.

Gupta, H. V., Kling, H., Yilmaz, K.K., Martinez, G.F., 2009. Decomposition of the mean squared error and NSE performance criteria: Implications for improving hydrological modelling. J. Hydrol. 377, 80–91. https://doi.org/10.1016/j.jhydrol.2009.08.003

Hain, C.R., Crow, W.T., Anderson, M.C., Mecikalski, J.R., 2012. An ensemble Kalman filter dual assimilation of thermal infrared and microwave satellite observations of soil moisture into the Noah land surface model. Water Resour. Res. 48. https://doi.org/10.1029/2011WR011268

Hamill, T.M., Snyder, C., 2000. A Hybrid Ensemble Kalman Filter–3D Variational Analysis Scheme. Mon. Wea. Rev. 128, 2905–2919. https://doi.org/10.1175/1520-0493(2000)128<2905:AHEKFV>2.0.CO;2

Johnell, A., Lindström, G., Olsson, J., 2007. Deterministic evaluation of ensemble streamflow predictions in Sweden. Nord. Hydrol. 38, 441–450. https://doi.org/10.2166/nh.2007.022

Kalman, R.E., 1960. A New Approach to Linear Filtering and Prediction Problems. J. Basic Eng. 82, 35. https://doi.org/10.1115/1.3662552

Khajehei, S., Ahmadalipour, A., Moradkhani, H., 2018. An effective post-processing of the North American multi-model ensemble (NMME) precipitation forecasts over the continental US. Clim. Dyn. 51, 457–472. https://doi.org/10.1007/s00382-017-3934-0

Kirtman, B.P., Min, D., Infanti, J.M., Kinter, J.L., Paolino, D.A., Zhang, Q., van den Dool, H., Saha, S., Mendez, M.P., Becker, E., Peng, P., Tripp, P., Huang, J., DeWitt, D.G., Tippett, M.K., Barnston, A.G., Li, S., Rosati, A., Schubert, S.D., Rienecker, M., Suarez, M., Li, Z.E., Marshak, J., Lim, Y.-K., Tribbia, J., Pegion, K., Merryfield, W.J., Denis, B., Wood, E.F., 2014. The North American Multimodel Ensemble: Phase-1 Seasonal-to-Interannual Prediction; Phase-2 toward Developing Intraseasonal Prediction. Bull. Am. Meteorol. Soc. 95, 585–601. https://doi.org/10.1175/BAMS-D-12-00050.1

Komma, J., Blöschl, G., Reszler, C., 2008. Soil moisture updating by Ensemble Kalman Filtering in real-time flood forecasting. J. Hydrol. 357, 228–242. https://doi.org/10.1016/j.jhydrol.2008.05.020

Komma, J., Reszler, C., Blöschl, G., Haiden, T., 2007. Ensemble prediction of floods - catchment non-linearity and forecast probabilities. Nat. Hazards Earth Syst. Sci. 7, 431–444. https://doi.org/10.5194/nhess-7-431-2007

Koster, R.D., Mahanama, S.P.P., Livneh, B., Lettenmaier, D.P., Reichle, R.H., 2010. Skill in streamflow forecasts derived from large-scale estimates of soil moisture and snow. Nat. Geosci. 3, 613–616. https://doi.org/10.1038/ngeo944

Kumar, S. V., Dong, J., Peters-Lidard, C.D., Mocko, D., Gómez, B., 2016. Role of forcing uncertainty and model error background characterization in snow data assimilation. Hydrol. Earth Syst. Sci. Discuss. 1–24. https://doi.org/10.5194/hess-2016-581

Kumar, S. V., Peters-Lidard, C.D., Mocko, D., Reichle, R., Liu, Y., Arsenault, K.R., Xia, Y., Ek, M., Riggs, G., Livneh, B., Cosh, M., 2014. Assimilation of remotely sensed soil moisture and snow depth retrievals for drought estimation. J. Hydrometeorol. 15, 2446–2469. https://doi.org/10.1175/JHM-D-13-0132.1

Lacava, T., Matgen, P., Brocca, L., Bittelli, M., Pergola, N., Moramarco, T., Tramutoli, V., 2012. A first assessment of the SMOS soil moisture product with in situ and modeled data in Italy and Luxembourg. IEEE Trans. Geosci. Remote Sens. 50, 1612–1622. https://doi.org/10.1109/TGRS.2012.2186819

Liang, X., Lettenmaier, D.P., Wood, E.F., Burges, S.J., 1994. A simple hydrologically based model of land surface water and energy fluxes for general circulation models. J. Geophys. Res. 99, 14415. https://doi.org/10.1029/94JD00483

Lin, P., Rajib, M.A., Yang, Z.L., Somos-Valenzuela, M., Merwade, V., Maidment, D.R., Wang, Y., Chen, L., 2018. Spatiotemporal Evaluation of Simulated Evapotranspiration and Streamflow over Texas Using the WRF-Hydro-RAPID Modeling Framework. J. Am. Water Resour. Assoc. 54, 40–54. https://doi.org/10.1111/1752-1688.12585

Liu, J.S., Chen, R., Logvi-, T., 2001. Sequential Monte Carlo Methods in Practice, in: Sequential Monte Carlo Methods in Practice. https://doi.org/10.1007/978-1-4757-3437-9

Liu, Y., Gupta, H. V., 2007. Uncertainty in hydrologic modeling: Toward an integrated data assimilation framework. Water Resour. Res. 43, 1–18. https://doi.org/10.1029/2006WR005756

Liu, Y.Y., Parinussa, R.M., Dorigo, W. a., De Jeu, R. a M., Wagner, W., M. Van Dijk, a. I.J., McCabe, M.F., Evans, J.P., 2011. Developing an improved soil moisture dataset by blending passive and active microwave satellite-based retrievals. Hydrol. Earth Syst. Sci. 15, 425–436. https://doi.org/10.5194/hess-15-425-2011

Loikith, P.C., Detzer, J., Mechoso, C.R., Lee, H., Barkhordarian, A., 2017. The Influence of Recurrent Modes of Climate Variability on the Occurrence of Monthly Temperature Extremes Over South America. J. Geophys. Res. Atmos. 122, 10297–10311. https://doi.org/10.1002/2017JD027561

Ma, N., Niu, G.Y., Xia, Y., Cai, X., Zhang, Y., Ma, Y., Fang, Y., 2017. A Systematic Evaluation of Noah-MP in Simulating Land-Atmosphere Energy, Water, and Carbon Exchanges Over the Continental United States. J. Geophys. Res. Atmos. 122, 12,245–12,268. https://doi.org/10.1002/2017JD027597

Madadgar, S., Moradkhani, H., 2013. A Bayesian Framework for Probabilistic Seasonal Drought Forecasting. J. Hydrometeorol. 14, 1685–1705. https://doi.org/10.1175/JHM-D-13-010.1

Maneta, M.P., Howitt, R., 2014. Stochastic calibration and learning in nonstationary hydroeconomic models. Water Resour. Res. 50, 3976–3993. https://doi.org/10.1002/2013WR015196

Martinez, J.A., Dominguez, F., Miguez-Macho, G., 2016. Effects of a Groundwater Scheme on the Simulation of Soil Moisture and Evapotranspiration over Southern South America. J. Hydrometeorol. 17, 2941–2957. https://doi.org/10.1175/JHM-D-16-0051.1

Mitchell, K.E., Lohmann, D., Houser, P.R., Wood, E.F., Schaake, J.C., Robock, A., Cosgrove, B. a, Sheffield, J., Duan, Q., Luo, L., Higgins, R.W., Pinker, R.T., Tarpley, J.D., Lettenmaier, D.P., Marshall, C.H., Entin, J.K., Pan, M., Shi, W., Koren, V., Meng, J., Ramsay, B.H., Bailey, A. a, 2004. The multi-institution North American Land Data Assimilation System (NLDAS): Utilizing multiple GCIP products and partners in a continental distributed hydrological modeling system. J. Geophys. Res. 109, D07S90–. https://doi.org/10.1029/2003JD003823

Molteni, F., Buizza, R., Marsigli, C., Montani, A., Nerozzi, F., Paccagnella, T., 2001. A strategy for high-resolution ensemble prediction. I: Definition of representative

members and global-model experiments. Q. J. R. Meteorol. Soc. 127, 2069–2094. https://doi.org/10.1002/qj.49712757612

Moradkhani, H., 2008. Hydrologic remote sensing and land surface data assimilation. Sensors 8, 2986–3004. https://doi.org/10.3390/s8052986

Moradkhani, H., Dechant, C.M., Sorooshian, S., 2012. Evolution of ensemble data assimilation for uncertainty quantification using the particle filter-Markov chain Monte Carlo method. Water Resour. Res. 48, W12520. https://doi.org/10.1029/2012WR012144

Moradkhani, H., Hsu, K.-L., Gupta, H., Sorooshian, S., 2005a. Uncertainty assessment of hydrologic model states and parameters: Sequential data assimilation using the particle filter. Water Resour. Res. 41. https://doi.org/10.1029/2004WR003604

Moradkhani, H., Nearing, G., Abbaszadeh, P., Pathiraja, S., 2018. Fundamentals of Data Assimilation and Theoretical Advances, in: Handbook of Hydrometeorological Ensemble Forecasting. pp. 1–26. https://doi.org/10.1007/978-3-642-40457-3_30-1

Moradkhani, H., Sorooshian, S., Gupta, H. V., Houser, P.R., 2005b. Dual state-parameter estimation of hydrological models using ensemble Kalman filter. Adv. Water Resour. 28, 135–147. https://doi.org/10.1016/j.advwatres.2004.09.002

Nijssen, B., Schnur, R., Lettenmaier, D.P., 2001. Global Retrospective Estimation of Soil Moisture Using the Variable Infiltration Capacity Land Surface Model, 1980–93. J. Clim. 14, 1790–1808. https://doi.org/10.1175/1520-0442(2001)014<1790:GREOSM>2.0.CO;2

Niu, G.Y., Yang, Z.L., Mitchell, K.E., Chen, F., Ek, M.B., Barlage, M., Kumar, A., Manning, K., Niyogi, D., Rosero, E., Tewari, M., Xia, Y., 2011. The community Noah land surface model with multiparameterization options (Noah-MP): 1. Model description and evaluation with local-scale measurements. J. Geophys. Res. Atmos. 116, 1–19. https://doi.org/10.1029/2010JD015139

Oglesby, R.J., Erickson III, D.J., 1989. Soil moisture and the persistence of north american drought. J. Clim. 2, 1362–1380. https://doi.org/10.1175/1520-0442(1989)002<1362:smatpo>2.0.co;2

Oleson Lawrence, D. M., Bonan, G. B., Flanner, M. G., K.W., Kluzek Lawrence, P. J., Levis, S., Swenson, S. C., Thornton, E., P. E. A., Decker, M., Dickinson, R., Feddema, J., D., Heald Hoffman, F., Lamarque, J.-F., Mahowald, N., C.L., Niu Qian, T., Randerson, J., Running, S., Sakaguchi, G.-Y., K. A., Stockli, R.,

Wang, A., Yang, Z.-L., Zeng, X., S., Zeng, X.B., 2010. Technical Description of version 4.0 of the Community Land Model. Report.

Olsson, J., Lindstrom, G., 2008. Evaluation and calibration of operational hydrological ensemble forecasts in Sweden. J. Hydrol. 350, 14–24. https://doi.org/10.1016/j.jhydrol.2007.11.010

Omranian, E., Sharif, H.O., Tavakoly, A.A., 2018. How well can Global Precipitation Measurement (GPM) capture hurricanes? Case study: Hurricane harvey. Remote Sens. 10. https://doi.org/10.3390/rs10071150

Parajka, J., Naeimi, V., Blöschl, G., Wagner, W., Merz, R., Scipal, K., 2006. Assimilating scatterometer soil moisture data into conceptual hydrologic models at the regional scale. Hydrol. Earth Syst. Sci. 10, 353–368. https://doi.org/10.5194/hess-10-353-2006

Park, Y.Y., Buizza, R., Leutbecher, M., 2008. TIGGE: Preliminary results on comparing and combining ensembles. Q. J. R. Meteorol. Soc. 134, 2029–2050. https://doi.org/10.1002/qj.334

Pathiraja, S., Anghileri, D., Burlando, P., Sharma, a., Marshall, L., Moradkhani, H., 2018a. Insights on the impact of systematic model errors on data assimilation performance in changing catchments. Adv. Water Resour. 113, 202–222. https://doi.org/10.1016/j.advwatres.2017.12.006

Pathiraja, S., Anghileri, D., Burlando, P., Sharma, A., Marshall, L., Moradkhani, H., 2018b. Time-varying parameter models for catchments with land use change: The importance of model structure. Hydrol. Earth Syst. Sci. 22, 2903–2919. https://doi.org/10.5194/hess-22-2903-2018

Pathiraja, S., Marshall, L., Sharma, A., Moradkhani, H., 2016a. Detecting non-stationary hydrologic model parameters in a paired catchment system using data assimilation. Adv. Water Resour. 94, 103–119. https://doi.org/10.1016/j.advwatres.2016.04.021

Pathiraja, S., Marshall, L., Sharma, A., Moradkhani, H., 2016b. Hydrologic modeling in dynamic catchments: A data assimilation approach. Water Resour. Res. 52, 3350–3372. https://doi.org/10.1002/2015WR017192

Pathiraja, S., Moradkhani, H., Marshall, L., Sharma, A., Geenens, G., 2018c. Data-Driven Model Uncertainty Estimation in Hydrologic Data Assimilation. Water Resour. Res. 54, 1252–1280. https://doi.org/10.1002/2018WR022627

Piazzi, G., Thirel, G., Campo, L., Gabellani, S., 2018. A Particle Filter scheme for multivariate data assimilation into a point-scale snowpack model in Alpine environment. Cryosph. Discuss. 1–37. https://doi.org/10.5194/tc-2017-286

Rana, A., Moradkhani, H., 2016. Spatial, temporal and frequency based climate change assessment in Columbia River Basin using multi downscaled-scenarios. Clim. Dyn. 47, 579–600. https://doi.org/10.1007/s00382-015-2857-x

Rebel, K.T., De Jeu, R.A.M., Ciais, P., Viovy, N., Piao, S.L., Kiely, G., Dolman, A.J., 2012. A global analysis of soil moisture derived from satellite observations and a land surface model. Hydrol. Earth Syst. Sci. 16, 833–847. https://doi.org/10.5194/hess-16-833-2012

Reichle, R.H., Koster, R.D., Liu, P., Mahanama, S.P.P., Njoku, E.G., Owe, M., 2007. Comparison and assimilation of global soil moisture retrievals from the Advanced Microwave Scanning Radiometer for the Earth Observing System (AMSR-E) and the Scanning Multichannel Microwave Radiometer (SMMR). J. Geophys. Res. 112, D09108. https://doi.org/10.1029/2006JD008033

Ridler, M.E., Madsen, H., Stisen, S., Bircher, S., Fensholt, R., 2014. Assimilation of SMOS-derived soil moisture in a fully integrated hydrological and soil-vegetation-atmosphere transfer model in Western Denmark. Water Resour. Res. 50, 8962–8981. https://doi.org/10.1002/2014WR015392

Ridler, M.E., Van Velzen, N., Hummel, S., Sandholt, I., Falk, A.K., Heemink, A., Madsen, H., 2014. Data assimilation framework: Linking an open data assimilation library (OpenDA) to a widely adopted model interface (OpenMI). Environ. Model. Softw. 57, 76–89. https://doi.org/10.1016/j.envsoft.2014.02.008

Rodell, M., Houser, P.R., Jambor, U., Gottschalck, J., Mitchell, K., Meng, C.-J., Arsenault, K., Cosgrove, B., Radakovich, J., Bosilovich, M., Entin, J.K., Walker, J.P., Lohmann, D., Toll, D., 2004. The Global Land Data Assimilation System. Bull. Am. Meteorol. Soc. 85, 381–394. https://doi.org/10.1175/BAMS-85-3-381

Roulin, E., 2006. Skill and relative economic value of medium-range hydrological ensemble predictions. Hydrol. Earth Syst. Sci. Discuss. 3, 1369–1406. https://doi.org/10.5194/hessd-3-1369-2006

Roulin, E., Vannitsem, S., 2005. Skill of Medium-Range Hydrological Ensemble Predictions. J. Hydrometeorol. 6, 729–744. https://doi.org/10.1175/JHM436.1

Schaake, J., Buizza, R., Clark, M., Krahe, P., Hamill, T., Hartman, R., Howard, C., Restrepo, P., Seo, D.J., Thielen, J., Toth, Z., Wood, E., Ssg, H., 2006. Hydrologic

Ensemble Prediction : Past , Present and Opportunities for the Future, in: International Commission for the Hydrology of the Rhine Basin. Expert Consulation Workshop, 30 and 31 March 2006, Bern, Switzerland.

Schaake, J.C., Hamill, T.M., Buizza, R., Clark, M., 2007. HEPEX: The hydrological ensemble prediction experiment. Bull. Am. Meteorol. Soc. 88, 1541–1547. https://doi.org/10.1175/BAMS-88-10-1541

Schaake, J.C., Koren, V.I., Duan, Q.Y., Mitchell, K., Chen, F., 1996. Simple water balance model for estimating runoff at different spatial and temporal scales. J. Geophys. Res. Atmos. 101, 7461–7475. https://doi.org/10.1029/95JD02892

Scipal, K., Scheffler, C., Wagner, W., 2005. Soil moisture-runoff relation at the catchment scale as observed with coarse resolution microwave remote sensing. Hydrol. Earth Syst. Sci. Discuss. 2, 417–448. https://doi.org/10.5194/hessd-2-417-2005

Shanley, J.B., Chalmers, A., 1999. The effect of frozen soil on snowmelt runoff at Sleepers River, Vermont. Hydrol. Process. 13, 1843–1857. https://doi.org/10.1002/(SICI)1099-1085(199909)13:12/13<1843::AID-HYP879>3.0.CO;2-G

Shaw, J.A., Daescu, D.N., 2016. An ensemble approach to weak-constraint four-dimensional variational data assimilation, in: Procedia Computer Science. pp. 496–506. https://doi.org/10.1016/j.procs.2016.05.329

Sheffield, J., Goteti, G., Wen, F., Wood, E.F., 2004. A simulated soil moisture based drought analysis for the United States. J. Geophys. Res. D Atmos. 109, 1–19. https://doi.org/10.1029/2004JD005182

Shutts, G., 2005. A kinetic energy backscatter algorithm for use in ensemble prediction systems. Q. J. R. Meteorol. Soc. 131, 3079–3102. https://doi.org/10.1256/qj.04.106

Slater, A.G., Bohn, T.J., McCreight, J.L., Serreze, M.C., Lettenmaier, D.P., 2007. A multimodel simulation of pan-Arctic hydrology. J. Geophys. Res. Biogeosciences 112. https://doi.org/10.1029/2006JG000303

Smith, M.B., Koren, V.I., Zhang, Z., Reed, S.M., Pan, J.J., Moreda, F., 2004. Runoff response to spatial variability in precipitation: An analysis of observed data, in: Journal of Hydrology. pp. 267–286. https://doi.org/10.1016/j.jhydrol.2004.03.039

Strahler, A.N., 1952. Hypsometric (area-altitude) analysis of erosional topography. Bull. Geol. Soc. Am. 63, 1117–1142. https://doi.org/10.1130/0016-7606(1952)63[1117:HAAOET]2.0.CO;2

Strömberg, D., 2007. Natural Disasters, Economic Development, and Humanitarian Aid. J. Econ. Perspect. 21, 199–222. https://doi.org/10.1257/jep.21.3.199

Thirel, G., Rousset-Regimbeau, F., Martin, E., Habets, F., 2008. On the Impact of Short-Range Meteorological Forecasts for Ensemble Streamflow Predictions. J. Hydrometeorol. 9, 1301–1317. https://doi.org/10.1175/2008JHM959.1

Twedt, T.M., Schaake Jr., J.C., Peck, E.L., 1977. NATIONAL WEATHER SERVICE EXTENDED STREAMFLOW PREDICTION., in: Proceedings of The Western Snow Conference. pp. 52–57.

Uccellini, L.W., 2014. The Record Front Range and Eastern Colorado Floods of September 11 – 17, 2013.

Verbunt, M., Walser, A., Gurtz, J., Montani, A., Schär, C., 2007. Probabilistic Flood Forecasting with a Limited-Area Ensemble Prediction System: Selected Case Studies. J. Hydrometeorol. 8, 897–909. https://doi.org/10.1175/JHM594.1

Walker, J.P., Houser, P.R., 2001. A methodology for initializing soil moisture in a global climate model: Assimilation of near-surface soil moisture observations. J. Geophys. Res. Atmos. 106, 11761–11774. https://doi.org/10.1029/2001JD900149

Wei, M., Toth, Z., Wobus, R., Zhu, Y., Bishop, C.H., Wang, X., 2006. Ensemble Transform Kalman Filter-based ensemble perturbations in an operational global prediction system at NCEP. Tellus, Ser. A Dyn. Meteorol. Oceanogr. 58, 28–44. https://doi.org/10.1111/j.1600-0870.2006.00159.x

Wood, A.W., Lettenmaier, D.P., 2008. An ensemble approach for attribution of hydrologic prediction uncertainty. Geophys. Res. Lett. 35, 1–5. https://doi.org/10.1029/2008GL034648

Woods, R., Sivapalan, M., 1999. A synthesis of space-time variability in storm response: Rainfall, runoff generation, and routing. Water Resour. Res. https://doi.org/10.1029/1999WR900014

Xia, Y., Mitchell, K., Ek, M., Cosgrove, B., Sheffield, J., Luo, L., Alonge, C., Wei, H., Meng, J., Livneh, B., Duan, Q., Lohmann, D., 2012a. Continental-scale water and energy flux analysis and validation for North American Land Data Assimilation

System project phase 2 (NLDAS-2): 2. Validation of model-simulated streamflow. J. Geophys. Res. Atmos. 117, n/a–n/a. https://doi.org/10.1029/2011JD016051

Xia, Y., Mitchell, K., Ek, M., Sheffield, J., Cosgrove, B., Wood, E., Luo, L., Alonge, C., Wei, H., Meng, J., Livneh, B., Lettenmaier, D., Koren, V., Duan, Q., Mo, K., Fan, Y., Mocko, D., 2012b. Continental-scale water and energy flux analysis and validation for the North American Land Data Assimilation System project phase 2 (NLDAS-2): 1. Intercomparison and application of model products. J. Geophys. Res. Atmos. 117, n/a–n/a. https://doi.org/10.1029/2011JD016048

Xia, Y., Mocko, D., Huang, M., Li, B., Rodell, M., Mitchell, K.E., Cai, X., Ek, M.B., 2017. Comparison and Assessment of Three Advanced Land Surface Models in Simulating Terrestrial Water Storage Components over the United States. J. Hydrometeorol. 18, 625–649. https://doi.org/10.1175/JHM-D-16-0112.1

Yan, H., DeChant, C.M., Moradkhani, H., 2015. Improving Soil Moisture Profile Prediction With the Particle Filter-Markov Chain Monte Carlo Method. IEEE Trans. Geosci. Remote Sens. 53, 6134–6147. https://doi.org/10.1109/TGRS.2015.2432067

Yan, H., Moradkhani, H., 2016. Combined assimilation of streamflow and satellite soil moisture with the particle filter and geostatistical modeling. Adv. Water Resour. 94, 364–378. https://doi.org/10.1016/j.advwatres.2016.06.002

Yan, H., Moradkhani, H., Zarekarizi, M., 2017. A probabilistic drought forecasting framework: A combined dynamical and statistical approach. J. Hydrol. 548, 291–304. https://doi.org/10.1016/j.jhydrol.2017.03.004

Yan, H., Zarekarizi, M., Moradkhani, H., 2018. Toward improving drought monitoring using the remotely sensed soil moisture assimilation: A parallel particle filtering framework. Remote Sens. Environ. 216, 456–471. https://doi.org/10.1016/j.rse.2018.07.017

Yang, Z.L., Niu, G.Y., Mitchell, K.E., Chen, F., Ek, M.B., Barlage, M., Longuevergne, L., Manning, K., Niyogi, D., Tewari, M., Xia, Y., 2011. The community Noah land surface model with multiparameterization options (Noah-MP): 2. Evaluation over global river basins. J. Geophys. Res. Atmos. 116, 1–16. https://doi.org/10.1029/2010JD015140

Zaitchik, B.F., Rodell, M., Reichle, R.H., 2008. Assimilation of GRACE Terrestrial Water Storage Data into a Land Surface Model: Results for the Mississippi River Basin. J. Hydrometeorol. 9, 535–548. https://doi.org/10.1175/2007JHM951.1

Zarekarizi, M., Rana, A., Moradkhani, H., 2017. Precipitation extremes and their relation to climatic indices in the Pacific Northwest USA. Clim. Dyn. https://doi.org/10.1007/s00382-017-3888-2

Zhang, G., Chen, F., Gan, Y., 2016. Assessing uncertainties in the Noah-MP ensemble simulations of a cropland site during the tibet joint international cooperation program field campaign. J. Geophys. Res. 121, 9576–9596. https://doi.org/10.1002/2016JD024928

Zupanski, M., Fletcher, S.J., Navon, I.M., Uzunoglu, B., Heikes, R.P., Randall, D.A., Ringler, T.D., Daescu, D., 2006. Initiation of ensemble data assimilation. Tellus, Ser. A Dyn. Meteorol. Oceanogr. 58, 159–170. https://doi.org/10.1111/j.1600-0870.2006.00173.x